




Publicly Accessible Penn Dissertations

1-1-2015

The Effect of Cell Contractility and Packing on Extracellular Matrix and Soft Tissue Rheology

Anne Sofieke Geertruide Van Oosten
University of Pennsylvania, annevanoostenphd@gmail.com

Follow this and additional works at: <http://repository.upenn.edu/edissertations>

 Part of the [Biomechanics Commons](#), [Biomedical Commons](#), and the [Mechanics of Materials Commons](#)

Recommended Citation

Van Oosten, Anne Sofieke Geertruide, "The Effect of Cell Contractility and Packing on Extracellular Matrix and Soft Tissue Rheology" (2015). *Publicly Accessible Penn Dissertations*. 2075.
<http://repository.upenn.edu/edissertations/2075>

This paper is posted at Scholarly Commons. <http://repository.upenn.edu/edissertations/2075>
For more information, please contact libraryrepository@pobox.upenn.edu.

The Effect of Cell Contractility and Packing on Extracellular Matrix and Soft Tissue Rheology

Abstract

In the past decades it has become clear that the mechanical properties of tissues are important for healthy functioning. The mechanical properties of tissues and their load-bearing components found in the extracellular matrix (ECM) have been tested mechanically to provide more insight. However, there is a discrepancy between tissue and ECM mechanics. In this thesis this discrepancy is investigated with a novel multiaxial rheology method, which addresses a physiologically relevant combination of shear and axial strains. Blood clots are used to study the effect of cell traction and cell packing on ECM mechanics.

The results show that ECM networks compression soften and extension stiffen in a typical asymmetric manner. The apparent Young's moduli and shear moduli are decoupled, and are strongly influenced by a modest degree of axial strain. Cell traction induced pre-stress does not change the direction of this response but makes it more symmetrical and increases shear moduli. Close red cell packing in blood clots reverses the behavior of the clots from compression softening to stiffening, and from extension and shear strain stiffening to softening, resembling soft tissues. The same effects can be mimicked by embedding chemically inert beads into a fibrin network at densities approaching the jamming threshold for granular and colloidal materials. The overall conclusion is that cell jamming is likely to be the determining factor of soft tissue mechanics. This has implications for the understanding of tissue mechanics in physiological and pathological situations as well as the modeling of tissues.

Degree Type

Dissertation

Degree Name

Doctor of Philosophy (PhD)

Graduate Group

Bioengineering

First Advisor

Paul A. Janmey

Keywords

Blood clotting, Collagen, Fibrin, Non linear viscoelasticity, Rheology

Subject Categories

Biomechanics | Biomedical | Mechanics of Materials

**ON THE ORIGIN OF TISSUE MECHANICS:
THE EFFECT OF CELL CONTRACTILITY AND PACKING ON
EXTRACELLULAR MATRIX AND SOFT TISSUE RHEOLOGY**

Anne S. G. van Oosten

A DISSERTATION

in

Bioengineering

Presented to the Faculties of the University of Pennsylvania

in

Partial Fulfillment of the Requirements for the

Degree of Doctor of Philosophy

2015

Supervisor of Dissertation

Paul A. Janmey, PhD
Professor of Physiology

Graduate Group Chairperson

Jason A. Burdick, PhD
Professor of Bioengineering

Dissertation Committee

Rebecca G. Wells, MD
Associate Professor of Medicine (Chair)

Vivek B. Shenoy, PhD
Professor of Physics

John W. Weisel, PhD
Professor of Medicine

THE EFFECT OF CELL CONTRACTILITY AND PACKING ON EXTRACELLULAR
MATRIX AND SOFT TISSUE RHEOLOGY
COPYRIGHT

2015

Anne S. G. van Oosten

This work is licensed under the
Creative Commons Attribution-
NonCommercial-ShareAlike 3.0
License

To view a copy of this license, visit

<http://creativecommons.org/licenses/by-nc-sa/3.0/>

Dedicated to all women in science who paved this path before me

ACKNOWLEDGMENT

First and foremost I would like to thank my adviser Paul Janmey. I am deeply indebted to him, for giving me the opportunity to come to Penn to pursue my PhD. I would also like to thank the members of my committee, Rebecca Wells, John Weisel and Vivek Shenoy, for valuable advice and guidance.

I am grateful for having worked with many wonderful colleagues in the Janmey lab. LiKang Chin, Pete Galie, Katrina Cruz, Robert Bucki, Melissa Mendez, Dikla Raz, Eric Wang, Maria Murray, Dave Slochower, Fitzroy Byfield, Kasia Pogoda, Elisabeth Charrier and Anne Herrmann.

I am thankful to Maryna Perepelyuk from the Wells lab, and Richard Li from the Diamond lab for supplying blood (products) for my experiments.

Fred MacKintosh and his lab members, Mahsa Vahabi, Albert Licup and Abhinav Sharma, developed and performed the simulations presented in this thesis. I greatly appreciate their work and knowledge.

I am honored and grateful to have received a Fulbright Science and Technology Award and a Kuitse – Prins Bernhard Culture Fund Fellowship.

Lastly, I am extremely grateful having the support of my family in the Netherlands. I couldn't have done this without their support.

ABSTRACT

THE EFFECT OF CELL CONTRACTILITY AND PACKING ON EXTRACELLULAR MATRIX AND SOFT TISSUE RHEOLOGY

Anne S. G. van Oosten

Paul A. Janmey

In the past decades it has become clear that the mechanical properties of tissues are important for healthy functioning. The mechanical properties of tissues and their load-bearing components found in the extracellular matrix (ECM) have been tested mechanically to provide more insight. However, there is a discrepancy between tissue and ECM mechanics. In this thesis this discrepancy is investigated with a novel multiaxial rheology method, which addresses a physiologically relevant combination of shear and axial strains. Blood clots are used to study the effect of cell traction and cell packing on ECM mechanics.

The results show that ECM networks compression soften and extension stiffen in a typical asymmetric manner. The apparent Young's moduli and shear moduli are decoupled, and are strongly influenced by a modest degree of axial strain. Cell traction induced pre-stress does not change the direction of this response but makes it more symmetrical and increases shear moduli. Close red cell packing in blood clots reverses the behavior of the clots from compression softening to stiffening, and from extension and shear strain stiffening to softening, resembling soft tissues. The same effects can be mimicked by embedding chemically inert beads into a fibrin network at densities approaching the jamming threshold for granular and colloidal materials. The overall conclusion is that cell jamming is likely to be the determining factor of soft tissue mechanics. This has implications for the understanding of tissue mechanics in physiological and pathological situations as well as the modeling of tissues.

TABLE OF CONTENTS

ACKNOWLEDGMENT IV

ABSTRACT..... V

TABLE OF CONTENTS..... VI

LIST OF ILLUSTRATIONS..... X

CHAPTER 2: BACKGROUND..... 5

2.1 Tissue = cells + extracellular matrix 5

 2.1.1 Collagen: the most common extracellular matrix protein..... 6

 2.1.2 Fibrin: the extracellular matrix of blood clots..... 7

 2.1.3 Blood clots and how they compare to soft tissues 8

2.2 Measuring ECM and tissue mechanics 11

 2.2.1 Understanding basic mechanical properties 11

 2.2.2 Biological materials are viscoelastic materials12

 2.2.3 Rheometers are devices to measure mechanical properties of materials14

 2.3.4 Multiaxial measurements with a shear rheometer17

2.3 The extraordinary mechanical properties of the extracellular matrix.18

 2.3.1 Mechanical properties of reconstituted collagen and fibrin networks 18

 2.3.2 ECM networks are remarkably strong 20

 2.3.3 ECM networks show typical non linear behavior when subjected to deformation..... 22

2.4 Tissue mechanics in health and disease25

 2.4.1 Tissue mechanics in health 25

 2.4.2 Tissue mechanics in disease 26

**CHAPTER 3: THE EFFECT OF AXIAL STRAIN ON THE SHEAR RHEOLOGY OF
EXTRACELLULAR MATRIX NETWORKS 28**

3.1 Abstract..... 28

3.2 Introduction 28

3.3 Methods 30

 3.3.1 Preparation of fibrin.....30

 3.3.2 Preparation of collagen type 131

 3.3.3 Preparation of composite networks with collagen and hyaluronic acid.....31

3.3.4 Preparation of cross-linked hyaluronic acid gels	31
3.3.5 Preparation of soft polyacrylamide gels	32
3.3.6 Rheometry	32
3.3.7 Tensile testing	34
3.4 Results	34
3.4.1 Verification of experimental method with polyacrylamide gels	34
3.4.2 Shear strain-stiffening onset and amplitude of semiflexible biopolymer networks is altered when networks are axially strained.....	35
3.4.3 Storage moduli of semiflexible biopolymer networks drop in compression and increase in extension	39
3.4.4 Axial stress-strain curves have different slopes in compression and extension	41
3.4.5 Uncoupling of the axial and shear moduli of semiflexible biopolymer networks	45
3.4.6 Composite gels of collagen and hyaluronic acid behave similar as collagen.....	46
3.4.7 Cross-linked hyaluronic acid networks show different response to axial strain.....	49
3.5 Discussion.....	50
 CHAPTER 4: DYNAMICS OF EXTRACELLULAR MATRIX NETWORKS UNDER SHEAR, COMPRESSION AND EXTENSION	
55	
4.1 Abstract.....	55
4.2 Introduction	55
4.3 Materials and methods	57
4.3.1 Preparation of coarse and fine fibrin clots	57
4.3.2 Preparation of collagen gels and composites of collagen and hyaluronic acid.	58
4.3.3 Shear rheometry	58
4.4 Results	59
4.4.1 The dynamics of storage moduli and axial stresses during compression and extension ...	59
4.4.2 Stress-relaxation in compression, extension and shear	66
4.5 Discussion.....	72
 CHAPTER 5: THE EFFECT OF CELL CONTRACTILITY ON MULTIAXIAL RHEOLOGY OF EXTRACELLULAR MATRIX NETWORKS.....	
78	
5.1 Abstract.....	78
5.2 Introduction.....	79
5.3 Materials and methods.....	80
5.3.1 Preparation of platelet-rich and platelet-poor plasma.....	80
5.3.2 Whole blood clots.....	81

5.3.3 Rheometry.....	81
5.3.3 Imaging	81
5.4 Results	82
5.4.1 Platelet contractility increases storage moduli of whole blood and plasma clots	82
5.4.2 Pre-stressed clots weaken when compressed and shear strengthen in extension, with symmetry between compression and extension	84
5.4.3 Inhibiting platelet contractility in whole and plasma clots results in clots that resemble fibrin networks.....	86
5.4.4 Stress-relaxation is changed by platelet-contractility.....	88
5.4.5 Strain amplitude dependence decreases in pre-stressed networks.....	92
5.5 Discussion.....	93
CHAPTER 6: THE EFFECT OF CELL PACKING DENSITY ON MULTIAXIAL RHEOLOGY OF EXTRACELLULAR MATRIX AND MODEL TISSUES.....	97
6.1 Abstract.....	97
6.2 Introduction	97
6.3 Materials and methods	98
6.3.1 Contracted clots from rat blood.....	98
6.3.2 Fibrin networks with beads	99
6.3.3 Rheometry	99
6.4 Results.....	100
6.4.1 Contracted clots respond oppositely to axial strain as whole blood clots, plasma clots, and reconstituted networks.	100
6.4.2 Shear rheology of contracted clots can be mimicked by embedding beads in a fibrin network, in absence of contractile cells.....	101
6.4.3 Dynamics and stress-relaxation of contracted clots and constructs	106
6.4.4 Non-linear behavior at high shear strains changes at high cell and bead packing densities	110
6.5 Discussion.....	113
6.5.1 Jamming to explain tissue rheology	114
CHAPTER 7: CONCLUSIONS AND FUTURE DIRECTIONS	118
7. 1 Summary of results.....	118
7.2 Future directions	119
7.2.1 Deepening the understanding of semiflexible network physics.....	120
7.2.2 Stress-relaxation	120
7.2.3 Generalization of multiaxial rheology principles to rigid, and flexible biopolymers, and polyelectrolytes.	121

7.2.4 Influence of platelet contraction on fibrin network mechanics.....	122
7.2.5 Jamming of beads inside networks	122
7.2.6 Effect of cell attachments on multiaxial rheology	123
7.2.7 Extension of multiaxial rheology to tissues with varying cell to ECM ratio; cellular traction and anisotropy	124
BIBLIOGRAPHY	125

LIST OF ILLUSTRATIONS

Figure 2.1: The ECM and cells in a tissue. Schematic representation (left) and microscope image (right) of connective tissue, showing cells embedded in extracellular matrix. Picture adopted from ⁵.

Figure 2.2: Interaction between membrane receptors and ECM. Schematic representation of a cell membrane with integrin receptors in the membrane making connections with extracellular matrix constituents. Picture adopted from ³.

Figure 2.3: Collagen self-assembly. Collagen peptide chains form tropocollagen and subsequently assemble into collagen fibrils and fibers. Picture adopted from ⁷.

Figure 2.4: Fibrin polymerization. Schematic representation of fibrinogen polymerization into fibrin fibers. Picture adopted from ¹.

Figure 2.5: Fibrin and whole blood clot. Electron micrograph of (A) a reconstituted fibrin network and (B) a whole blood clot. The fibrin network is pulled on by aggregated platelets with red blood cells trapped in the network, plasma fills the open spaces. Images adopted from ¹¹. Bar = 5 μm

Figure 2.6: Contracted blood clot. Electron micrographs of interior (A) and exterior (B) of a contracted blood clot. In (A) the polyhedral shape of the tightly packed red blood cells can be seen. In (B) the fibrin network can be seen stretching over the red blood cells on the outside of the clot. Picture from ¹². Bar = 10 μm

Figure 2.7: Depicting compressive, extensional and shear deformation and showing how stress and moduli are determined. Pictures adopted from ⁴.

Figure 2.8: Typical stress after application of constant strain for an elastic solid, a viscous fluid, an viscoelastic solid and viscoelastic fluid. Graphs adopted from ².

Figure 2.9: Explanation of central force rigidity threshold. The hinging structure of a bathroom mirror collapses upon the slightest touch. This structure consists of 2 beams intersecting. The cytoskeleton in the cell consists of networks with 2 intersecting fibers. A rigid dome of 3 intersecting beams can withstand large forces without deforming. Picture from ⁹.

Figure 2.10: Linear deformation of a spring as an example of linear elasticity. The change of the spring length and the force needed for that particular elongation (or compression) are plotted. This results in a straight line. The slope is constant hence the modulus is constant. Image adapted from ⁶.

Figure 2.11: Strain-stiffening of biopolymers. The modulus of many biopolymer networks increases with increasing shear strain ⁸.

Figure 2.12: Biopolymers show negative normal stress, polyacrylamide does not. Shear (circles) and normal (triangles) stresses as a function of shear strain for various biopolymers compared to polyacrylamide. Graphs from ¹⁰.

Figure 3.1: Experimental set-up for multiaxial rheology method. A shear rheometer is used with a parallel plate geometry. Biopolymer samples are polymerized between the plates; after polymerization buffer is added around the sample to prevent drying and allow free fluid flow to in and out of the sample. The gap between the plates is changed to apply axial strain; the lower plate is rotated to apply shear strain. The torque and axial force are recorded.

Figure 3.2: Testing of multiaxial rheology method with linear elastic polyacrylamide gels. Showing the storage modulus (a), and axial stress (b). The data from (a) are obtained with the rheometer; the data in (b) are obtained separately with a tensile tester. The reported Young's modulus in (b) is the slope of the axial stress-strain.

Figure 3.3: Semiflexible biopolymer networks strain-stiffen when axially strained, but onset and amplitude is altered. Strain amplitude dependence of fibrin clots of (a) 2 mg/ml and (c) 10 mg/ml when 12.5% extended, 20% compressed and at 0% axial strain; and (b) collagen gels of 2.5 mg/ml at 2.5% extension, 20% compression and 0% axial strain. (d), (e). Storage modulus versus shear strain for a diluted phantomized triangular network with $L/L_c = 6.67$; with varying pre-stress: without any axial strain, with 10% extension and with 10% compression. The normalised bending modulus $\tilde{\kappa} = 10^{-3}$ (d) corresponds with fibrin; $\tilde{\kappa} = 2 \times 10^{-4}$ with collagen (e).

Figure 3.4: Example of storage modulus of fibrin network followed in time during the initial steps of a typical compression sequence. The storage modulus of a 10 mg/ml fibrin network is shown as a function of time during compression from 0% to 1% and from 1% to 2%. The relaxed value of the storage modulus is taken right before the next level of compression is applied, as pointed out by the arrows. The same approach is used for the storage modulus in extension and the axial stress.

Figure 3.5: Collagen type 1 networks soften in compression and stiffen in extension. Rheology of a 2.5 mg/ml collagen gel at low shear strains (2%) at increasing levels of axial strain, showing the storage modulus (a), axial stress (b) and loss tangent (c). The data from (a) and (c) are obtained simultaneously with the shear rheometer; the data in (b) are obtained separately with the tensile tester.

Figure 3.6: Coarse fibrin clots of 10 mg/ml soften in compression and stiffen in extension. Rheology of a coarse fibrin clot with factor XIIIa cross-linking with a concentration of 10 mg/ml measured at low shear strains (2%) at increasing levels of axial strain, showing the storage modulus (a), axial stress (b) and loss tangent (c). The data from (a) and (c) are obtained simultaneously with the shear rheometer;

the data in (b) were obtained separately with the tensile tester. For tensile measurements the sample diameter was between 22.5 mm and 25 mm, with a 1mm gap.

Figure 3.7: Coarse fibrin clots of 2 mg/ml soften in compression and stiffen in extension. Rheology of a coarse fibrin clot with factor XIIIa cross-linking with a concentration of 2 mg/ml measured at low shear strains (2%) at increasing levels of axial strain, showing the storage modulus (a), axial stress (b), and loss tangent (c)

Figure 3.8: Simulations of storage moduli and axial stresses predict multiaxial behavior of semiflexible biopolymers. Simulation for a diluted phantomized triangular network (3D) with $L/L_c = 6.67$. (a) shows the storage modulus, (b) shows the axial stresses. The normalised bending modulus $\tilde{\kappa} = 10^{-3}$ corresponds with fibrin $\tilde{\kappa} = 2 \times 10^{-4}$ with collagen.

Figure 3.9: Increasing the viscosity of the solvent phase of collagen networks does not change multiaxial rheology. Rheology of composites with 2.5 mg/ml collagen and 4 mg/ml linear hyaluronic acid at low shear strains (2%) showing the storage modulus (a), axial stress (b), and loss tangent (c). Experimental method is identical as experiments with collagen gels as shown in Figure 3.4; with the modification that samples are allowed longer relaxation times; between 15 and 30 minutes.

Figure 3.10: Composite collagen-hyaluronic acid networks strain-stiffen significantly. Strain amplitude dependency of composite networks with 2.5 mg/ml collagen and 4 mg/ml linear hyaluronic acid (in absence of axial strain).

Figure 3.11: Cross-linked hyaluronic acid gel shown different behavior compared to semiflexible biopolymer networks. Rheology of 8 mg/ml thiol-modified hyaluronic acid cross-linked with thiol reactive PEGDA at low shear strains (2%) at increasing levels of axial strain, showing the storage modulus (a) and axial stress (b). Both measured with the shear rheometer.

Figure 4.1: Dynamics of storage moduli and axial stresses of 10 mg/ml fibrin networks. Coarse networks (a-f) and fine networks (g, h) subjected to 1% (a, b) or 10% (c-h) axial strain, with a sample diameter of 8mm (a-d, g, h) or 25mm (e, f). Storage modulus is measured with oscillatory shear strain of 2%. The mean of 3 samples is shown. 3-10% of data points are depicted with a symbol.

Figure 4.2: Peak storage moduli normalized to initial storage moduli for 10 mg/ml fibrin networks subjected to varying axial strain, with varying plate sizes and permeability. The initial modulus is calculated as an average over 10 sec before axial strain application, the peak is the highest point reached during or immediately after axial strain application. A value of 1 indicates there is no peak but the modulus moves to the new steady state without relaxation.

Figure 4.3: Dynamics of storage moduli and axial stresses of 2.5 mg/ml collagen networks. Collagen networks (a-e) and composite collagen – HA networks

(**f, g**) subjected to 0.5 compression% (**a**), 0.25% extension (**b**) or 5% compression (**c, e**) 2.5% compression (**f**) or 2.5% extension (**d, g**). Sample diameter was 25 mm (**a-d, f, g**) or 8 mm (**e**). Storage modulus is measured with oscillatory shear strain of 2%. The mean of 3 samples is shown. 3-10% of data points are depicted with a symbol.

Figure 4.4: Peak storage moduli normalized to initial storage moduli for collagen networks subjected to varying axial strain, with varying plate sizes and permeability. The initial modulus is calculated as an average over 10 sec before axial strain application, the peak is the highest point reached during or immediately after axial strain application. A value of 1 indicates there is no peak but the modulus moves to the new steady state without relaxation.

Figure 4.5: Dynamics of storage moduli and axial stresses of coarse and fine fibrin network at 2 mg/ml. Coarse networks (**a**) and fine networks (**b**) with a sample diameter of 50 mm subjected to 5% compression. The mean of 3 samples is shown. 3-10% of data points are depicted with a symbol.

Figure 4.6: Relaxation of storage moduli and axial stresses of fibrin networks at 10 mg/ml after an axial step strain. The axial strain, plate size and permeability were varied. The storage moduli (**a, b**) and axial stresses (**c, d**) were normalized to the peak value that was reached after axial strain application. The mean of 3 samples is shown.

Figure 4.7: Relaxation of storage moduli and axial stresses of collagen networks after an axial step strain. The axial strain, plate size and permeability were varied. The storage moduli (**a, b**) and axial stresses (**c, d**) were normalized to the peak value of each sample. The mean of 3 samples is shown. 3-10% of data points are depicted with a symbol.

Figure 4.8: Relaxation of storage moduli and axial stresses of coarse and fine fibrin networks of 2 mg/ml after a 5% compression. The storage moduli (**a**) and axial stresses (**b**) were normalized to the peak value of each sample. The mean of 3 samples is shown. 3-10% of data points are depicted with a symbol

Figure 4.9: Axial stress-relaxation compared to shear relaxation. A step strain was imposed on a collagen network (**a**), 10 mg/ml coarse fibrin network (**b**), a composite collagen-hyaluronic acid network (**c**) and a 10 mg/ml fine fibrin network (**d**) in compression, extension and shear. The resulting stress was followed as a function of time. The stress is normalized to the peak value; the mean of 3 samples is shown. 3-10% of data points are depicted with a symbol.

Figure 4.10: Frequency-dependence of collagen and composite collagen-hyaluronic acid networks in axial and shear direction. A 1% oscillatory strain was imposed on a collagen network (**a**) and a composite collagen-hyaluronic acid network (**b**) in compression, extension and shear. The average \pm SD of 5 cycles is shown for 1 sample. The shear moduli were obtained with the shear rheometer, the Young's moduli with the tensile tester. The dependence of the modulus to the frequency is determined by fitting a power-law over the whole range of frequencies.

Figure 5.1: Imaging of fibrin network in whole blood clots. Native state (left) and with blebbistatin treatment (right). Fluorescent imaging of fibrin network by incorporation of Alexa Fluor 488-fibrinogen.

Figure 5.2: Storage moduli of whole blood, plasma and fibrin clots. The storage modulus of whole blood clots at 1% shear strain; and of plasma clots and fibrin at 2% shear strain, all in absence of axial strain. For whole clots and fibrin the mean of 3 samples is shown \pm SD; for prp 1 sample is shown, for ppp the mean of 2 samples is shown \pm SD

Figure 5.3: Native and blebbistatin-treated whole clots, platelet-rich and platelet-poor plasma clot show compression softening and extension stiffening. Rheology of native, blebbistatin-treated whole clots, ppp, and prp at low shear strains (1-2%) at increasing levels of axial strain, showing the storage moduli (**a**), axial stresses (**b**), loss tangents (**c**), and normalized storage moduli (**d**). The data from (**a**), (**b**) and (**c**) are obtained simultaneously with the shear rheometer. For prp 1 sample is shown. For ppp the mean of 2 samples \pm SD is shown, for whole clots 3 samples \pm SD.

Figure 5.4: Simulations of storage moduli and axial stresses predict multiaxial behavior of semiflexible biopolymers. Simulation for a diluted phantomized triangular network (3D) with varying pre-stress and $L/L_c = 6.67$. (**a**, **c**) show the storage modulus, (**b**, **d**) show the axial stresses. The normalised bending modulus $\tilde{\kappa} = 10^{-3}$ corresponds with fibrin (**a**, **b**), $\tilde{\kappa} = 2 \times 10^{-4}$ with collagen (**c**, **d**).

Figure 5.5: Dynamics of storage moduli and axial stresses of native and blebbistatin-treated whole blood clots. A 5% compression (**a**, **c**) or extension (**b**, **d**) was applied to native (**a**, **b**) or a blebbistatin-treated (**c**, **d**) clots. The storage modulus is measured with a 1% shear strain.

Figure 5.6: Stress-relaxation of native and blebbistatin-treated whole blood clots. The axial stress in compression and extension, and shear stress after a 5% strain is followed in time and normalized to the peak stress. The mean of 3 samples is shown.

Figure 5.7: Strain-amplitude dependence of the storage moduli of native and blebbistatin-treated clots compared to fibrin networks. The storage modulus is shown as a function of the applied shear strain at a constant frequency of 1 rad/s.

Figure 6.1: Contracted clots compression stiffen and extension weaken. Rheology of contracted rat blood clots at low shear strains (2%) at increasing levels of axial strain, showing the storage modulus (**a**), axial stress (**b**) and loss tangent (**c**). The data from (**a**), and (**c**) are obtained simultaneously with the shear rheometer. The axial stress data in (**b**) are obtained with the tensile tester. The mean of 5 samples is shown \pm SD.

Figure 6.2: Imaging of 3 jammed beads within fibrin network at different depths. A 50% bead- fibrin construct is shown. Images show fibrin network imaged with ALEXA-488 Fbg incorporation (**a, b, c, d**). Phase contrast image of beads (**e**) corresponding with fluorescent image (**a**).

Figure 6.3: Beads embedded in a fibrin network change multiaxial rheology to resemble tissues when bead density reaches a critical value. Rheology of fibrin-bead constructs at low shear strains (2%) at increasing levels of axial strain, showing the storage modulus (**a**), axial stress (**b**) and loss tangent (**c**). The data from (**a**), (**b**) and (**c**) are obtained simultaneously with the shear rheometer.

Figure 6.4: Dynamics of storage moduli and axial stresses of contracted clots and fibrin-bead constructs. A 5% compression (**a, c, e, g**) or extension (**b, d, f, h**) was applied, to contracted clots (**a, b**), and 5 mg/ml fibrin networks with 50% beads (**c, d**), 60% beads (**e, f**), and 70% beads (**g, h**). The mean of 3 samples is shown, except for compressed contracted clots and 70% (n=4). 3-5% of data points is depicted with a symbol.

Figure 6.5: Relaxation of storage modulus after axial strain application of contracted clots and fibrin-bead constructs Stress-relaxation in compression, extension and shear is shown, normalized to the peak stress of (**a**) contracted clots (**b**) fibrin-bead construct with 50% beads, (**c**) constructs with 60% beads and (**d**) constructs with 70% beads.

Figure 6.6: Stress-relaxation of contracted clots and fibrin-bead constructs after a step axial or shear strain. Stress-relaxation in compression, extension and shear is shown, normalized to the peak stress of (**a**) contracted clots (**b**) fibrin-bead construct with 50% beads, (**c**) constructs with 60% beads and (**d**) constructs with 70% beads.

Figure 6.7: Strain amplitude dependence of contracted clots. The storage modulus of contracted rat blood clots is shown with increasing shear strains.

Figure 6.8: Strain amplitude dependence of fibrin-bead constructs at varying axial strain. The storage modulus of fibrin-bead constructs with a bead density of (**a**) 50% (**b**) 60% and, (**c**) 70% is shown with increasing shear strains at 20% extension, 35% compression and 0% axial strain.

Figure 6.9: Overview of strain-stiffening and weakening behavior, comparing normalized storage moduli of contracted clots and fibrin-beads constructs. The storage modulus was normalized to the value at the lowest shear stress (1% for contracted clots, 2% for constructs).

CHAPTER 1: INTRODUCTION

When you study the material properties of tissues, you can't help but to be impressed. It is most intriguing that a material that is so soft and flexible can be equally strong and resilient at the same time. The load bearing components of tissues, a class of materials called biopolymers, are found both inside and around cells and have remarkable and unique mechanical properties. Tissue strength is for good reason; the tissues in our bodies and subsequently the cells in the tissues are constantly subjected to mechanical stimuli. Often one will think of extreme events such as high impact sports when considering mechanical stimuli on the body. However, all tissues are constantly mechanically challenged. Even when lying perfectly still when you sleep, muscle movements in the cardiovascular system, lungs and intestines are pushing and pulling tissues. Also, gravitational forces are acting on tissues. These forces are necessary for healthy functioning of tissues but can quickly become pathological when outside a relatively narrow range.

The direct effect of forces on tissue function and development was documented as early as 150 years ago. Henry Davis, an American orthopedic surgeon, made observations on the production of new tendon as a response to tension ¹³. Three German orthopedic surgeons separately published theories on the effect of forces on skeletal development. Carl Hueter and Richard von Volkmann both concluded that an abnormally high level of pressure slows down bone growth and that a lower level of pressure increased bone growth ^{14,15}. Julius Wolff stated that *'every change in the function of bone is followed by certain definite changes in internal architecture and external conformation in accordance with mathematical laws'* ¹⁶. Another important work that emphasized the

importance of forces in the development of a wide variety of tissues and organisms was published in 1917. This book, *On growth and form* composed by Sir D'Arcy Wentworth Thompson, is now considered one of the classical publications in the natural sciences ¹⁷.

Standard tissue culture techniques started to develop around the same time in history as the publications mentioned above. Being able to study cells outside of the body resulted in a flight of knowledge on the functioning of organisms. However, the belief that tissues and cells respond to mechanical stimuli was not perpetuated into common biological practice. On the contrary, most cell biologists operated under the belief that cells respond merely to chemical cues, such as hormones. Consequently, to this day the standard tool for cell culture remains the rigid (plastic or glass) dish, closely resembling the version developed by Julius Petri while in Robert Koch's lab ¹⁸. Though in their field, microbiology, one used the dish as a carrier for agar or gelatin, scientists started growing body cells directly in Petri dishes. However, tissue cells in the body are surrounded by material that is much softer than glass or plastic – with the exception of bone – hence the mechanical cues cells receive from being cultured in a plastic dish are unphysiological. A breakthrough for the study of cell mechanics was the development of the elastic substrate for cell culture by Albert Harris in 1980 ¹⁹. In the mid 1990s the use of elastic substrates for cell culture had been refined and scientists started to study the effect of the material properties of these substrates on many aspects of cell behavior. We now know that cell functionalities like morphology, cell traction, locomotion, differentiation, and protein synthesis are influenced by the mechanical properties of the substrate they grow on ²⁰⁻²³. Extrapolating these findings to cell behavior within tissues in the body remains challenging as the properties of the materials in the body are much more complex compared to the elastic substrates used in tissue culture.

Tissues consist of cells surrounded by a network of proteins, sugary molecules and hybrids thereof. This structure, called the extracellular matrix or ECM in short, is often considered the mechanical backbone of tissues. The building blocks of the ECM can be isolated from tissues and reconstituted in the lab. In order to better understand the mechanical environment of cells in the body the mechanical properties of reconstituted ECM networks have been investigated; mostly in shear, and to a lesser extent in extension and compression. These experiments showed that the ECM has unique mechanical properties that are not seen in simple rubber materials - like the elastic substrates used to study cells *in vitro*. However, knowing the mechanical properties of reconstituted ECM networks does not allow you to deduce the mechanical environment of cells *in vivo*. The mechanical properties of these networks reported in literature show a rather extreme variability. Another issue is that a deformation in the body is hardly ever unidirectional, often there is a combination of shear and extension or compression. Most importantly, there is a discrepancy between the mechanics of reconstituted ECM networks and whole tissues. For example, ECM networks show an opposite response to shear deformation compared to whole tissues, as shown in this thesis.

The primary goal of this thesis is to elucidate the factors contributing to the disparity between ECM and tissue mechanics. This is done with a novel multiaxial rheology approach, hereby also addressing a physiologically relevant combination of shear and axial strains. **Chapter 3** investigates the multiaxial rheology of semiflexible ECM networks formed by collagen and fibrin, and also touches upon non-fibrillar ECM constituents and composites of fibrillar and non-fibrillar ECM constituents. **Chapter 4** discusses the dynamics of the mechanical properties of these networks during multiaxial deformation.

The obvious difference between a tissue and an ECM network is the presence of cells in a tissue. Cells could change the mechanics of the ECM network in several ways. Here blood clots are used as a model for soft tissues, to test the effect of cells on a fibrin network.

Chapter 5 addresses the effect of cell contractility on the multiaxial rheology of plasma and blood clots. **Chapter 6** addresses the effect of cell packing in fibrin networks both with and without platelets.

CHAPTER 2: BACKGROUND

2.1 Tissue = cells + extracellular matrix

Tissues are formed by cells and extracellular matrix (ECM). The cells, which are the smallest functional units of the tissue, perform all vital functions such as energy production and synthesis of proteins. The ECM is the supporting structure around the cells. It is an intricate network formed by proteins, such as collagen, sugary fibers such as hyaluronic acid, and other components that the cells synthesize and organize around them. Especially connective tissues have a very abundant extracellular matrix ²⁴. (Figure 2.1)

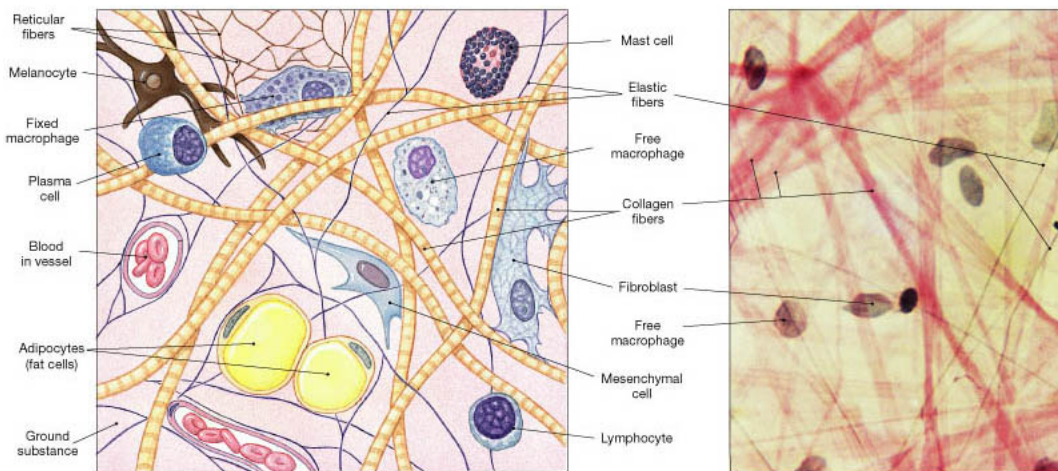


Figure 2.1: The ECM and cells in a tissue. Schematic representation (left) and microscope image (right) of connective tissue, showing cells embedded in extracellular matrix. Picture adopted from 5

The extracellular matrix was often thought of as an inert substance, a space-filler necessary for water retention, and in some cases mechanical strength. It has become clear over the past decades that the ECM is a highly dynamic material that has an

important role in preserving both chemical and mechanical homeostasis is tissue. In addition, cells actively interact with their ECM, through receptors on the cell surface. (Figure 2.2) These receptors are in turn attached to the cytoskeleton inside the cell; which allows the cells to exert forces on the surrounding ECM ²⁵.

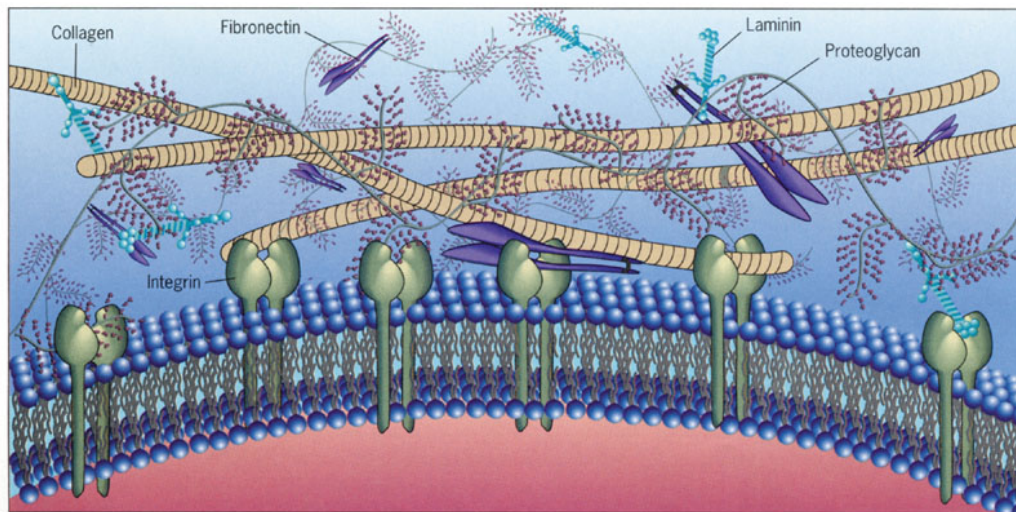


Figure 2.2: Interaction between membrane receptors and ECM. Schematic representation of a cell membrane with integrin receptors in the membrane making connections with extracellular matrix constituents. Picture adopted from ³.

2.1.1 Collagen: the most common extracellular matrix protein

The major ECM constituent in mammals is the protein collagen. There are as many as 28 types of collagen known; collagen type 1 is by far the most abundant in the body. The hallmark of a collagen is the chain of continuous glycine-X-Y amino acid repeats in which X and Y can be any amino acid. For fibril forming collagens like collagen type 1 usually the second amino acid is a proline, and the third a hydroxyproline. Three of such so-called α -chains twist around each other to form a tropo-collagen. Tropocollagen

monomers self-assemble into larger structures. Fibrils can further aggregate into even larger fibers. (Figure 2.3) Some collagens form networks or associate with other collagen fibrils. In the body the fibrils or fibers are cross-linked by specific enzymes such as lysyl oxidases or transglutaminases ²⁶. Reconstituted collagen networks do not contain these enzymes and therefore lack covalent cross-links, these network are entangled.

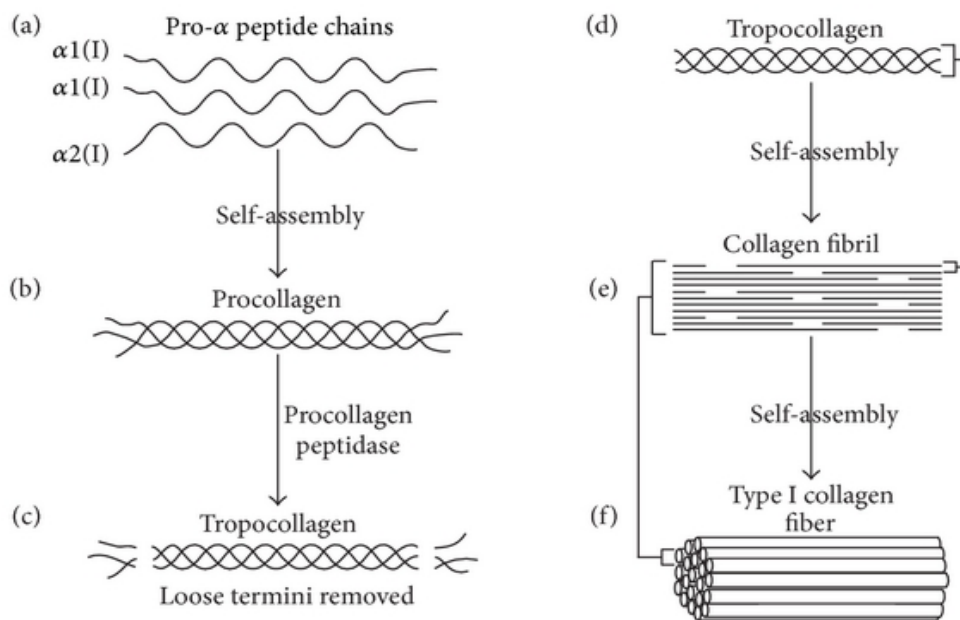


Figure 2.3: Collagen self-assembly. Collagen peptide chains form tropocollagen and subsequently assemble into collagen fibrils and fibers. Picture adopted from 7.

2.1.2 Fibrin: the extracellular matrix of blood clots

A protein called fibrin forms the extracellular matrix of blood clots, it is formed by monomers called fibrinogen which are always present in the blood. The enzyme thrombin is needed to form fibrin fibers from fibrinogen. Thrombin cleaves off

fibrinopeptides after which the fibrinogen monomers assemble in a typical lateral manner. The smallest assemblies are called protofibrils. The protofibrils pack together to form larger fibers, which can branch out. (Figure 2.4) Fibrin fibers can be cross-linked by specific enzymes. The transglutaminase factor XIIIa cross-links the fibrinogen monomer ends within the fiber. Factor XIII is activated by thrombin as well but only in the presence of calcium. When fibrin networks are reconstituted in the lab they form branched, entangled networks ¹¹.

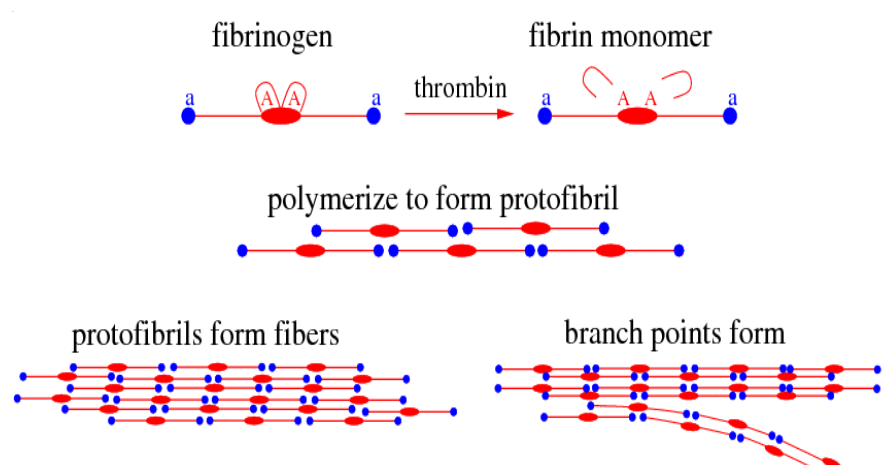


Figure 2.4: Fibrin polymerization. Schematic representation of fibrinogen polymerization into fibrin fibers. Picture adopted from ¹.

2.1.3 Blood clots and how they compare to soft tissues

Blood clots are a unique tissue, as they are only formed in pathological situations. When a vessel is damaged, chemicals are released that set the blood clotting cascade in motion; which leads to thrombin activation among other things. The most important cells involved in blood clotting are platelets. The platelets attach to the fibrin network, often in aggregates, and pull on the network thus contracting it. In certain situations red blood

cells are trapped in the network, as well as immune cells. When the fibrin network is contracted by platelets, fluid (blood serum) is squeezed out and a very tight seal is formed that stops bleeding ¹¹.

In a laboratory setting different variants of blood clots can be formed: a plasma clot, a whole clot or a contracted clot. *In vivo* plasma clots can be formed in the arterial system. In the lab this can be mimicked with blood from which the red blood cells are removed by centrifugation. The plasma clot is then formed from the remaining platelet-rich plasma (prp).

When blood is clotted in a container to which the fibrin attaches sufficiently, the platelets are not able to pull the fibrin network together or squeeze out fluid. All of the blood constituents remain in the clot and is it therefore called a whole blood clot. The whole clot generally has a fibrin concentration of around 2 mg/ml and a red blood cell volume density of 40-50%. Hence, there is still a large volume of plasma present in the clot.

(Figure 2.5)

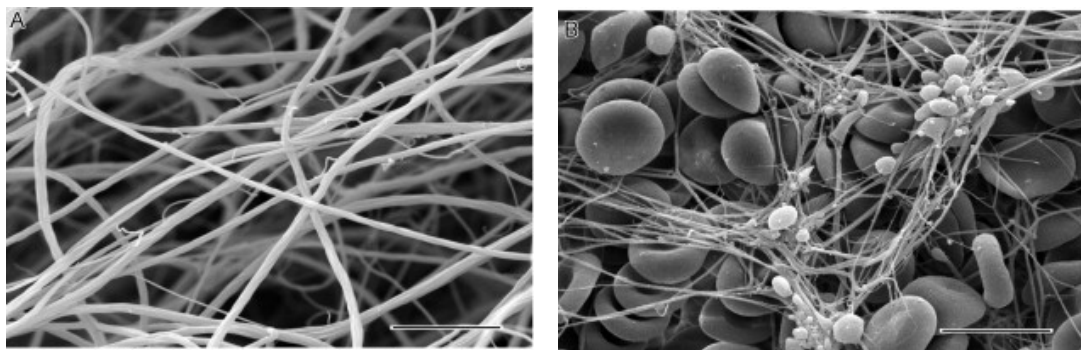


Figure 2.5: Fibrin and whole blood clot. Electron micrograph of (A) a reconstituted fibrin network and (B) a whole blood clot. The fibrin network is pulled on by aggregated platelets with red blood cells trapped in the network, plasma fills the open spaces. Images adopted from ¹¹. Bar = 5 μ m

In contracted clots red blood cells are trapped, and all the fluid (serum) has been squeezed out. A contracted clot is made in the lab by letting the blood clot form in a container to which the fibrin network does not attach. The platelets can contract the fibrin network so vigorously that the red blood cells trapped in the network deform to polyhedrals. (Figure 2.6) *In vivo* red blood cells get trapped in the fibrin network as well, mostly in the venous system ¹².

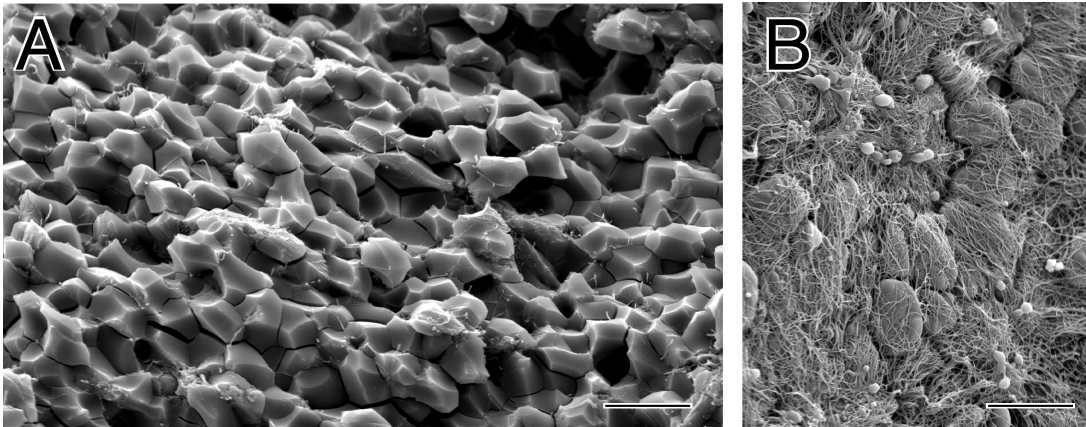


Figure 2.6: Contracted blood clot. Electron micrographs of interior (A) and exterior (B) of a contracted blood clot. In (A) the polyhedral shape of the tightly packed red blood cells can be seen. In (B) the fibrin network can be seen stretching over the red blood cells on the outside of the clot. Picture from ¹². Bar = 10 μm

Blood clots form a simple model system for soft tissues; in most soft tissues there is a modest extracellular matrix surrounding a densely packed cell formation. However, the soft tissue cells form many contacts with the ECM surrounding them. Blood clots allow studying the effect of volume conservation and cell traction separately. The volume conserving red blood cells are considered mostly non-adhesive. The platelets form contacts with the fibrin network and put tension on the network, but form a very small volume fraction of the total blood clot.

2.2 Measuring ECM and tissue mechanics

2.2.1 Understanding basic mechanical properties

When you poke something you can feel whether it is soft or hard. Measuring material mechanics is simply a more sophisticated way of poking and feeling. The three most common ways of testing mechanical properties of materials are by compressing, extending or shearing them, as depicted in Figure 2.7. The stress τ on a material is defined as the force F over the area A on which the force is applied:

$$\tau = F/A \quad (2.1)$$

With stress in Pa, force in N and area in m^2 . (Note sometimes the symbol σ is used to depict stress.)

The modulus (E in axial direction and G in shear) is a quantitative measure of material strength. It is calculated by observing the deformation γ (or strain) of a material when a known stress is applied, or by measuring stress when a known strain is applied.

$$E \text{ (or } G) = \tau/\gamma \quad (2.2)$$

With modulus in Pa. (Note sometimes the symbol ϵ is used to depict stress.)

For linear isotropic elastic solids the shear modulus and axial modulus are related by the Poisson's ratio ν of the material by:

$$E = 2 G (1 + \nu) \quad (2.3)$$

For Newtonian fluids the stress is directly related to the change in deformation $\dot{\gamma}$ (strain rate) and viscosity μ as follows:

$$\tau = \mu \dot{\gamma} \quad (2.4)$$

With dynamic viscosity in Pa*s and strain rate in s⁻¹.

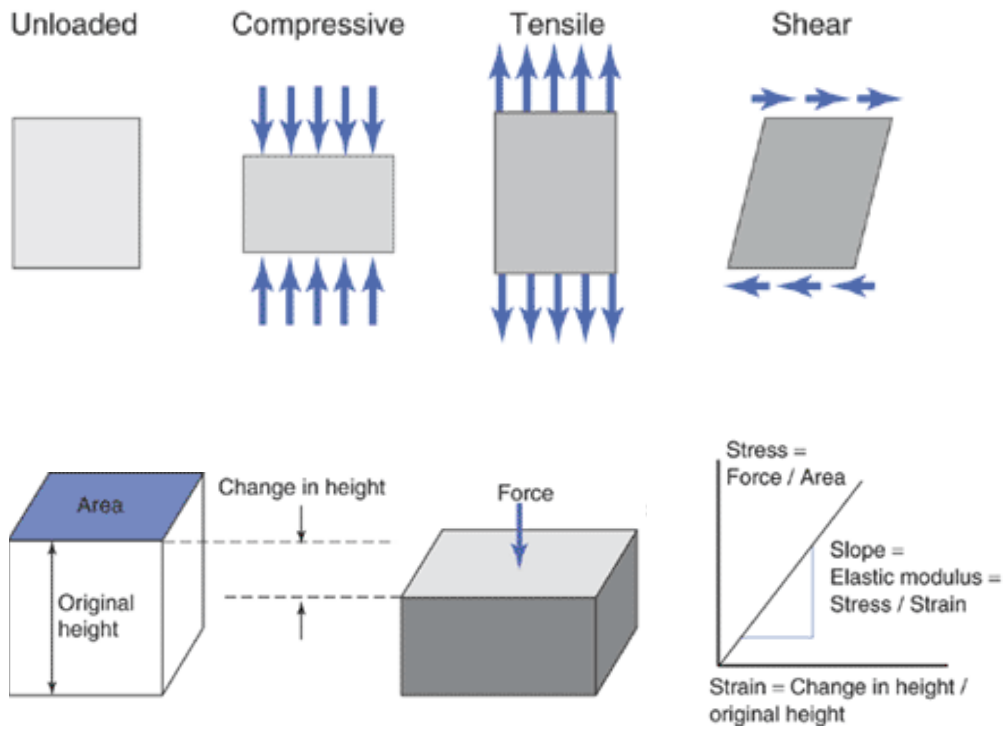


Figure 2.7: Depicting compressive, extensional and shear deformation and showing how stress and moduli are determined. Pictures adopted from 4.

2.2.2 Biological materials are viscoelastic materials

Most tissues and biopolymer networks, including extracellular matrices like collagen and fibrin networks, are viscoelastic. Their mechanical behavior lies in between an elastic

solid like rubber and a viscous fluid like honey ²⁷⁻³⁴. Viscoelastic materials show time dependent behavior like stress-relaxation. Figure 2.8 shows examples of the response of an elastic, viscous and viscoelastic material to a quick deformation (or strain) that is kept constant. An elastic solid like a rubber band will deform immediately and the resulting tension (stress) in the rubber band will be maintained, or 'stored', which is often modeled as a spring. As a result, the rubber band will snap back quickly and return fully to its original shape. On the other hand, when deforming a viscous fluid like honey, the tension dissipates immediately; hence the energy put into the movement is 'lost', often modeled as a dashpot. Viscoelastic materials show behavior between these two extremes, for a viscoelastic solid only a part of the energy will dissipate, for a viscoelastic fluid all energy will dissipate eventually ².

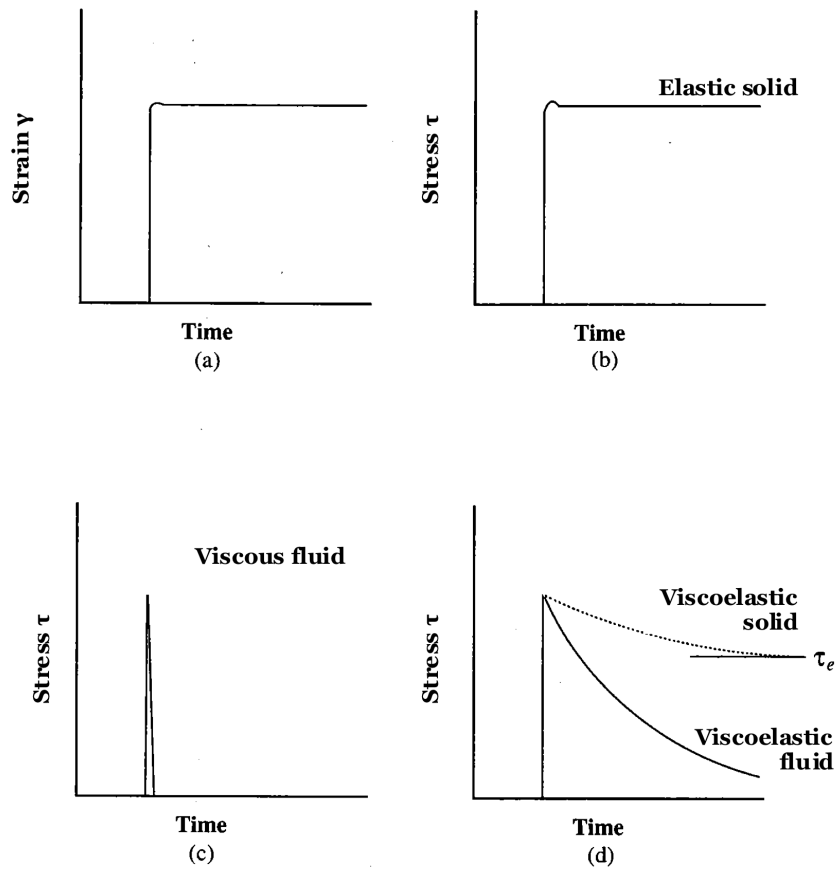


Figure 2.8: Typical stress after application of constant strain for an elastic solid, a viscous fluid, an viscoelastic solid and viscoelastic fluid. Graphs adopted from ².

2.2.3 Rheometers are devices to measure mechanical properties of materials

Rheometers, literally machines that measure how materials flow, come in all shapes and sizes. The rheometers used in the presented thesis research measure macroscopic material properties of a piece of tissue or network constrained between 2 parallel plates. One of the plates moves to apply a well-defined strain to the samples, while the stress response is monitored. The tensile tester applies a known compression or extension by moving the upper plate up or down. It continuously records the axial force the sample

exerts on a force transducer that is attached to the upper plate. Equations 2.1 and 2.2 are used to calculate the modulus of the materials.

The shear rheometer applies a shear strain by rotating the bottom plate. A force transducer is attached to the upper plate, which measures the torque that the sample exerts on the plate. The working equations of the shear rheometer are far more complicated than those of the axial rheometer.

When a shear strain is applied by rotating a parallel plate the strain field is not homogeneous. The shear strain varies with radius r , hence it is maximum on the edge and zero in the center. Furthermore, the strain at position $r = R$ depends on the angular displacement θ , and the distance between the plates or gap height h :

$$\gamma = \frac{\theta R}{h} \quad (2.5)$$

With angular displacement in radians, gap and radius in m.

Hence the shear rate at a position $r = R$ depends on the angular velocity as follows:

$$\dot{\gamma} = \frac{\Omega R}{h} \quad (2.6)$$

With angular velocity in rad/s.

The shear stress is calculated from the torque balance M on the upper plate:

$$\tau = \frac{M}{2\pi R^3} \left[3 + \frac{d \ln M}{d \ln \dot{\gamma}} \right] \quad (2.7)$$

With the torque balance in Nm.

Shear rheometers are often used in an oscillatory mode as this allows to continuously measure material properties over long time scales at small strains. In this particular set-up the shear strain oscillates sinusoidally with a given frequency ω :

$$\gamma = \gamma_0 \sin \omega t \quad (2.8)$$

With frequency in rad/s,

In the linear regime the stress will oscillate sinusoidally at the same frequency as the strain but in the case of viscous fluids and viscoelastic materials the stress response will be shifted by a phase angle δ .

$$\tau = \tau_0 \sin(\omega t + \delta) \quad (2.9)$$

With the phase angle in rad.

For elastic solids the stress-strain response is completely in phase, the phase angle is 0° . For viscous fluids the stress response is completely out of phase with the strain, the phase angle is 90° . Viscoelastic materials have a phase angle between 0° and 90° , which allows to decompose the stress response in an in-phase fraction τ' and out-of-phase fraction τ'' as follows:

$$\tau = \tau' + \tau'' = \tau'_0 \sin \omega t + \tau''_0 \cos \omega t \quad (2.10)$$

This in turn allows to express the modulus of the material in an elastic in-phase contribution, given by the storage modulus G' . The viscous out-of-phase contribution is given by the loss modulus G'' . The two can be combined in a complex modulus G^* as follows:

$$G^* = G' + iG'' \quad (2.11)$$

Equation 2.8 - 2.10 also allows one to deduct that the tangent of the phase angle δ is simply:

$$\tan \delta = \frac{G''}{G'} \quad (2.12)$$

The loss tangent is a useful way of expressing where on the spectrum of viscoelasticity a material falls.

2.3.4 Multiaxial measurements with a shear rheometer

As mentioned in the previous section, a shear rheometer is normally used to measure material properties in shear and a tensile tester is used for compression and extension testing. In the presented research, the shear rheometer is used to do both. The gap between the rheometer plates can be changed manually and thereby used to apply axial strain, while the rheometer is programmed to apply shear strain.

2.3 The extraordinary mechanical properties of the extracellular matrix.

2.3.1 Mechanical properties of reconstituted collagen and fibrin networks

(adapted from Van Oosten, Galie, Janmey, '*Mechanical properties of hydrogels*', from Gels Handbook, Fundamentals, Properties and Applications of hydrogels, World Scientific Publishing Company)

2.3.1.1 Collagen

In the presented research we will focus on the fibrillar collagen type 1, which is the predominant type of collagen *in vivo* and the most common collagen used to create collagen hydrogels *in vitro*. The situation *in vivo* is much more complex because of the addition of other collagen types^{35,36} and other ECM components such as hyaluronic acid³⁷, chondroitin sulfate³⁶ fibronectin and laminin³⁸, which alter the structure and mechanics of hydrogels based on collagen type 1.

The mechanical behavior of collagen gels in the linear regime has been tested extensively, both in shear and uniaxial deformation. Generally, the variability of mechanical measurements of collagen hydrogels is rather large due to differences in the collagen source, hydrogel preparation and testing conditions.³⁹⁻⁴¹ For example the fibril diameter and striation are modified by fluctuations in polymerization temperature, pH, and ionic strength⁴²⁻⁴⁴. The isolation method of collagen also affects the mechanical properties of the networks; when acid-extraction is used the collagen telo-peptides remain intact, whereas during pepsin digestion the telopeptides are cleaved, thereby eliminating important cross-linking sites³⁹⁻⁴¹.

The shear storage modulus of collagen hydrogels in the concentration range of 0.5 – 10 mg/ml falls between 2 and 150 Pa. The loss modulus is typically 10-20% of the elastic modulus. The shear moduli show little frequency dependence^{35,45}.

In contrast to the relatively low magnitudes of shear storage moduli, tensile testing of 0.3 – 3 mg/ml collagen at fast loading rates or short times after deformation, reveals an elastic modulus between 1.5 and 24.3 kPa^{46,47} and an equilibrium modulus between 0.5 and 5 kPa for gels ranging from 1 – 10 mg/ml⁴⁸⁻⁵⁰. The orders of magnitude differences between the tensile and shear moduli are striking, but a systematic direct comparison of identical samples in shear and uniaxial deformation has not yet been reported. In prolonged confined compression at large strains, collagen gels have been observed to have low moduli in the order of single Pascals; eventually collapsing when compression is continued^{41,51}.

The non-linear properties of collagen hydrogels in shear deformation are similar to those of many other networks of reconstituted biopolymers, showing strain-stiffening^{8,39,52} and negative normal stress¹⁰. The critical strain for the onset of non-linear behavior starts between 5-30% strain and shows dependence on concentration^{35,39,42,45}.

Upon recurring large strains collagen networks show a shift of the critical strain; the non-linear mechanical response starts occurring at higher strains⁵². However, strain-stiffening behavior is remarkably reversible unless rupture occurs, which is typically around 100% strain^{39,45}. (non-linear behavior is explained in more detail in 2.3.3)

2.3.1.2 Fibrin

Fibrin hydrogels, like collagen, are used extensively in both *in vivo* and *in vitro* applications⁵³. Because of this prevalence, their mechanical properties are well-characterized. Fibrin forms from thrombin-activated monomers that assemble into protofibrils of approximately 10 nm diameter⁵⁴. Depending on the pH and ionic strength of the solution, protofibrils aggregate laterally to create fibers of varying diameter and branching frequency, which affects the pore size of the mesh and consequently tunes the

mechanical properties of the hydrogels. These fibers can reach 100s of nm diameter, and span roughly the same size scale as collagen fibers. From a mechanical perspective, fibrin fibers are somewhat more flexible than collagen fibers of the same length and diameter. Like collagen gels, fibrin is strongly strain stiffening at strain magnitudes greater than 10% and can withstand strain as large as 100% ^{55,56}.

Fibrin, like most biomaterials, demonstrates a viscoelastic response to mechanical loading: its resistance to deformation depends on the rate at which it's deformed. In contrast to other protein hydrogels like collagen, the material behaves remarkably elastically at low strain rates when it is covalently reinforced by Factor XIIIa ⁵⁷. There is evidence that bending of the fibers causes this elastic behavior at low strain rates. Fibrin also exhibits the viscoelastic property of creep, meaning that the material undergoes plastic deformation to a constant load. Previous studies suggest that slippage between fibers is responsible for this property ⁵⁸.

2.3.2 ECM networks are remarkably strong

Networks formed by elastic polymers like rubber – also called elastomers- get stronger the higher the density of the polymers is. This relation between the strength and the mass density of the polymer is linear for elastomers; when the concentration doubles, the strength increases twofold as well. Most networks formed by extracellular biopolymers such as collagen and fibrin, but also intracellular biopolymers such as actin, are much stronger than an elastomer of the same mass density ^{32,59,60}.

For these biopolymer networks that are entangled the relation between the modulus and concentration is:

$$\text{Modulus} \sim \text{concentration}^{11/5} \quad (2.13)$$

For networks with permanent cross-links this relation is:

$$\text{Modulus} \sim \text{concentration}^{5/2} \quad (2.14)$$

This unexpected strength of the biopolymer networks is even more remarkable if one considers another important structural feature. The intersections or nodes in the biopolymer networks consist of maximum 2 fibrils or fibers. Maxwell's theorem states that for a stable conformation in a 3D network the intersections need to be formed by 3 intersecting fibers ⁶¹. This is known as the central-force rigidity threshold, and is illustrated in Figure 2.9. It has been theorized that biopolymer networks have a stable conformation in 3D because there is internal stress in the network ⁶²⁻⁶⁴.

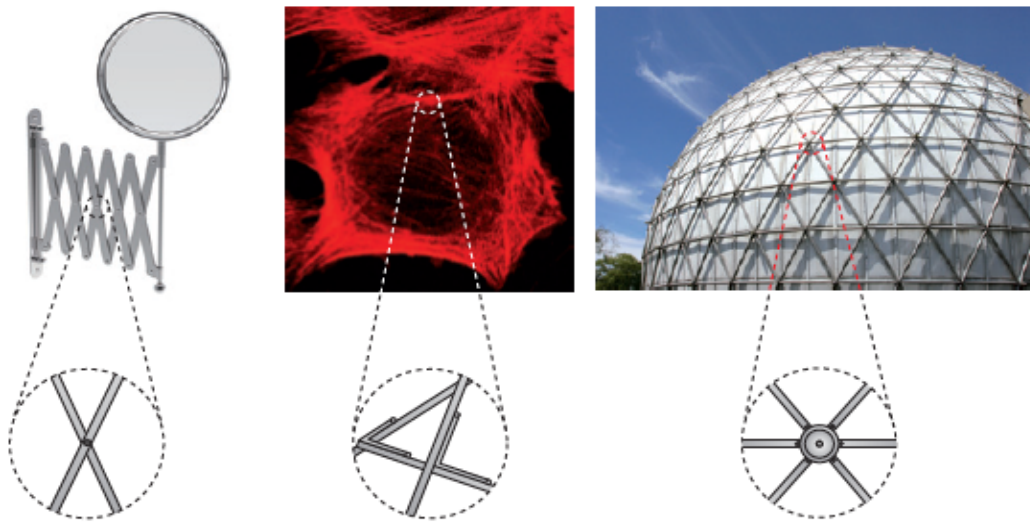


Figure 2.9: Explanation of central force rigidity threshold. The hinging structure of a bathroom mirror collapses upon the slightest touch. This structure consists of 2 beams intersecting. The cytoskeleton in the cell consists of networks with 2 intersecting fibers. A rigid dome of 3 intersecting beams can withstand large forces without deforming. Picture from 9.

2.3.3 ECM networks show typical non linear behavior when subjected to deformation

When rubber is stretched the deformation is linearly related to the force; a plot of the extension as a function of the force needed to accomplish that extension is a straight line (Figure 2.10). As a result the modulus is independent of the level of strain.

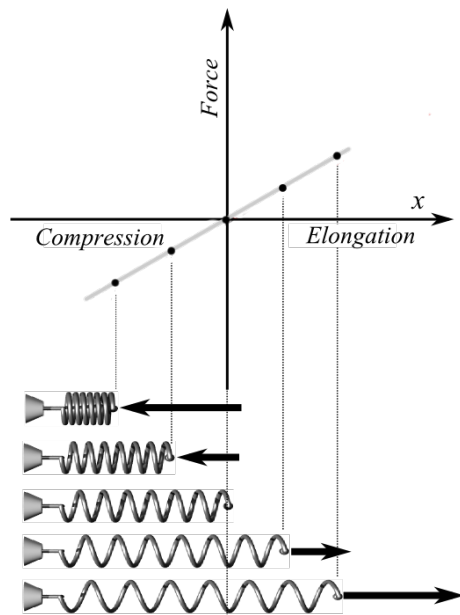


Figure 2.10: Linear deformation of a spring as an example of linear elasticity.

The change of the spring length and the force needed for that particular elongation (or compression) are plotted. This results in a straight line. The slope is constant hence the modulus is constant. Image adapted from ⁶.

Biopolymer networks will initially respond linearly to deformation. However, at some point the network starts to resist more deformation, and its stress will increase faster than the increasing strain, consequently leading to higher moduli ⁸. This phenomenon is called strain-hardening or strain-stiffening, and it is thought to be an important feature for proper functioning of tissues. A good example is skin; it needs to be flexible enough to move freely without discomfort. However, it can't stretch too far in order to maintain the structural integrity. Many biopolymer networks show this strain-stiffening behavior, as shown in Figure 2.11.

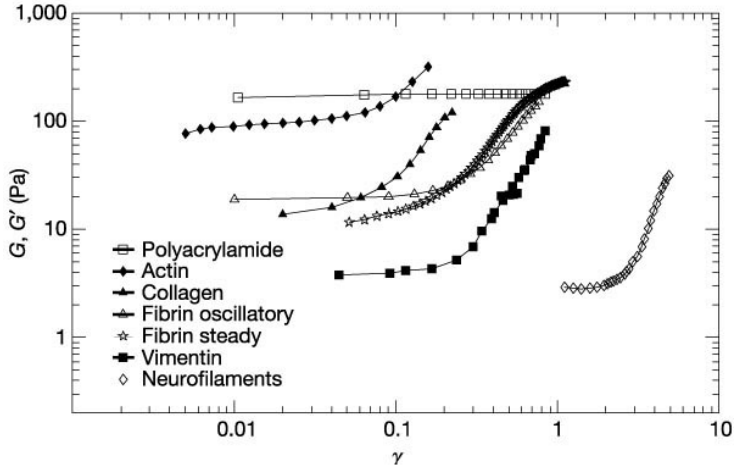


Figure 2.11: Strain-stiffening of biopolymers.
The modulus of many biopolymer networks increases with increasing shear strain ⁸.

Another non-linear feature of biopolymer networks is seen when deforming the networks in shear. An elastomer will expand when it is sheared; a biopolymer network tends to collapse when it is sheared ¹⁰. To perform shear experiments the sample is held between two plates that are kept at a constant distance, hence a sample will not be able to expand or collapse. Instead the machine measures the force that the sample exerts on the plates between which it is restrained. In this case the elastomer (polyacrylamide or PAA) will push against the plates, shown in Figure 2.12 (f) as a positive normal stress. The biopolymer network will pull on the plates, in Figure 2.12 (a-e) shown as a negative normal stress.

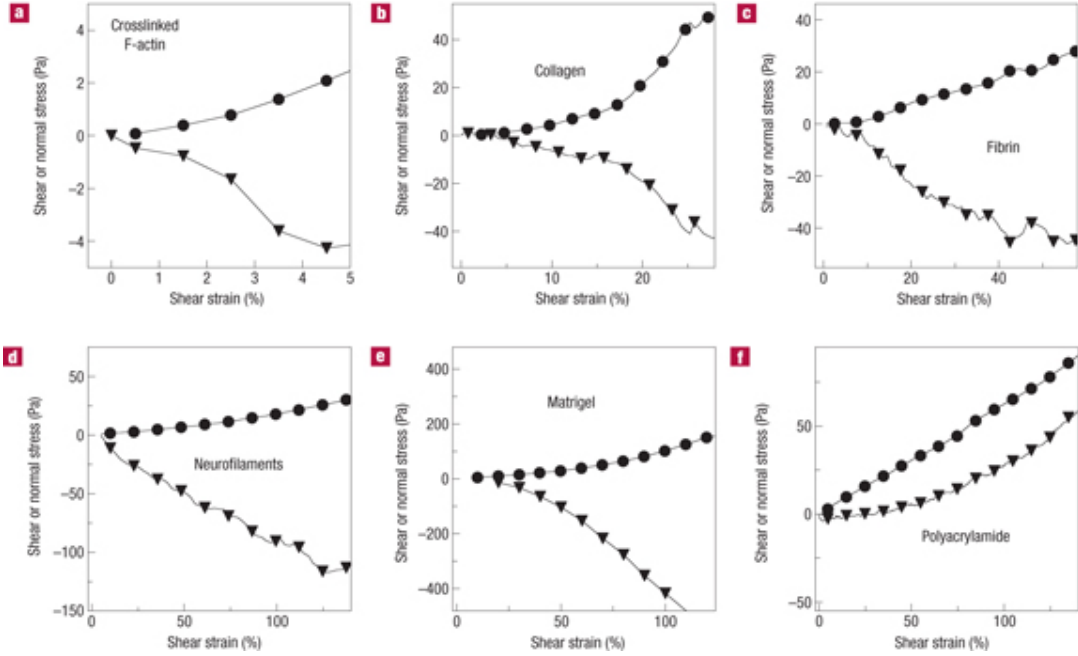


Figure 2.12: Biopolymers show negative normal stress, polyacrylamide does not. Shear (circles) and normal (triangles) stresses as a function of shear strain for various biopolymers compared to polyacrylamide. Graphs from ¹⁰.

2.4 Tissue mechanics in health and disease

2.4.1 Tissue mechanics in health

The mechanical properties of tissues vary widely. On the lowest end of the spectrum is a unique tissue mechanically speaking; blood is a viscous fluid ⁶⁵. Blood is closely followed by viscoelastic fluids like mucus ⁶⁶ and synovial fluid ⁶⁷. The softest viscoelastic solids include brain, fat and mammary glands, which measure in the range of 0.1-1 kPa. On the higher end of the range you find cartilage and tendon, which are in the MPa range and at considerable distance is bone, which is in the order of GPa. Overall, most tissues are viscoelastic materials in a range of 1 kPa through 20 kPa; and show a considerable amount of stress-relaxation. The behavior of whole tissues with increasing strains varies. Many connective tissues like lung ⁶⁸, arteries ⁶⁹, cornea ⁷⁰, skin ^{71,72}, ligaments ^{73,74}, and tendons ⁷⁵⁻⁷⁷ do show strain-stiffening, though the onset varies. The issue with interpreting mechanical measurements on whole tissues is that there is a large variability depending on testing methods, and particularly the directionality, as the organization of tissues is often highly anisotropic.

Tissues with an obvious mechanical function such as bone, skin, muscle, tendon, blood vessels, lung and cartilage have been the subjects of mechanical tests for decades ^{33,78-80}. Soft tissues have been tested to a much lesser extent and also suffered from a lack of appropriate measuring methods resulting in large variances ⁸¹. Some of these soft tissues were reported to strain-weaken when deformed in shear, for example brain ^{82,83}, liver ^{84,85} and fat ^{86,87}. The mechanics of soft tissues such as brain, liver, fat and kidney have gained more interest recently however, due to the role of mechanics in pathologies.

2.4.2 Tissue mechanics in disease

Changes in the mechanical properties of the extracellular matrix have been linked to many pathologies, such as cancer, atherosclerosis and fibrosis, which will be discussed in more detail below. Increased tissue stiffness is often linked to an increased deposition of collagen, specifically collagen type 1. Other factors include increased cross-linking of the already existent and newly deposited extracellular matrix⁸⁸⁻⁹³.

Many tumors have a significantly stiffer stroma than healthy tissue. This has always been intuitive to physicians who use palpation during physical exams to assess the presence of lumps in skin, thyroid, testes and breast tissue. Tumor stroma in breast malignancies can be up to 10x stiffer compared to healthy mammary tissue⁹⁴, and breast tumor stiffness is an indicator of metastasis potential⁹⁵. Other types of tumors that are stiffer compared to healthy tissue include colorectal cancer⁹⁶ and liver⁹⁷. Gliomas did not have higher moduli in shear but showed significantly higher compression stiffening. Hence with the increased pressure in brain tumors cells are likely to experience a higher stiffness in gliomas *in vivo*⁸³. Tumor progression *in vivo* has been linked to the collagen cross-linking enzyme lysyl oxidase⁹⁸. *In vitro* studies have shown that a malignant phenotype can be modulated by substrate stiffness⁹⁹.

Fibrosis occurs when tissue damage causes fibroblasts to transform to myofibroblasts. The myofibroblasts produce scar-like collagen tissue and contract the matrix. Unfortunately, the stiffening of tissue itself is a trigger for more myofibroblast transition. Due to this positive-feedback it is difficult to stop the fibrotic process. Vulvular fibroblasts cultured on a stiff substrates for 5 days were able to revert their phenotype on a physiological substrate¹⁰⁰. However, lung fibroblasts that experienced a pathologically stiff substrate for as little as 2 weeks permanently changed¹⁰¹. Fibrosis of the lung

parenchyma eventually destroys lung function completely. The mechanics of lung tissues is significantly changed even in mildly abnormal parenchyma ¹⁰². *In vitro*, substrate stiffness was shown to promote matrix deposition by alveolar cells ¹⁰³ and fibroblasts ¹⁰⁴.

Liver fibrosis is seen as a result of excessive drinking or hepatitis infections. It has been shown that in the case of liver, the increase in matrix stiffness precedes the deposition of collagen, shown by histological staining ¹⁰⁵. *In vitro* a stiff substrate was necessary for hepatic stellate cells to differentiate into myofibroblasts ^{106,107}. Proliferation of hepatocytes was shown to be altered by collagen gel structure ¹⁰⁸. Metabolic rates and albumin secretion were shown to depend on substrate compliance as well ¹⁰⁹.

Stiffening of the arteries always happens gradually in aging, when the ratio of elastin to collagen in vessel walls decreases ¹¹⁰. This process is often enhanced in pathological situations. It is known that increased arterial stiffening is correlated with higher incidences of numerous cardiovascular diseases ^{111,112}. *In vitro* it was shown that endothelial cell layers become more permeable on substrates of supra-physiological stiffness ^{113,114} and endothelial cells are more sensitive to inflammatory agents with increasing substrate stiffness ¹¹⁵.

Overall the importance of the mechanical homeostasis in tissues has been established in many systems.

CHAPTER 3: THE EFFECT OF AXIAL STRAIN ON THE SHEAR RHEOLOGY OF EXTRACELLULAR MATRIX NETWORKS

(Adapted from: *Uncoupling shear and uniaxial elastic moduli of semiflexible biopolymer networks: compression-softening and stretch-stiffening*, Anne S. G. van Oosten, Mahsa Vahabi, Albert Licup, Abhinav Sharma, Fred C. MacKintosh, Paul A. Janmey, Scientific Reports, 2015)

3.1 Abstract

Gels formed by semiflexible filaments such as most biopolymers show strong non-linear behavior in shear deformation with a pronounced negative normal stress that also affects the relation between shear and Young's moduli. Here we report measurements and simulations of axial and shear stresses exerted by a range of hydrogels subjected to simultaneous deformation in both compression or extension and shear. These studies show that in contrast to volume-conserving linear elastic hydrogels such as polyacrylamide, the Young's moduli of cross-linked networks formed by the stiffer biopolymers collagen and fibrin are not proportional to their shear moduli and both moduli are strongly affected by even modest degrees of uniaxial strain.

3.2 Introduction

Networks formed by filamentous biopolymers - intracellular proteins like actin and vimentin; as well as extracellular proteins like collagen and fibrin - show distinct nonlinear viscoelastic mechanical responses when deformed in shear. The shear storage modulus, G' , of such networks is higher than for flexible polymer networks with the same mass density⁶⁰, and this increases with concentration as $G' \propto c^x$, where $x \cong 2.2 - 2.5$ for both intracellular and extracellular networks^{32,59,116-120}. The large elastic moduli and their

strong dependence on polymer density occur even though biopolymer networks fall below the isostatic threshold of 6-fold connectivity for minimal mechanical stability of networks in 3D with only central-force (i.e., stretching) interactions ⁶¹: the nodes of such networks consist of either 2 intersecting fibrils linked together or of branching points. Thus, the elasticity of biopolymer networks must be due to additional factors, such as the bending rigidity of fibrils or internal stresses such as those applied by motor proteins ^{62-64,121}.

Semiflexible polymer networks also show dramatic nonlinear elastic effects, including strain stiffening at relatively low shear strains, depending on network density and polymer stiffness ⁸. Strain-stiffening can be understood either by the non-linear force extension relation of semiflexible polymers due to thermal undulations at the filament level or by collective rearrangements and alignment of filaments at the network level ¹²². When sheared, these networks also exhibit large negative axial (or normal) stress, in contrast flexible elastomers that exhibit a much smaller positive (compressive) normal stress. Therefore, biopolymer networks would tend to collapse upon shear whereas linear elastic polymer networks would expand ¹⁰.

Nearly all measurements of the non-linear rheology of semiflexible polymer networks have been made in shear deformation, with the assumption that the Young's modulus is 2 to 3 times larger, depending on the Poisson's ratio of the materials. Direct measurements of Young's moduli have been made on collagen and fibrin gels, but not directly related to rheology under shear strain.

Interest in biopolymer mechanics has increased since it has been shown that mechanical properties of cell substrates or extracellular matrix (ECM), influence cell functions ²³.

Changes of the ECM have been linked to, or even precede common pathologies such as cancer ⁹⁹, atherosclerosis ¹¹¹ and fibrosis ¹⁰⁵.

Tissue engineering requires detailed knowledge of the mechanics of materials used as scaffolds to replace tissues. For this purpose, reconstituted networks and tissues have been characterized with either shear or uniaxial testing methods. However, most tissues are subjected to multiaxial mechanical stimuli at a variety of time scales.

In the present work we adapt common rheological techniques to provide a mechanical characterization of collagen and fibrin networks undergoing multiaxial deformations that mimic strains that can occur *in vivo*. We show that shear moduli decrease to an equilibrium value when networks are compressed but show a constant increase when samples are extended. Young's moduli are significantly lower in compression compared to extension. When comparing apparent Young's and shear moduli over a range of axial strains, the networks' apparent Young's moduli are not linearly related to their shear moduli.

3.3 Methods

3.3.1 Preparation of fibrin

Plasminogen depleted fibrinogen (Fbg) isolated from human plasma and (CalBioChem, EMD Millipore, Billerica, MA, USA) was dissolved in 1X T7 buffer (50mM Tris, 150 mM NaCl at pH 7.4), the fibrinogen solution was allowed to dissolve at room temperature without disturbing the solution. Thrombin (Thr) isolated from salmon plasma (SeaRun Holdings, Freeport, ME, USA) was diluted in ddH₂O at 1000U/ml. Solutions were aliquoted and snap frozen for future use. Salmon thrombin clotting properties for human fibrinogen were checked previously ^{123,124} and found to be near identical to human

thrombin at the Fbg and Thr concentrations used in this study. Factor XIII cross-linking was checked with an SDS PAGE gel and no difference was found between human and salmon thrombin.

To prepare fibrin networks, solutions were warmed to room temperature; fibrinogen stock solution, 1X T7 buffer, CaCl₂ stock and thrombin were added at appropriate ratios to yield a 2 or 10 mg/ml fibrinogen, 15mM Ca²⁺ /mg Fbg and 1 or 0.5 U thrombin / mg Fbg. The 2 mg/ml samples were polymerized at 37°C, 10 mg/ml samples at 25°C.

3.3.2 Preparation of collagen type 1

Collagen type 1 isolated from calf skin (MP Biomedicals, Santa Ana, CA) was dissolved in 0.02N acetic acid. To prepare collagen networks 10X PBS, 0.1M NaOH and ddH₂O were added in appropriate ratios to yield a 2.5 mg/ml collagen concentration in 1X PBS solution with a pH between 7-7.5. The samples were polymerized at 37°C.

3.3.3 Preparation of composite networks with collagen and hyaluronic acid

To prepare composite networks of collagen and hyaluronic acid collagen networks were prepared similarly as described in 3.3.2. Water was replaced by a 8 mg/ml hyaluronic acid solution (hyaluronic acid sodium salt from Streptococcus equi, Sigma, St. Louis, MO) to result in a final HA concentration of 4 mg/ml. Samples were mixed thoroughly and centrifuged for 5-10 seconds at 2000 xG shortly to remove bubbles prior to pipetting the samples between the rheometer plates.

3.3.4 Preparation of cross-linked hyaluronic acid gels

Thiol-modified hyaluronic acid (HA; HyStem, Biotime, Alameda, CA) and poly(ethyleneglycol) diacrylate (PEGDA M_w=3400 Da, Extralink, Biotime) were used to prepare HA gels. HyStem was dissolved in degassed water for 30 minutes at 37°C.

Fibronectin was added to HyStem so that the final concentration was 0.1 mg/mL of protein in the gel. The HyStem solution was crosslinked with Extralink using a 1:4 v:v Extralink to HyStem ratio, resulting in 0.8% w/w HA in the gel. The HA was allowed to polymerize for 1.5 hour before starting measurements.

3.3.5 Preparation of soft polyacrylamide gels

40% acrylamide and 2% bis-acrylamide solutions (Biorad, Hercules, CA) were mixed with ddH₂O to yield a 7.5% acrylamide and 0.01% bis-acrylamide solution.

Polymerization was initiated by adding ammonium persulphate (APS) and tetramethylethylenediamine (TEMED). Gels were polymerized at room temperature in a well, allowed to swell in ddH₂O, and cut into shape with a circular punch prior to measurements.

3.3.6 Rheometry

A strain-controlled rotational rheometer (RFS3, TA Instruments, New Castle, DE) was used with a parallel plate with a diameter of 8 mm for 10 mg/ml fibrin and a 25 mm diameter for 2.5 mg/ml collagen and hyaluronic acid gels, all with a gap of 1 mm. A 50 mm with a 0.4 mm gap was used for 2 mg/ml fibrin samples. The bottom plate incorporated a Peltier plate allowing to control the sample temperature, 25°C for 10 mg/ml fibrin, PAA and HA and 37°C for collagen and 2 mg/ml fibrin samples. The biopolymer samples were pipetted between the plates prior to polymerization. After polymerization appropriate buffer was pipetted around the free edge of the sample, to prevent drying and allow free fluid flow in and out of the sample.

The shear moduli of the samples were measured by applying a low oscillatory shear strain of 2% at a frequency of 10 rad/sec. Axial strain was applied by changing the gap between the plates. Some samples were subjected to a fixed step compression or

extension after which a shear strain sweep was performed. Strain sweeps were performed in absence of axial strain, after applying 20% compression, and 12.5% extension (for fibrin) or 2.5% extension (for collagen). The shear strain was increased from 2% up to the point of breakage (depending on type of sample and level of axial strain) at a frequency of 1 rad/sec. The lower frequency was necessary to observe the response of the axial stress to the shear stress.

Other samples were subjected to either an incremental compression or extension series. The step-size was optimized for axial strain in each direction, separately for collagen, hyaluronic acid and fibrin, to yield optimal resolution and prevent the sample from tearing (in extension). During the axial strain series the samples were allowed to relax before continuing to the next level of axial strain. For a precise application of axial strain the plate was moved at a low speed of 2 $\mu\text{m/s}$. The axial stress was collected simultaneously from the analog signal of the rheometer and using a ProLink instrument amplifier and Logger Pro software (Vernier Software and Technology, Beaverton, OR).

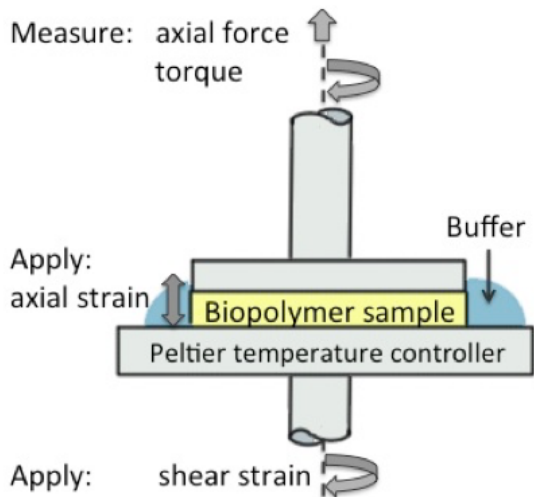


Figure 3.1: Experimental set-up for multi-axial rheology method. A shear rheometer is used with a parallel plate geometry. Biopolymer samples are polymerized between the plates; after polymerization buffer is added around the sample to prevent drying and allow free fluid flow to in and out of the sample. The gap between the plates is changed to apply axial strain; the lower plate is rotated to apply shear strain. The torque and axial force are recorded.

3.3.7 Tensile testing

To obtain additional data on the mechanical properties of networks under axial deformation, a tensile tester was used (5564, Instron, Norwood, MA) with parallel platens at a gap of 1 mm, using similar volumes of fluid as used for rheometry. To obtain data on fully relaxed networks; samples were subjected to 10 μm steps of compression or extension at 2 $\mu\text{m/s}$, which were allowed to relax for 15 minutes between consecutive steps. Tensile testing was done on 10 mg/ml fibrin networks and collagen networks with and without HA.

All results show the mean of 3 samples \pm standard deviation.

3.4 Results

3.4.1 Verification of experimental method with polyacrylamide gels

The strain-stiffening and negative normal stress of semiflexible polymer gels suggests that shear moduli might be altered by internal stresses generated by applying axial strain orthogonal to the shear plane. Figure 3.1 shows the experimental system, which allows uniaxial compression or extension to be applied to disk-shaped samples while their shear modulus is measured by oscillatory shear displacements. A strain-controlled rheometer with a parallel-plate geometry was used to apply axial strain by changing the height of the gap after the network was fully formed. A reservoir of solvent surrounds the gels in order to allow volume change by fluid flow across the free edges of the sample. As a control, linearly elastic soft polyacrylamide gels were tested.

Figure 3.2a shows the storage moduli are independent of the level of axial extension. The axial stress of PAA is linear with axial strain; independent of the direction. (Figure 3.2b) The Young's modulus of PAA is 2.8 times G' over the entire range of deformations, in

close agreement with its linear elasticity and the reported Poisson's ratio of 0.486¹²⁵. The axial stress observed with the shear rheometer confirmed the trend of the axial stress observed with the tensile tester.

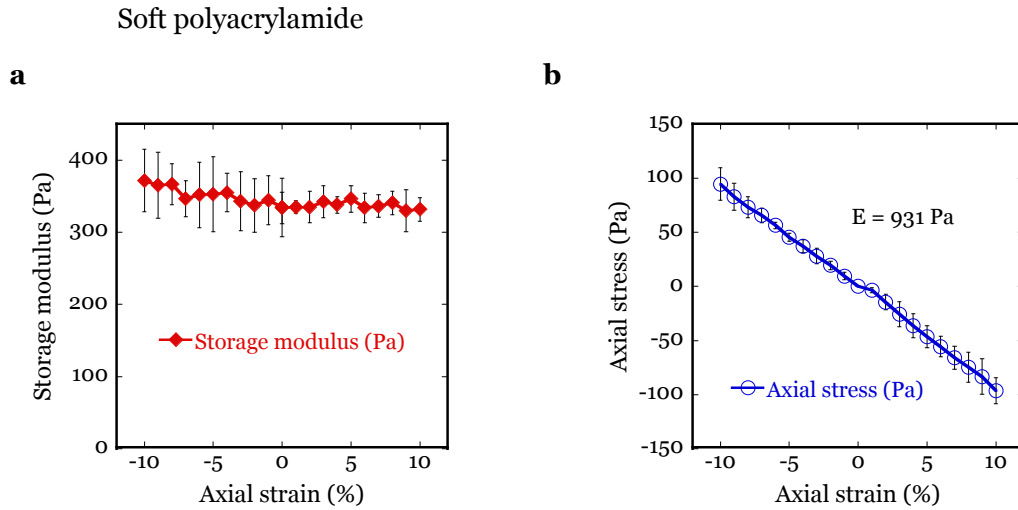


Figure 3.2: Testing of multiaxial rheology method with linear elastic polyacrylamide gels. Showing the storage modulus (**a**), and axial stress (**b**). The data from (**a**) are obtained with the rheometer; the data in (**b**) are obtained separately with a tensile tester. The reported Young's modulus in (**b**) is the slope of the axial stress-strain.

3.4.2 Shear strain-stiffening onset and amplitude of semiflexible biopolymer networks is altered when networks are axially strained

Networks of collagen at 2.5 mg/ml and fibrin at 2 and 10 mg/ml were subjected to increasing shear strain amplitudes after static uniaxial compression or extension. An oscillatory shear strain of constant frequency (1 rad/s) and increasing magnitude was applied to measure the shear moduli of the networks. The behaviour of the shear storage moduli is compared to strain-stiffening in the absence of axial strain (Figure 3.3).

Collagen and fibrin networks strain-harden, both when extended and compressed, although the initial storage modulus -at low shear strains- is altered dramatically by application of axial strain. It is lower in compression and larger in extension compared to uncompressed samples. For fibrin networks the degree of strain-stiffening is higher in compression and lower in extension. However, the onset, critical strain (reversal of strain-stiffening to weakening) and absolute peak value are similar for the three levels of axial strain. The storage moduli converge at higher levels of shear strains. (Figure 3.3a and c)

For collagen the onset of strain-stiffening occurs at larger shear strains in compression, but the critical strain at which strain-weakening occurs is similar. In extension, collagen networks show a similar onset of strain-stiffening, but the critical strain is lower compared to the samples without axial strain. (Figure 3.3b)

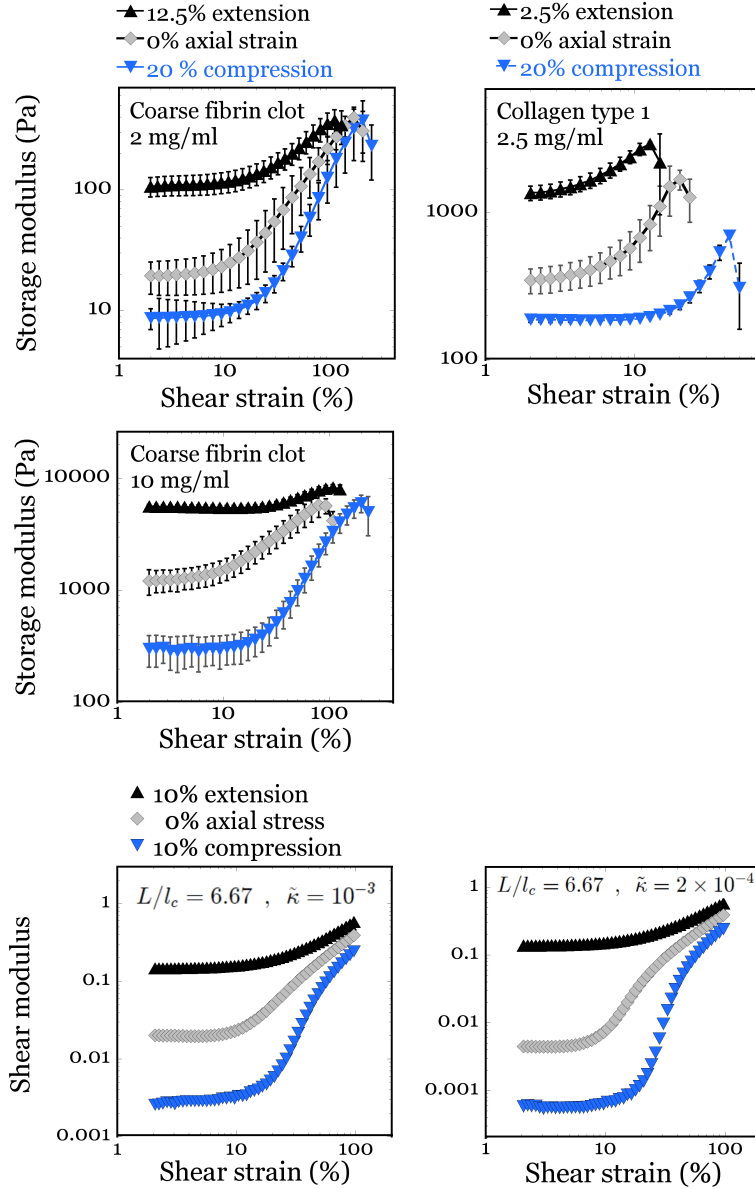


Figure 3.3: Semiflexible biopolymer networks strain-stiffen when axially strained, but onset and amplitude is altered. Strain amplitude dependence of fibrin clots of (a) 2 mg/ml and (c) 10 mg/ml when 12.5% extended, 20% compressed and at 0% axial strain; and (b) collagen gels of 2.5 mg/ml at 2.5% extension, 20% compression and 0% axial strain. (d), (e). Storage modulus versus shear strain for a diluted phantomized triangular network with $L/l_c = 6.67$; with varying pre-stress: without any axial strain, with 10% extension and with 10% compression. The normalised bending modulus $\tilde{\kappa} = 10^{-3}$ (d) corresponds with fibrin; $\tilde{\kappa} = 2 \times 10^{-4}$ with collagen (e).

The negative (downward) axial stress observed when samples are sheared is also observed in extended samples; however, in compressed samples there is a positive axial stress with increasing shear strains (data not shown).

To model networks of fibrin and collagen, disordered, lattice-based networks were generated that are constructed such that the average coordination number (connectivity) is 3.4, consistent with direct observations of collagen networks ¹²⁶. This connectivity is well below the point of marginal stability for purely spring/stretching interactions ⁶¹ suggesting that the stability (finite shear modulus) of such networks arises from additional stabilizing interactions, such as bending and applied stress. We model the total elastic energy \mathcal{H} of the network by combining bending and stretching contributions of all the fibers f :

$$\mathcal{H} = \sum_f \left[\int \frac{\kappa}{2} \left| \frac{d\hat{t}}{ds_f} \right|^2 ds_f + \int \frac{\mu}{2} \left(\frac{dl}{ds_f} \right)^2 ds_f \right]. \quad (3.1)$$

Here, κ is the bending rigidity of the individual filaments and μ is their stretch modulus where the first term above represents bending and second term represents stretching energies ¹²⁷.

In order to model networks with local connectivity <4 , 3D networks are generated by dilution of a *phantomized* FCC structure, in which the six fibers crossing at a node are separated randomly into three cross-linked pairs ¹²⁸, using freely-hinged joints. To reduce any edge effects, periodic boundaries are used for networks under deformation.

The dimensionless bending rigidity $\tilde{\kappa} = \kappa/(\mu\ell^2)$, where ℓ is the lattice spacing. ℓ^2 , is varied, keeping $\mu=1$ fixed. For collagen and fibrin fibers the dimensionless bending

rigidity $\tilde{\kappa} = 2 \times 10^{-4}$, and $\tilde{\kappa} = 10^{-3}$ have been chosen respectively.

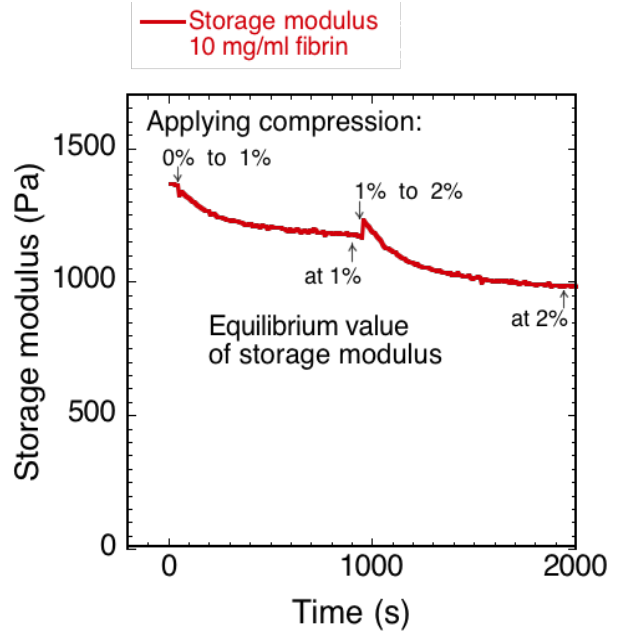
The shear modulus G is obtained from the ratio of the shear stress σ_s to shear strain γ , where the stress is calculated from the strain derivative of the minimized total elastic energy density H/V per unit volume V . Normal stresses are calculated from the energy changes due to an infinitesimal axial deformation $\delta\varepsilon$ using fixed lateral boundaries.

To compare with the experimental results seen in Figure 3.3**a,b** and **c**, the generated networks are imposed to a fixed compression or extension in addition to an increasing simple shear strain and compared to one in the absence of the axial strain. Figure 3**d** and **e** show the results for 3D network simulations with parameters quantifying the filament rigidity and network mesh size that are realistic for the experiments. Similar to the experimental results, applying axial stress changes the storage modulus.

3.4.3 Storage moduli of semiflexible biopolymer networks drop in compression and increase in extension

To test the effects of axial compression or extension on the shear storage moduli of fibrin and collagen networks in more detail, the networks were subjected to an incremental series of compressions or extensions while measuring the dynamic shear moduli at 2% shear strain and 10 rad/s. The networks were allowed to relax between 100 and 900 seconds (depending on the step size and sample) before applying the next step of axial deformation. An example of a 10 mg/ml fibrin network is shown in Figure 3.4. The storage modulus is shown monitored in time, while being compressed from 0% to 1% at 100 sec and from 1% to 2% at 1000 sec. The relaxed or steady-state values shown in Figure 3.5, 3.6, and 3.7 are taken right before application of the next step of axial strain.

Figure 3.4: Example of storage modulus of fibrin network followed in time during the initial steps of a typical compression sequence. The storage modulus of a 10 mg/ml fibrin network is shown as a function of time during compression from 0% to 1% and from 1% to 2%. The relaxed value of the storage modulus is taken right before the next level of compression is applied, as pointed out by the arrows. The same approach is used for the storage modulus in extension and the axial stress.



The relaxed values of the storage moduli were plotted for every level of axial strain. The storage moduli in absence of axial strain were $18.6 \text{ Pa} \pm 1.9 \text{ Pa}$, $1138 \text{ Pa} \pm 160 \text{ Pa}$ and $458 \text{ Pa} \pm 23 \text{ Pa}$ for 2 mg/ml and 10 mg/ml fibrin and collagen respectively. The storage moduli of both collagen and fibrin increase steadily when extended (positive axial strain), and collagen networks stiffen faster than fibrin. In compression (negative axial strain) the storage modulus shows a decrease, which levels out between 5-10% compression. At compression levels higher than 10% the storage modulus reaches an equilibrium value. (Figure 3.5 a, 3.6 a and 3.7 a) When the samples are returned to 0% axial strain from extension, the shear moduli return to their original value. When decompressed collagen samples return to the same value; however, fibrin samples return to a value that is slightly higher than their original value (data not shown).

The loss tangent (ratio of the loss and storage modulus, G''/G') of 2 mg/ml fibrin is 0.037 ± 0.005 and for 10 mg/ml fibrin 0.022 ± 0.006 in absence of axial deformation. Both

increase steadily under compression; when extended there initially is a slight decrease after which the loss tangent stays constant. (Figure 3.6 **c**, and 3.7 **c**) The trend of the loss tangent is different for collagen; from 0.064 ± 0.04 in absence of axial strain it reaches a slightly higher equilibrium value under compression but shows a constant decrease in extension. (Figure 3.5 **c**) These results indicate that filaments buckle under compression and filaments stretch when the networks are extended.

3.4.4 Axial stress-strain curves have different slopes in compression and extension

A tensile tester was used to measure the axial stress at similar relaxation times and levels of compression and extension (open circles) as were used with the shear rheometer, from which axial forces can also be measured, but with less accuracy (solid circles). A positive axial stress is recorded when the sample pushes against the plate (when compressed) and a negative stress is recorded when the sample pulls on the plates (in extension). The slope of the stress-strain curve is the Young's modulus (E). The axial stress is set to be 0 Pa before the measurement is started, by arbitrarily setting it to 0 in the software. However, often a small negative axial stress, in the order of single Pa, develops during polymerization.

Both collagen and 10 mg/ml fibrin networks show a similar trend. In extension the axial stress increases linearly with the axial strain over the entire range. In compression there is a toe region up to 4% compression after which stress changes linearly with axial deformation (Figure 3.5 **c** and 3.6 **c**). In compression the Young's modulus is calculated from the linear region between 4% and 10%. The Young's modulus is much higher in extension compared to compression. For collagen the Young's modulus in compression is 29.1 Pa and 6.52 kPa in extension. For 10 mg/ml fibrin the Young's modulus in compression is 128 Pa, and 10.7 kPa in extension. The axial stresses in 2 mg/ml fibrin

networks were only recorded with the rheometer and are very noisy, hence no moduli are calculated from these data.

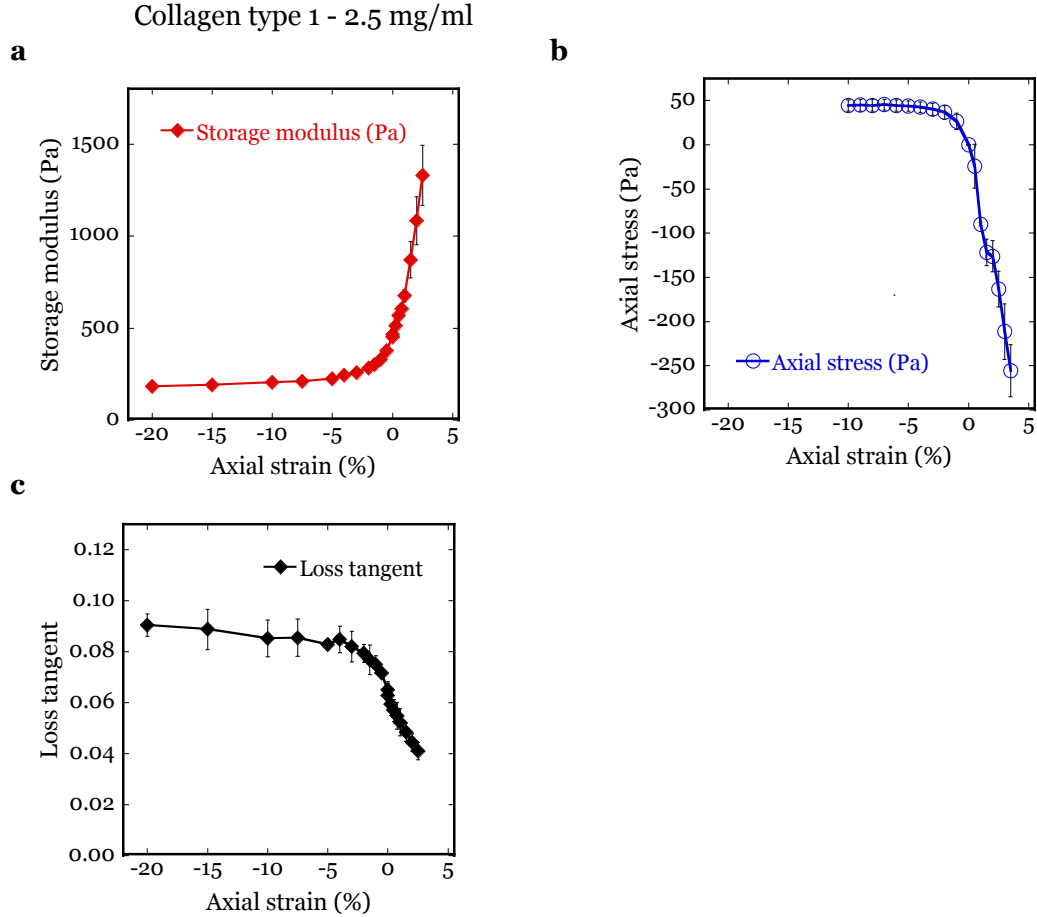


Figure 3.5: Collagen type 1 networks soften in compression and stiffen in extension. Rheology of a 2.5 mg/ml collagen gel at low shear strains (2%) at increasing levels of axial strain, showing the storage modulus (**a**), axial stress (**b**) and loss tangent (**c**). The data from (**a**) and (**c**) are obtained simultaneously with the shear rheometer; the data in (**b**) were obtained separately with the tensile tester.

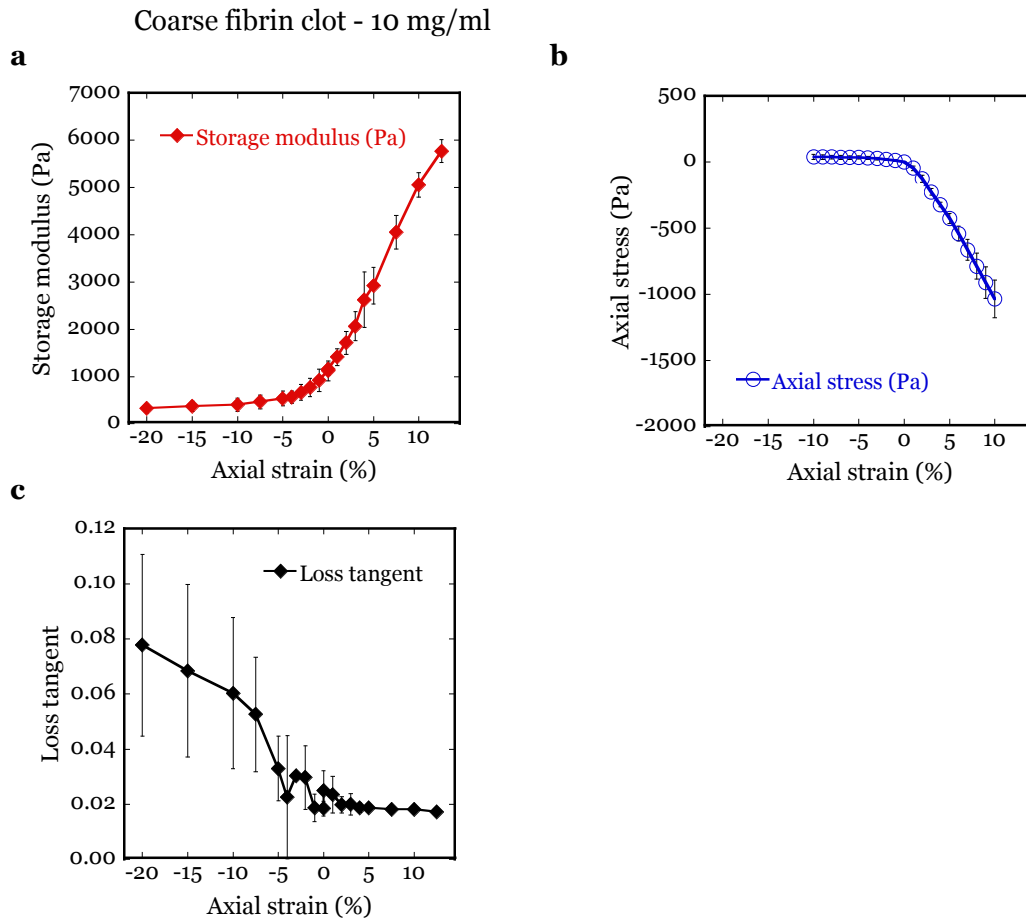


Figure 3.6: Coarse fibrin clots of 10 mg/ml soften in compression and stiffen in extension. Rheology of a coarse fibrin clot with factor XIIIa cross-linking with a concentration of 10 mg/ml measured at low shear strains (2%) at increasing levels of axial strain, showing the storage modulus (**a**), axial stress (**b**) and loss tangent (**c**). The data from (**a**) and (**c**) are obtained simultaneously with the shear rheometer; the data in (**b**) were obtained separately with the tensile tester. For tensile measurements the sample diameter was between 22.5mm and 25mm, with a 1mm gap.

Coarse fibrin clot - 2 mg/ml

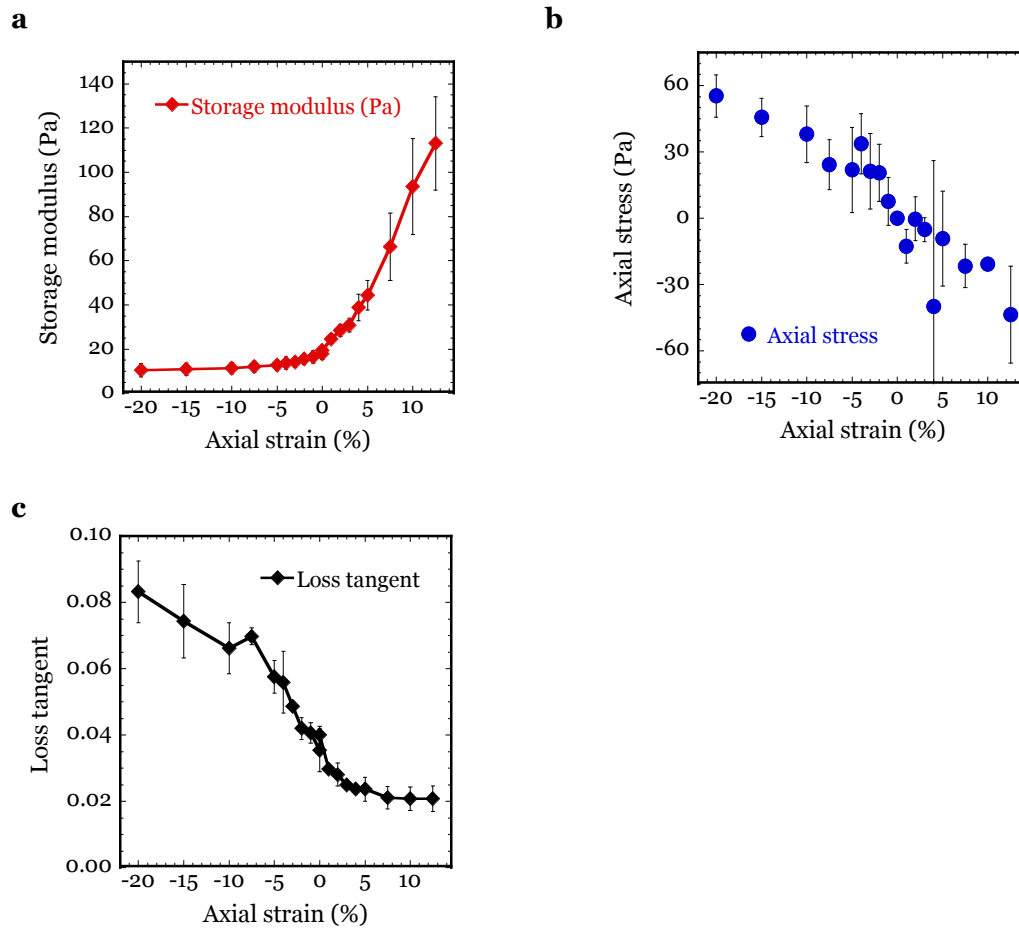


Figure 3.7: Coarse fibrin clots of 2 mg/ml soften in compression and stiffen in extension. Rheology of a coarse fibrin clot with factor XIIIa cross-linking with a concentration of 2 mg/ml measured at low shear strains (2%) at increasing levels of axial strain, showing the storage modulus (**a**), axial stress (**b**), and loss tangent (**c**)

3.4.5 Uncoupling of the axial and shear moduli of semiflexible biopolymer networks

In contrast to the results with polyacrylamide gels, the relationship between the storage and Young's moduli of fibrin and collagen varies with the axial strain. In extension the Young's modulus stays constant within the tested range, whereas the storage modulus continues to increase. When compressed both the storage and Young's moduli approach a new limiting value at large strains. However, between 4% and 10% compression the storage modulus of collagen is an order of magnitude larger than the Young's modulus. This result means that the resistance of the network to compression is failing while it is still able to resist a shear deformation.

To compare with the experimental results seen in Figure 3.5, 3.6 and 3.7, the simulated networks were subjected to increments of compression or extension, while measuring the linear shear modulus (at shear strains of 1%). At each step, the network is allowed to relax; the energy is minimized before applying the next axial strain. The results in Figure 3.8 agree well with the measured dependence of G' on axial strain. The model can account for the features observed in the experiments, including the qualitative differences between collagen and fibrin, e.g., the sharper onset of stiffening with axial strain.

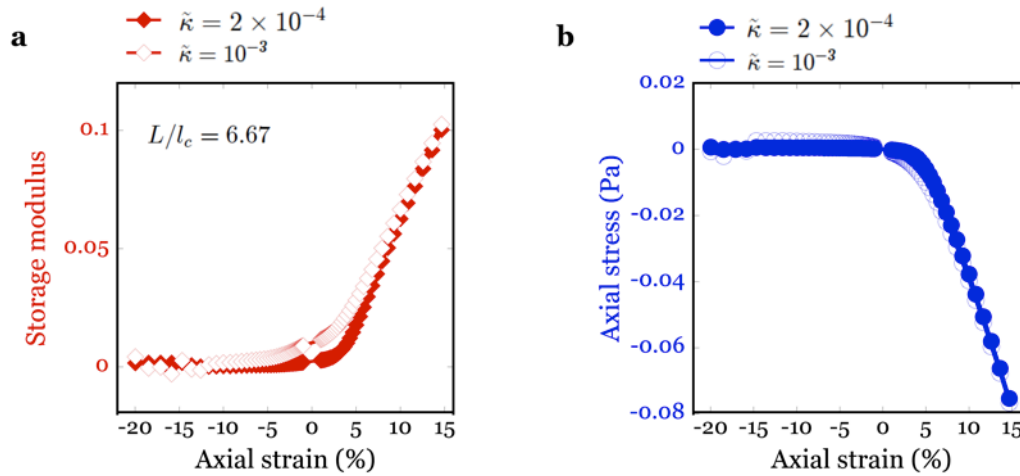


Figure 3.8: Simulations of storage moduli and axial stresses predict multiaxial behavior of semiflexible biopolymers. Simulation for a diluted phantomized triangular network (3D) with $L/l_c = 6.67$. (a) Shows the storage modulus, (b) shows the axial stresses. The normalised bending modulus $\tilde{\kappa} = 10^{-3}$ corresponds with fibrin, $\tilde{\kappa} = 2 \times 10^{-4}$ with collagen.

3.4.6 Composite gels of collagen and hyaluronic acid behave similar as collagen

The ECM *in vivo* contains other types of biopolymers aside from fibrillar collagen. Hyaluronic acid is a common component in the extracellular matrix; it is especially abundant in cartilaginous tissues, the eye and upregulated in wound-healing and developing tissues¹²⁹. HA has very different physical properties than collagen; it is a flexible, and highly anionic linear polymer build from disaccharide repeats. Due to this structure HA molecules have a high water retaining ability.

Composite networks are highly relevant from a physiological point of view. Testing HA-collagen composites has the additional objective to elucidate whether the particular multiaxial behavior of semiflexible networks can be modified by replacing the solvent of near-water viscosity by a viscoelastic fluid. The final concentration of HA in the composite networks is 4 mg/ml which by itself has a G' and G'' of 9 Pa and a loss tangent of 1. (data not shown) The viscoelastic characteristics of the HA solution will limit the free movement of the solvent. The anionic charge of HA can also have an effect on the rheological behavior.

The composite networks have a storage modulus $168 \text{ Pa} \pm 62 \text{ Pa}$ and a loss tangent of 0.31 ± 0.021 . Even though these networks are much more viscous, the response of the storage modulus, loss tangent and axial stress follows the same trend as pure collagen networks. (Figure 3.9) With the distinction that the relaxation times needed to reach equilibrium are much longer. Additionally, a strain sweep (in absence of axial strain) shows significant strain-stiffening, similar to collagen networks without hyaluronic acid. (Figure 3.10)

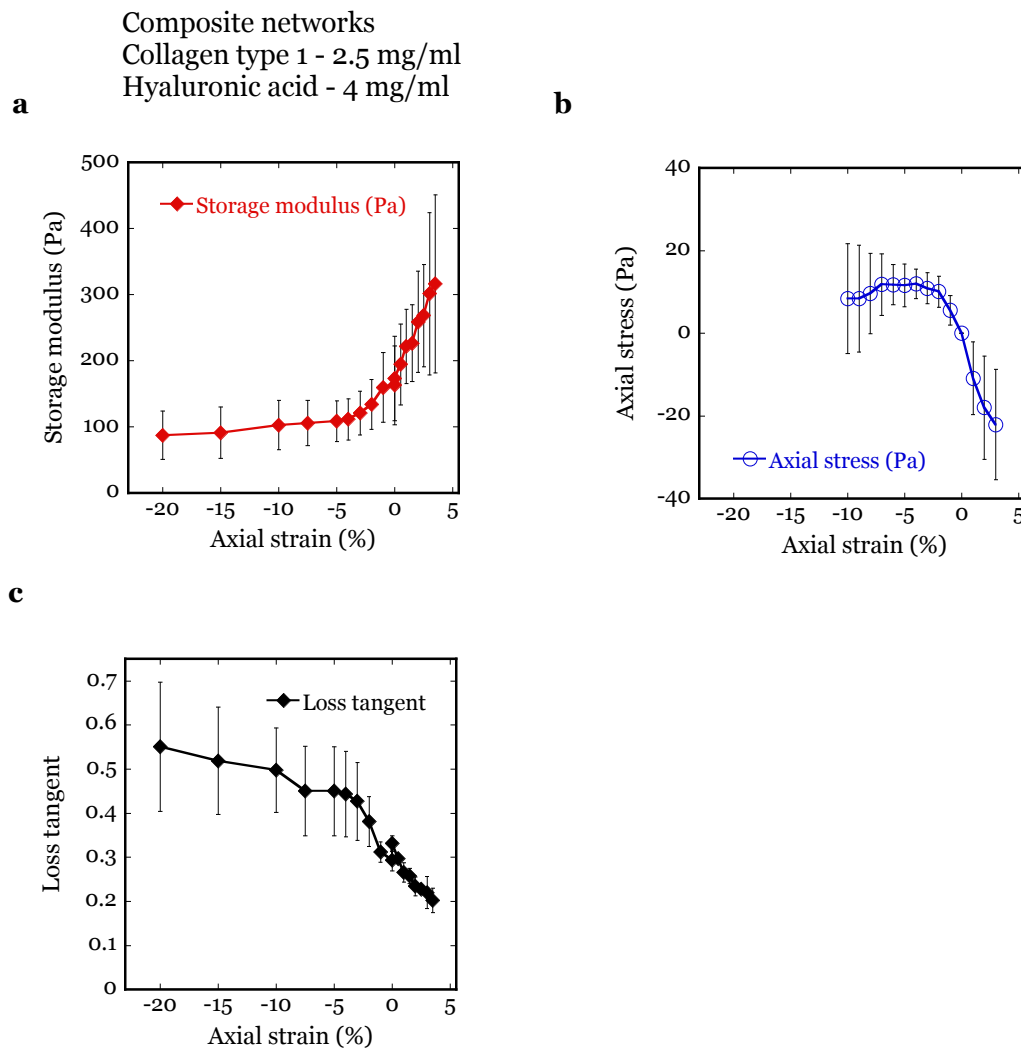


Figure 3.9: Increasing the viscosity of the solvent phase of collagen networks does not change multiaxial rheology. Rheology of composites with 2.5 mg/ml collagen and 4 mg/ml linear hyaluronic acid at low shear strains (2%) showing the storage modulus (a), axial stress (b), and loss tangent (c). Experimental method is identical as experiments with collagen gels as shown in Figure 3.4; with the modification that samples are allowed longer relaxation times; between 15 and 30 minutes.

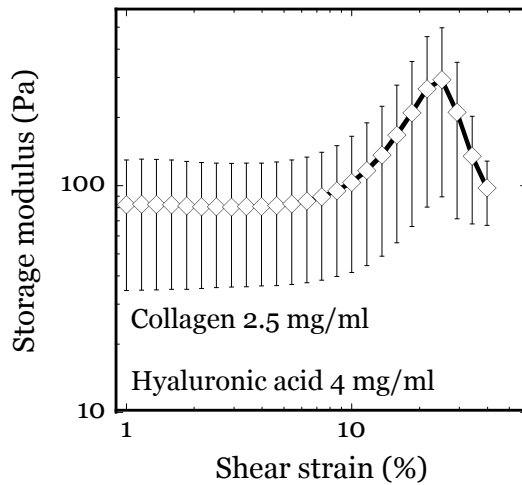


Figure 3.10: Composite collagen-hyaluronic acid networks strain-stiffen significantly. Strain amplitude dependency of composite networks with 2.5 mg/ml collagen and 4 mg/ml linear hyaluronic acid (in absence of axial strain).

3.4.7 Cross-linked hyaluronic acid networks show different response to axial strain

Hyaluronic acid in the body is usually cross-linked with proteoglycans such as aggrecan. Hereto, an 8 mg/ml thiol-modified hyaluronic acid mixture was lightly cross-linked with bi-functional PEGDA. A low concentration of fibronectin incorporated into the gels made the hyaluronic acid more adherent to the rheometer plates. The shear rheology is modified differently by axial strain compared to the semiflexible collagen and fibrin networks. In compression the storage moduli go up, in extension the moduli do not significantly change over the tested range. The trend in extension seems to be going up as well, however it was not possible to measure higher levels of extension due to adhesion problems. (Figure 3.11) A solution of linear hyaluronic acid at 8 mg/ml has a storage modulus of 50-60 Pa and a loss modulus of 40-45 Pa resulting in a loss tangent of around 0.75. However, the linear solution does not show a change in of the storage modulus with axial strain and is not able to bear loads in the axial direction. (data not shown)

Thiol-modified hyaluronic acid 8 mg/ml
Cross-linked with thiol reactive PEGDA

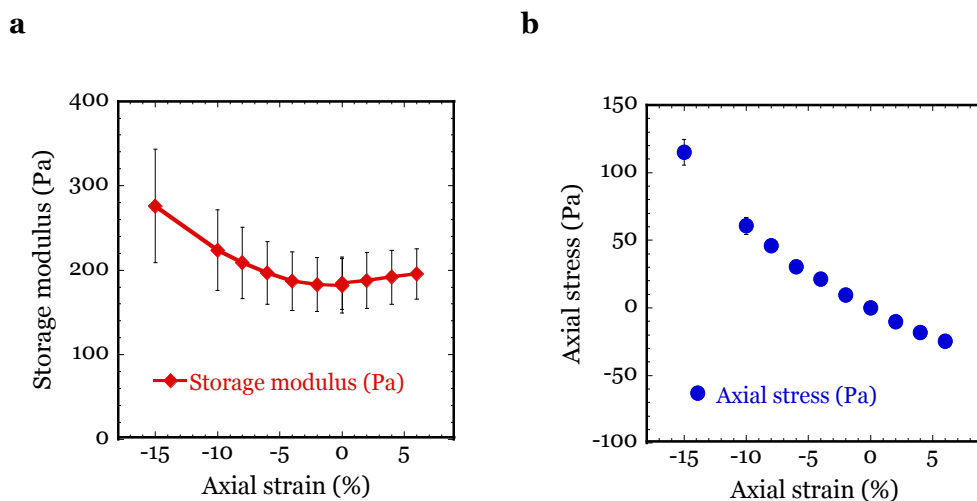


Figure 3.11: Cross-linked hyaluronic acid gel show different behavior compared to semiflexible biopolymer networks. Rheology of 8 mg/ml thiol-modified hyaluronic acid cross-linked with thiol reactive PEGDA at low shear strains (2%) at increasing levels of axial strain, showing the storage modulus (a) and axial stress (b). Both measured with the shear rheometer.

3.5 Discussion

Polymer networks in soft biological materials are subjected to simultaneous axial and shear deformation. For example blood vessels are subjected to shear strain from fluid flow and extensional and compressive strains from dilation and constriction. Adipose tissue is statically sheared and compressed at long intervals when sitting.

Analysis of such materials generally assumes a simple relationship between the resistance to axial compression and extension, defined by the Young's modulus E , and the resistance to shear deformation, defined by the shear modulus G . For elastic solids, these quantities are generally related by $E = 2G(1+\nu)$, where ν , the Poisson's ratio: the ratio of transverse strain to axial strain, which also quantifies the extent to which the

sample maintains volume when it is compressed. Nearly all simple materials have Poisson ratios $0 < \nu < 0.5$, meaning that $2G < E < 3G$, where the upper limits are for incompressible systems. This assumption underlies all measurements of elastic moduli by atomic force microscopes or other indentation probes, which produce strains that are combinations of simple shear, compression and extension. For hydrogels and other two-phase materials such as biopolymer networks, in which the solvent is incompressible but can move with respect to the compressible solid network phase, the elastic response to uniaxial stresses that potentially change volume can differ dramatically from the response to volume preserving simple shear: the short-time resistance to volume changes can be very high, even for materials that are very soft to shear.

The experiments reported here show that the elastic shear moduli of collagen and fibrin networks decrease under compression and increase when samples are extended. The Young's moduli are an order of magnitude lower in compression compared to extension. The change of the elastic shear modulus is decoupled from the change of the Young's modulus during compression and extension: in extension the Young's modulus is nearly constant, whereas the shear modulus continues to increase. Furthermore, when networks are compressed by only a small percentage of the original height, the Young's modulus drops below the shear modulus. When subjecting the samples to increasing shear strain under axial deformation, the strain-stiffening behaviour is altered both in onset and amplitude.

The simulations point towards these phenomena stemming from the difference between bending and stretching contributions of the filaments. The bending contribution of a stiff rod is:

$$k_{\parallel}(s_f) = 4\kappa/s_f r^2 \quad (3.2)$$

Whereas the stretching contribution is:

$$k_{\parallel}(s_f) = 3\kappa/s_f^3 \quad (3.3)$$

Where k is the stiffness, s_f is the segment length, r is the filament cross-section radius.

From this it becomes apparent that filaments are stiffer in stretch than when bend, which will lead to an asymmetrical force-extension, as opposed to springs that respond symmetrically in both directions ^{130,131}.

It is important to note that in the experiments here the samples are completely surrounded by buffer and fluid is allowed to flow freely in and out of the network when axially strained, allowing the sample volume to change. This change was visually observed by photographing the boundaries of the gels after axial strain, which remain the same for collagen and fibrin. The in/outflow of fluid and resulting compressibility of collagen has been described previously ¹³². We also verified the water outflow of a collagen network by incorporating food dye in the network and measuring outflow into the surrounding buffer after 10% compression. By contrast, in our experiments on PAA gels, we observe boundaries that bulge under axial compression and are concave in extension, consistent with the near incompressibility ($\nu \cong 1/2$) of PAA. Thus, our results are consistent with a vanishing Poisson ratio. Here, the Young's modulus coincides with the longitudinal modulus, in which the lateral dimensions of the sample do not change. For this reason, we impose fixed lateral boundaries in our simulations.

The volume change of collagen results in higher (lower) protein concentrations in compression (extension). But, the changes in the storage moduli cannot be explained by the change in volume; the increased polymer mass in compression and its dilution in extension make the effects of axial strain on storage moduli even more striking.

Additionally, composite networks of collagen and linear hyaluronic acid were tested. Though having longer stress-relaxation times, the equilibrium values of the axial stress and storage modulus showed the same trend as the collagen networks prepared with buffer with water-like viscosity, as did the composite networks show significant strain stiffening. However, when a lightly cross-linked HA solution was tested, it showed compression and extension stiffening. The cross-linked HA gels are expected to fully maintain their volume during compression and extension, and hence the gels will bulge when compressed and concave when extended. However, the same volume conservation happens in PAA gels, the storage modulus of which shows no dependence on the level of axial strain. It is therefore likely that this difference can be explained by the charges on the HA. In the composite network the HA, though showing viscoelastic characteristics, is in the solvent phase. Thus the charges are free to move and the composite as a whole will stay electrically neutral. Moreover, the charges will not act repulsively when being able to flow. The cross-linking of the HA changes this situation, now the network phase carries the anionic charge. When compressed the charges on the network will act repulsively. In extension this effect will be less but still present.

The few studies directly comparing mechanics in different directions show results consistent with our findings. In one study the compressive moduli of collagen gels measured with atomic force microscopy are between 2.85 Pa and 23.1 Pa, and the shear moduli measured with a rheometer are between 19.9 Pa and 152 Pa respectively, for collagen isolated from rats of increasing age ⁴¹. Another study compared creep in confined compression and shear and concluded that the modulus was higher in shear than in compression ⁵¹. It has been shown for fibrin gels that when compressed the shear modulus drops initially. The same study also imaged the networks during compression and showed directly that filaments buckle when compressed ¹³³.

The relation between E and G in viscoelastic solids has previously described to be extremely time dependent, with a Poisson's ratio ranging from -1 to ~ 0.3 .^{134,135}

However, in our experiments, the networks are allowed to relax considerably and show even larger variability in the relationship between E and G . Thus, the decoupling of E and G is not merely a time dependence issue but an intrinsic material property. Fluid flow into the gel might account for the differences observed in previous studies, where extension of these gels is often described as viscoelastic. The results with collagen-HA composites indicates that there is likely a poroelastic component to the behaviour of the semiflexible networks as well. A logical continuation on the research presented in this chapter is to analyse the time dependency of these systems.

Fibrin and collagen gels have often been suggested as scaffolds for cells in tissue engineering applications. The mechanical adequacy has been often debated due to the variability in reported moduli. In this study it becomes apparent that the ability of these networks to withstand compression and the combination of shear and compression is limited, which might pose a problem when these gels are used to replace damaged tissues. Hereto, it is vital to further study the mechanics of whole tissues and cell seeded biopolymer networks to deduct if this will improve the ability of constructs to resist mechanical loads.

Author Contributions

AvO and PAJ designed experiments. AvO performed experiments and data analysis. MV, AL, AS and FCM developed the computational model. MV and AL performed the simulations and MV analyzed the resulting data. All authors contributed to manuscript preparation.

CHAPTER 4: DYNAMICS OF EXTRACELLULAR MATRIX NETWORKS UNDER SHEAR, COMPRESSION AND EXTENSION

4.1 Abstract

Time-dependent behavior of biological materials is important as *in vivo* mechanical stimuli occur at a wide range of timescales. Here the dynamics of both the storage moduli and axial stresses of fibrin and collagen networks are explored after application of an axial step strain. The levels of axial strain, sample diameter, and permeability of the networks are varied. Shear stress relaxation after a step shear is compared to axial stress relaxation. The results show that for collagen and 2 mg/ml fibrin networks there is a poroelastic component to relaxation after axial strains, which is absent for pure shear deformation. The strong frequency dependence of axial moduli, and low frequency dependence of shear moduli explain the large variability of mechanical properties reported in literature.

4.2 Introduction

Biological materials, both soft tissues and reconstituted biopolymer networks, show time dependent responses in mechanical tests, such as stress-relaxation, creep, or hysteresis depending on the type of testing method. Time-dependence of biological systems is important because *in vivo* tissues experience loading at a large range of timescales. Quick loading occurs in sudden events associated with movement, the same tissues will experience long intervals of sustained loading during standing, sitting or lying down. The same diverse loading conditions will be experienced by biomaterials used in tissue engineering applications.

The time dependent responses of biological materials have been investigated, quite extensively in the case of some tissues, like cartilage ^{79,136}. The viscoelastic properties of fibrin and collagen networks have been well established in shear ^{27,137}, and are argued to play a role in the mechanics in the axial direction ^{46,138}.

However, hydrogels like collagen and fibrin gels consist of <1% protein. The remaining >99% is buffer, which, like interstitial fluid, can flow within the porous biopolymer network structure. When subjected to axial strains, these networks will change their volume and hence a poroelastic component of the mechanical behavior is to be considered, in which pressure differences cause fluid flow and local stress fields. The existence of interstitial fluid flow or poroelasticity in axial deformation has been well established experimentally, especially with collagen ^{51,132,139}. Modeling of these principles has been of great interest not only for biological materials, but for hydrogels in general ^{140,141}. Many models are able to account for parts of the behavior seen, such as the biphasic theory to model poroelasticity ^{132,142,143}, which has been added onto and modified to accommodate for the viscoelastic nature of the network phase, poroviscoelasticity ^{144,145} and the non-linear nature of the network phase, hyperelasticity ¹⁴⁶⁻¹⁴⁸. Other important factors such as tissue anisotropy, ionic charges, cell traction and remodeling have been accounted for more recently ^{138,149-151}.

In the previous chapter the multiaxial rheology of biopolymer networks at steady state was discussed. In this chapter the dynamical responses of these systems to multiaxial strains are explored. The response of both the storage moduli and axial stresses of fibrin and collagen networks are followed in time during application of shear and axial strains. To address the contributions of interstitial fluid flow and the viscoelastic properties of the network, the axial strain, sample size and network permeability were varied. The

relaxation of collagen networks changes with these parameters as expected from poro(visco)elastic theory. Fibrin networks at 2 mg/ml show a significant difference between highly permeable coarse clots and fine clots with a low permeability. Fibrin networks at 10 mg/ml show no apparent dependence on plate size and permeability at large axial strains, which is likely due to network anisotropy and experimental issues.

4.3 Materials and methods

4.3.1 Preparation of coarse and fine fibrin clots

Coarse fibrin clots were prepared identically as in Chapter 3. Briefly, fibrinogen (Fbg) isolated from human plasma dissolved in 1X T7 buffer (50mM Tris, 150 mM NaCl at pH 7.4), thrombin (Thr) isolated from salmon plasma, 1X T7 buffer, and CaCl₂ stock were added at appropriate ratios to yield a 2 or 10 mg/ml fibrinogen, 30mM Ca²⁺ and 1 or 0.5 U thrombin / mg Fbg. The 2 mg/ml samples were polymerized at 37°C, 10 mg/ml samples at 25°C.

Fine fibrin clots were prepared by dialyzing the fibrinogen solution against a 1X T8 buffer (50mM Tris, 450 mM NaCl at pH 8.4) overnight at 4°C in SnakeSkin dialysis tubing (Life Technologies, Carlsbad, CA). The solutions were spun down to remove aggregated protein, aliquoted, snap frozen and stored at -80°C until further use. To prepare fine clots, solutions were warmed to room temperature; fibrinogen stock solution, 1X T8 buffer, CaCl₂ stock and thrombin were added at appropriate ratios to yield a 2 or 10 mg/ml fibrinogen, 30mM Ca²⁺ and 1 or 0.5 U thrombin / mg Fbg. The 2 mg/ml samples were polymerized at 37°C, 10 mg/ml samples at 25°C.

4.3.2 Preparation of collagen gels and composites of collagen and hyaluronic acid.

Collagen type 1 gels and composite gels with hyaluronic acid were prepared identically as in Chapter 3. Briefly, to prepare collagen networks, 10X PBS, 0.1M NaOH and ddH₂O were added in appropriate ratios to yield a 2.5 mg/ml collagen concentration in 1X PBS solution with a pH between 7-7.5. The samples were polymerized at 37°C.

To prepare composite networks of collagen and hyaluronic acid collagen water was replaced by a 8 mg/ml hyaluronic acid solution to result in a final HA concentration of 2 mg/ml or 4 mg/ml. Samples were mixed thoroughly and centrifuged for 5 sec at 2000xG to remove bubbles prior to pipetting the samples between the rheometer plates.

The concentration of hyaluronic acid was lowered from 4 to 2 mg/ml in most experiments as the addition of HA made the gels less adherent to the rheometer plates. This made it difficult to obtain accurate data in extension.

4.3.3 Shear rheometry

The shear rheometer set-up used is identical to the one used in Chapter 3. A strain-controlled rotational rheometer (RFS3, TA Instruments, New Castle, DE) was used with a parallel plate with a diameter of 8 mm for 10 mg/ml fibrin and a 25 mm diameter for 2.5 mg/ml collagen and composite collagen-hyaluronic acid gels, all with a gap of 1 mm. A 50 mm with a 0.4 mm gap was used for 2 mg/ml fibrin samples.

The shear moduli of the samples were measured by applying a low oscillatory shear strain of 2% at a frequency of 10 rad/sec. Axial strain was applied by changing the gap between the plates. To obtain data on the dynamical changes of the samples, the storage modulus was sampled every 2 seconds for samples with quick anticipated relaxation rates, and up to 8 seconds per point for samples with slow anticipated relaxation rates.

The axial stress was collected simultaneously from the analog signal of the rheometer using a ProLink instrument amplifier and Logger Lite software (Vernier Software and Technology, Beaverton, OR). The sampling rate of the axial stress was varied between 0.25 – 5 sec/point depending on anticipated relaxation rates. The speed of axial strain application was varied between 2 – 25 $\mu\text{m/s}$.

Frequency sweeps were performed by changing the frequency of the applied oscillatory shear strain between 0.01 rad/s and 10 rad/s while keeping the strain constant at 1%. At each frequency 10 oscillations were performed of which the last 5 were used to calculate the moduli.

4.3.3 Axial frequency sweep with tensile tester

To obtain the frequency dependence of networks in the axial direction the tensile tester was used (5564, Instron, Norwood, MA) with parallel platens at a gap of 1 mm, using similar volumes of fluid as used for shear rheometry. For frequency sweeps, samples were subjected to a sawtooth shaped cyclic strain (compression or extension) with an amplitude of 10 μm at frequencies between 0.00159 Hz and 1.59 Hz. 10 cycles were measured, of which the last 5 cycles were used to calculate the Young's modulus.

4.4 Results

4.4.1 The dynamics of storage moduli and axial stresses during compression and extension

To obtain steady-state values of the axial stresses and storage moduli during the axial strain sequences, as they were presented in Chapter 3, these variables were followed in time. This presented the opportunity to look at the dynamics of the systems during the axial strain application of both the storage moduli and axial stresses. Additional

experiments were done increasing the axial step-size, and changing the sample diameter and permeability of the fibrin and collagen networks.

The fibrin samples shown in Figure 4.1 were all prepared at a 10 mg/ml fibrinogen concentration. The samples were axially strained 1% (**a, b**) or 10% (**c-h**). Additionally, samples were tested with a 25 mm diameter plate instead of 8 mm (**e, f**); and fine clots were tested, which have thinner fibrils and hence a smaller meshsize ¹⁵²⁻¹⁵⁴ (**g, h**). The axial strain is applied at $t = 10$ sec. With 1% axial strain the storage modulus moves to its new steady-state without an observable peak, which is lower than the initial value in compression, and higher when extended. The axial stress, however, shows a pronounced peak and subsequent relaxation. When a larger axial strain of 10% is applied, the storage modulus does show a significant increase both in compression and extension. When a larger plate is used or the permeability is lowered – using fine fibrin clots- the axial peak stress is higher.

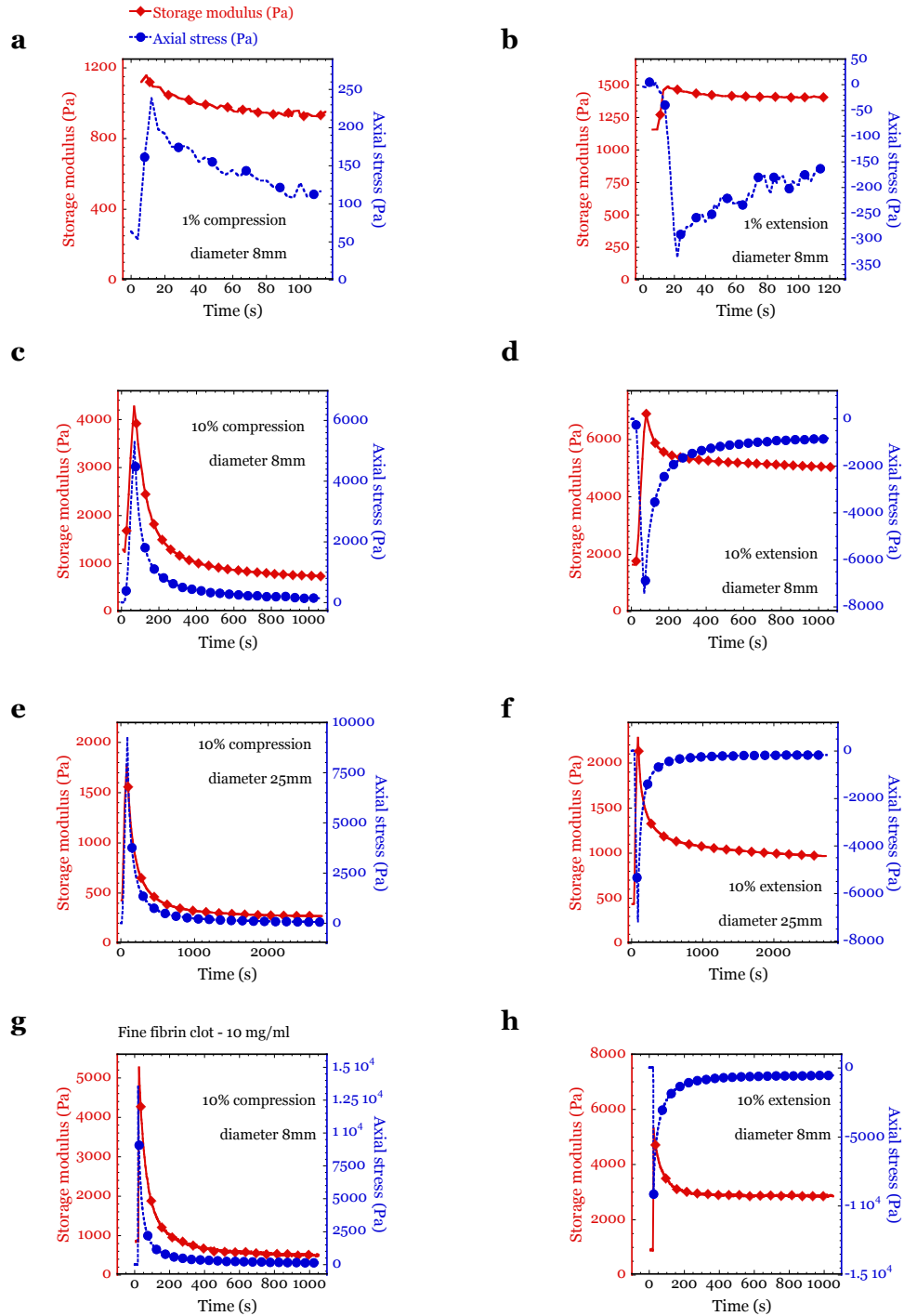


Figure 4.1: Dynamics of storage moduli and axial stresses of 10 mg/ml fibrin networks. Coarse networks (**a-f**) and fine networks (**g, h**) subjected to 1% (**a, b**) or 10% (**c-h**) axial strain, with a sample diameter of 8mm (**a-d, g, h**) or 25mm (**e, f**). Storage modulus is measured with oscillatory shear strain of 2%. The mean of 3 samples is shown. 3-10% of data points are depicted with a symbol.

However, the peak storage moduli do not show a clear trend, which is further obfuscated by the variability in the initial storage modulus. Hence in Figure 4.2 the ratio of the peak modulus G'_{peak} to the initial storage modulus G'_0 is shown. This shows that in compression the increased plate size does not result in a larger peak, but in extension the peak is larger with increased sample size. The decrease in permeability of the fine clots results in larger storage modulus peaks for both compression and extension.

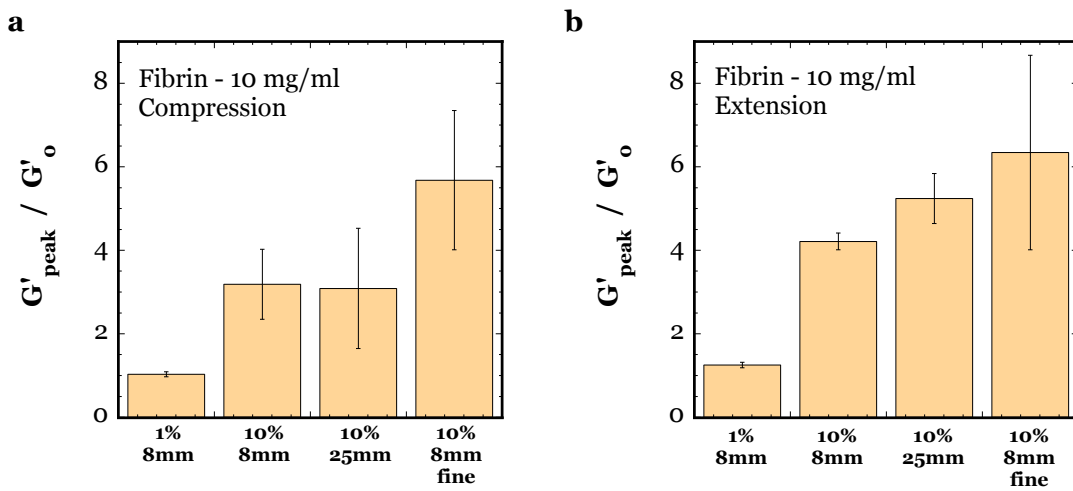


Figure 4.2: Peak storage moduli normalized to initial storage moduli for 10 mg/ml fibrin networks subjected to varying axial strain, with varying plate sizes and permeability. The initial modulus is calculated as an average over 10 sec before axial strain application, the peak is the highest point reached during or immediately after axial strain application. A value of 1 indicates there is no peak but the modulus moves to the new steady state without relaxation.

For collagen the same type of experiments are plotted in Figure 4.3. Again it is observed that the smallest step-size, 0.5% compression and 0.25% extension, results in a direct move of the storage modulus to its new value without a peak (**a, b**). The axial stress shows a pronounced peak even at these small axial strains. When the axial strain is

increased 10-fold, both the storage modulus and axial stress show a pronounced peak. In compression the relaxation to the new steady-state happens quickly, for both the storage modulus and axial stress. In extension, the axial stress relaxes quickly but the storage modulus shows a continuous decline over the test time. When a smaller plate is used (e) 5% compression still renders a peak in both the storage modulus and axial stress, though the peak values are lower. When 2 mg/ml hyaluronic acid is added to the networks the relaxation is slower. The peaks of the storage moduli were again normalized to the initial value (Figure 4.4). This shows that with increasing axial strain and decreasing permeability the peak increases, whereas the smaller sample diameter results in a smaller peak. For cross-linked hyaluronic acid networks, there is no relaxation observed after axial or shear strain, similar to soft polyacrylamide gels. (data not shown)

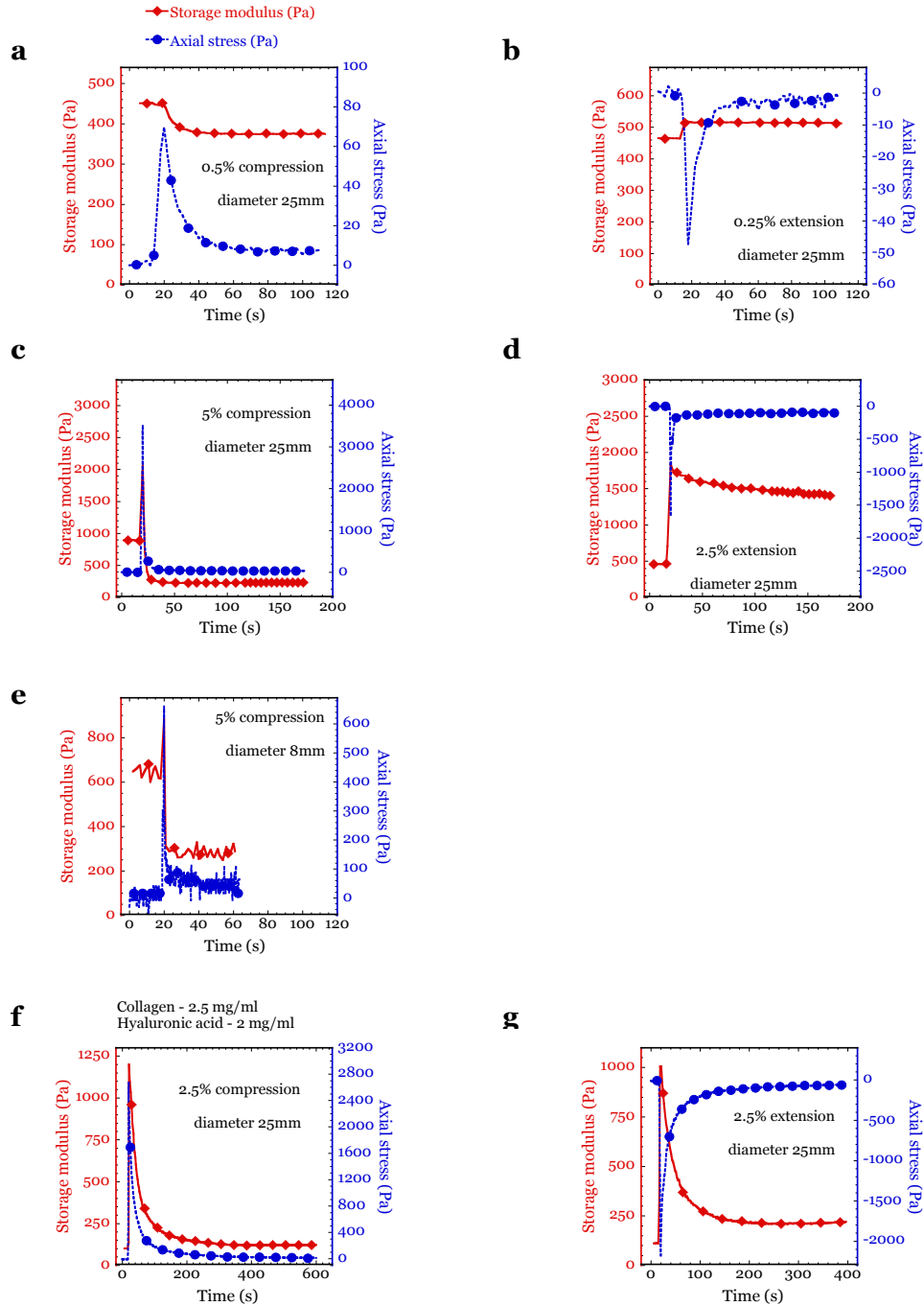


Figure 4.3: Dynamics of storage moduli and axial stresses of 2.5 mg/ml collagen networks. Collagen networks (**a-e**) and composite collagen – HA networks (**f, g**) subjected to 0.5% compression (**a**), 0.25% extension (**b**) or 5% compression (**c,e**) 2.5% compression (**f**) or 2.5% extension (**d, g**). Sample diameter was 25mm (**a-d, f, g**) or 8mm (**e**). Storage modulus is measured with oscillatory shear strain of 2%. The mean of 3 samples is shown. 3-10% of data points are depicted with a symbol.

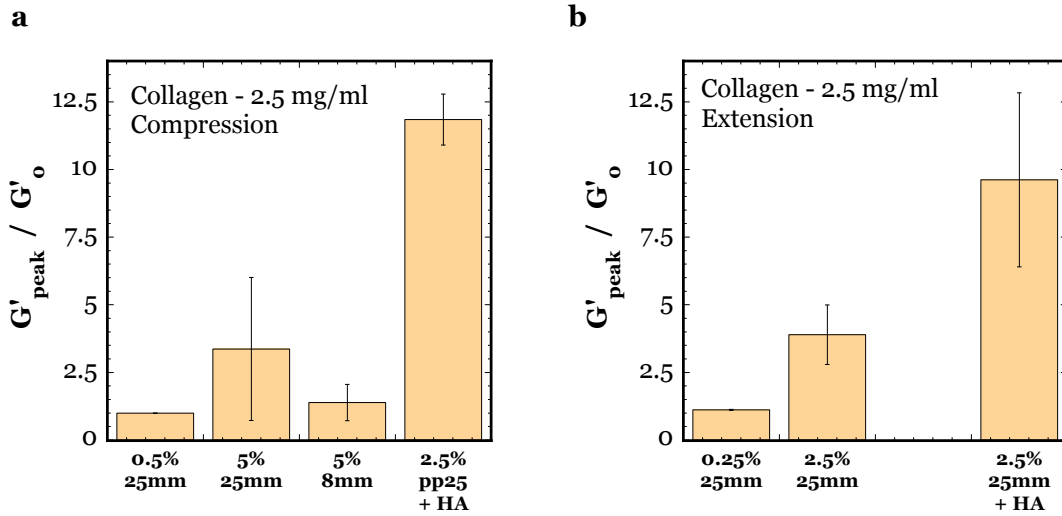


Figure 4.4: Peak storage moduli normalized to initial storage moduli for collagen networks subjected to varying axial strain, with varying plate sizes and permeability. The initial modulus is calculated as an average over 10 sec before axial strain application, the peak is the highest point reached during or immediately after axial strain application. A value of 1 indicates there is no peak but the modulus moves to the new steady state without relaxation.

Additionally, coarse and fine fibrin networks were tested at 5% compression. A distinct difference is observed in the dynamics, which is slower for the fine networks. (Figure 4.5)

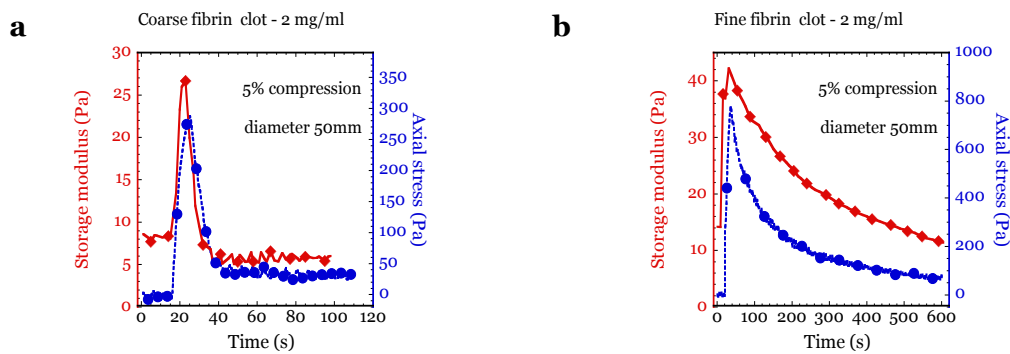


Figure 4.5: Dynamics of storage moduli and axial stresses of coarse and fine fibrin network at 2 mg/ml. Coarse networks (a) and fine networks (b) with a sample diameter of 50mm subjected to 5% compression. The mean of 3 samples is shown. 3-10% of data points are depicted with a symbol.

4.4.2 Stress-relaxation in compression, extension and shear

To assess the dynamics of these systems in more detail, the relaxations after axial strain application were plotted. In this case the storage moduli and axial stresses are normalized to the peak value, which in these systems occurs at the end of the axial strain application. For 10 mg/ml fibrin networks it becomes apparent that the stress-relaxation after 10% compression is similar for the samples of different diameters and permeability. (Figure 4.6a) In extension the storage moduli show little stress-relaxation. The axial stresses relax more in compression compared to extension. (4.6c, d)

The stress relaxation of the collagen samples shows more variability when test parameters are changed. In compression, the storage modulus barely relaxes at the low axial strain. With a larger strain the relaxation is more pronounced but still relatively quick. With the addition of HA the relaxation happens much slower, but the degree of relaxation is similar. A smaller plate size gives a faster and less pronounced relaxation. The axial stresses in compression show a similar pattern. When extended, the level of both the storage modulus and axial stress relaxation is low for the collagen networks. The relaxation of the composite collagen-HA networks looks similar in compression and extension.

Compared to 10 mg/ml fibrin networks, fine and coarse clots at 2 mg/ml show more distinction in their dynamics after 5% compression. The coarse clots are fully relaxed; in tens of seconds, the fine clots have not reached steady state after 300 sec. (Figure 4.8)

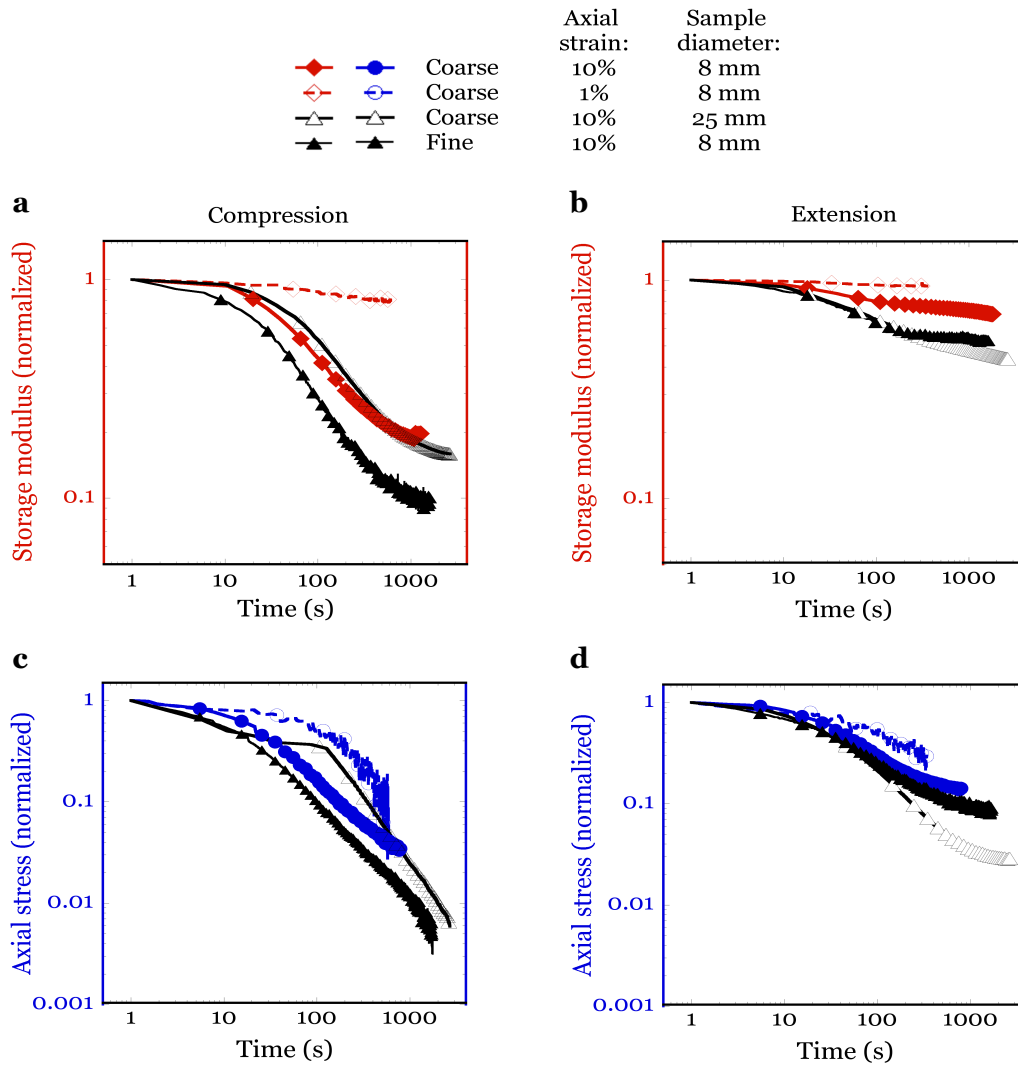


Figure 4.6: Relaxation of storage moduli and axial stresses of fibrin networks at 10 mg/ml after an axial step strain. The axial strain, plate size and permeability were varied. The storage moduli (**a**, **b**) and axial stresses (**c**, **d**) were normalized to the peak value that was reached after axial strain application. The mean of 3 samples is shown.

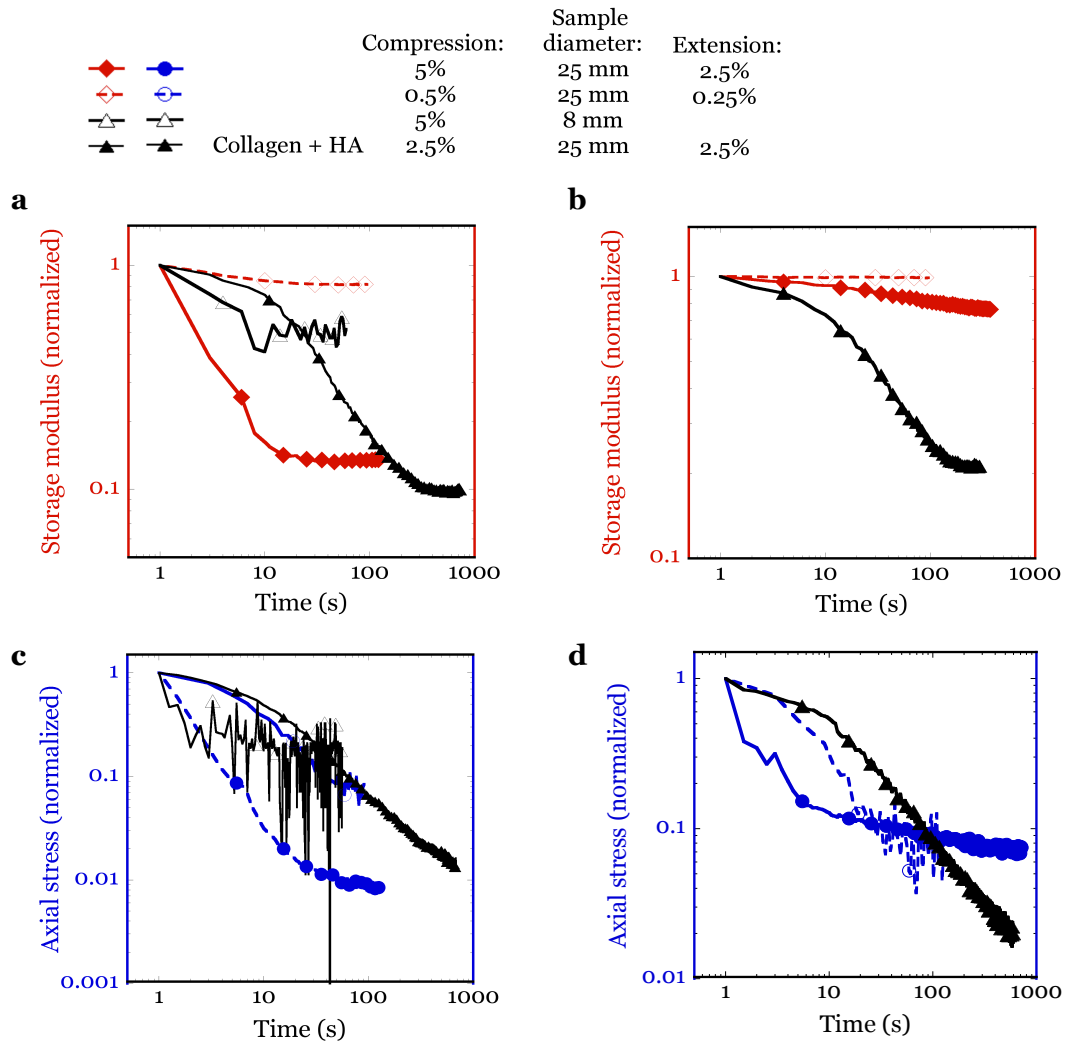


Figure 4.7: Relaxation of storage moduli and axial stresses of collagen networks after an axial step strain. The axial strain, plate size and permeability were varied. The storage moduli (**a**, **b**) and axial stresses (**c**, **d**) were normalized to the peak value of each sample. The mean of 3 samples is shown. 3-10% of data points are depicted with a symbol.

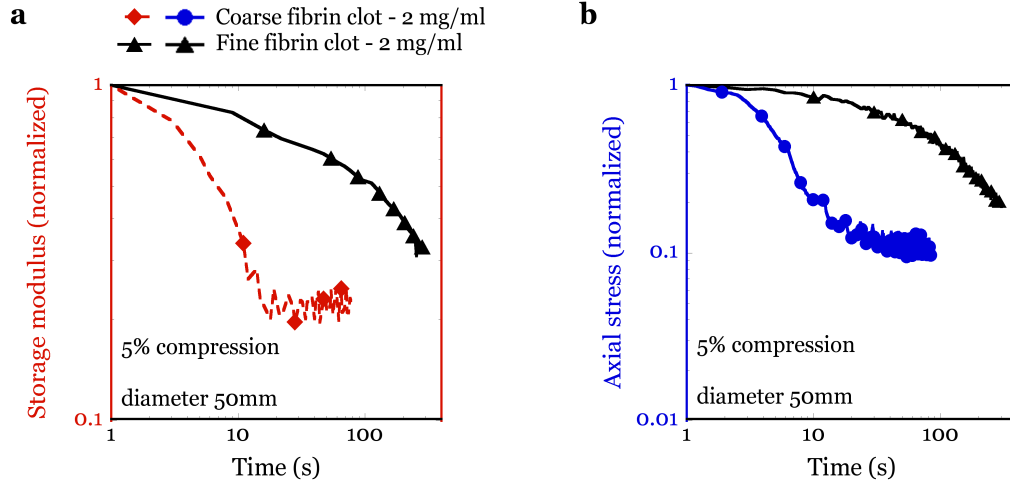


Figure 4.8: Relaxation of storage moduli and axial stresses of coarse and fine fibrin networks of 2 mg/ml after a 5% compression. The storage moduli (a) and axial stresses (b) were normalized to the peak value of each sample. The mean of 3 samples is shown. 3-10% of data points are depicted with a symbol

The measurement of the storage modulus during compression and extension is done with a small oscillatory shear strain. To compare shear stress relaxation with the axial stress relaxation, a step-shear strain of the same magnitude is applied. Figure 4.9 shows the stress in the axial or shear direction after a step-strain in the same direction is applied. This reveals that the shear stress relaxation is very minimal compared to the axial stress relaxation. It also shows that for collagen and fibrin networks, the compressive stress relaxes further than the extensional stress. However, the initial relaxation is similar. The composite collagen-HA networks show very similar relaxation in compression and extension.

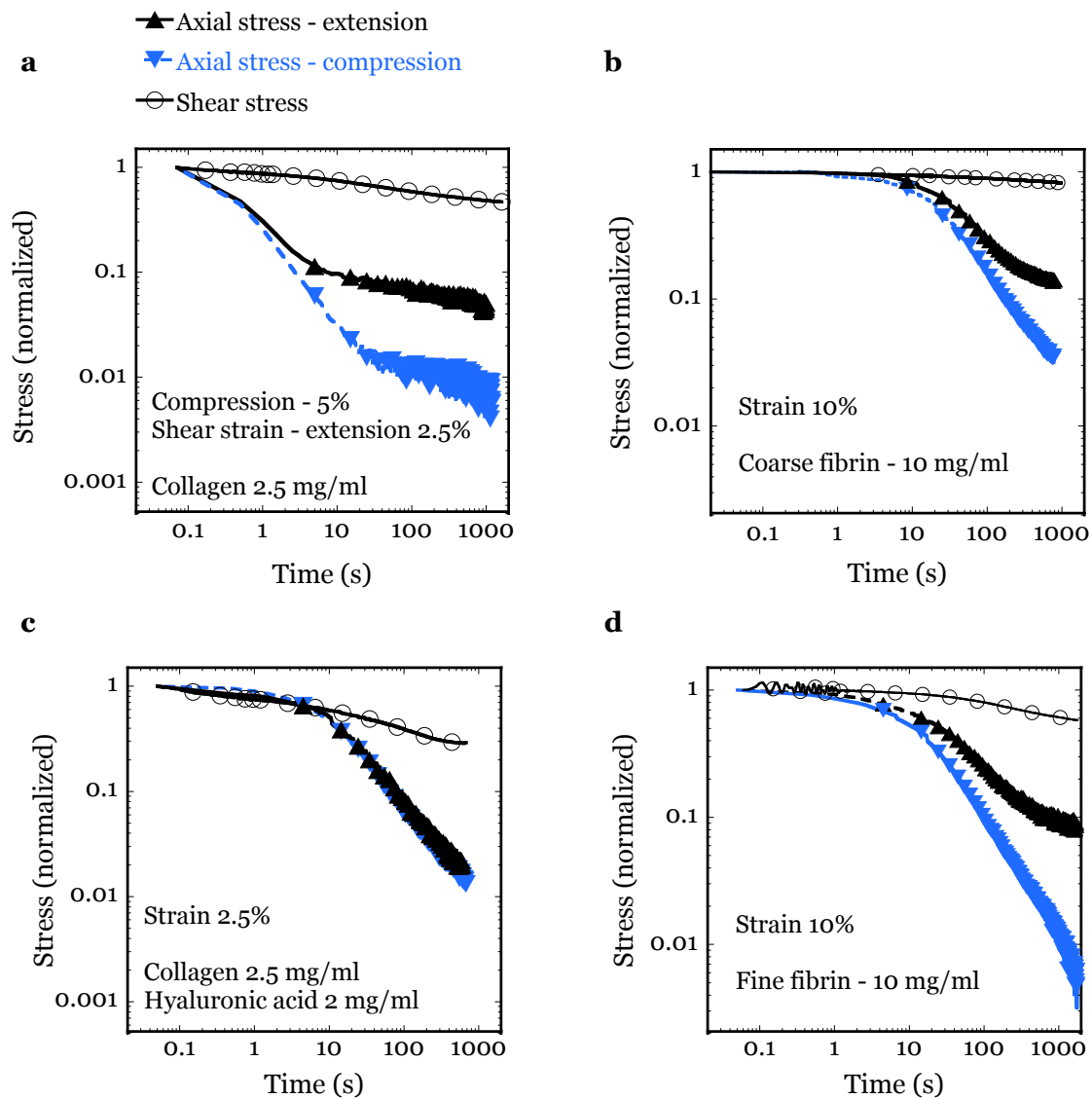


Figure 4.9: Axial stress-relaxation compared to shear relaxation. A step strain was imposed on a collagen network (a), 10 mg/ml coarse fibrin network (b), a composite collagen-hyaluronic acid network (c) and a 10 mg/ml fine fibrin network (d) in compression, extension and shear. The resulting stress was followed as a function of time. The stress is normalized to the peak value; the mean of 3 samples is shown. 3-10% of data points are depicted with a symbol.

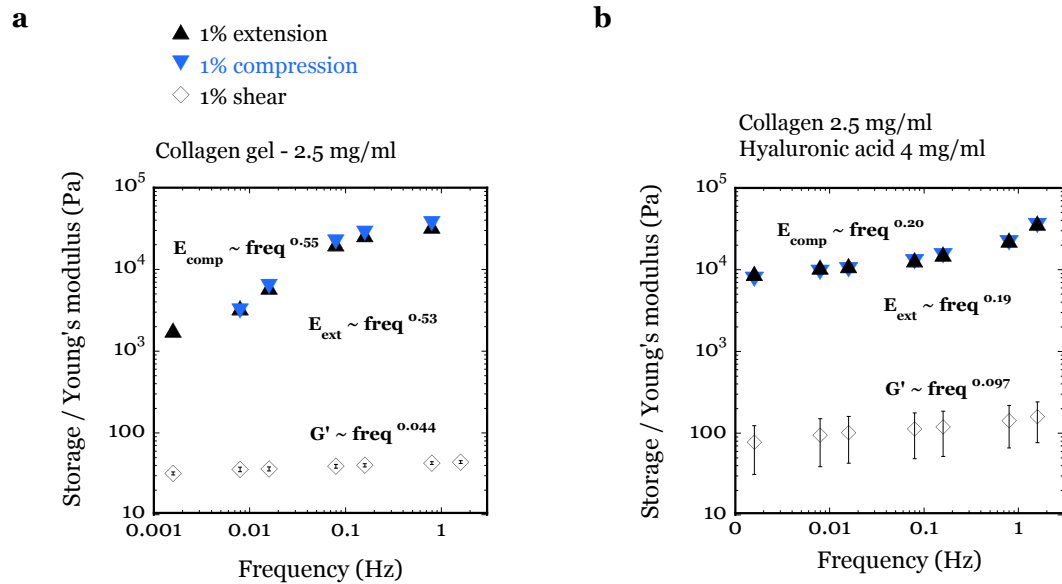


Figure 4.10: Frequency-dependence of collagen and composite collagen-hyaluronic acid networks in axial and shear direction. A 1% oscillatory strain was imposed on a collagen network (a) and a composite collagen-hyaluronic acid network (b) in compression, extension and shear. The average \pm SD of 5 cycles is shown for 1 sample. The shear moduli were obtained with the shear rheometer, the Young's moduli with the tensile tester. The dependence of the modulus to the frequency is determined by fitting a power-law over the whole range of frequencies.

Lastly, the frequency-dependence of collagen and composite networks was compared. This shows a dramatic difference between the frequency dependence of axial moduli and the elastic shear modulus, both for the collagen and composite networks. For the collagen networks, the Young's modulus varies in between 2 and 20kPa, and is the same in extension and compression, whereas the shear modulus varies between 30 and 50Pa. The modulus in compression varies with the frequency to the 0.55 power, and extensional modulus with a 0.53 power. The power is only 0.044 for the shear modulus.

This effect is less strong in the composite network, which is a 0.2, 0.19 and 0.097 power in compression, extension and shear respectively, though the difference between axial and shear moduli is still large. (Figure 4.10)

4.5 Discussion

In this chapter the dynamics of fibrin and collagen networks during multiaxial deformation were addressed. The stress field of a poroelastic material upon deformation is described by:

$$\sigma_{ij} = C_{ijkl}\varepsilon_{k,l} + \varphi_f \nabla p \quad (4.1)$$

In which the first term represents the solid phase of the material, the second term represents the fluid phase.

To distinguish viscoelastic and poroelastic contributions of the response, the axial strain, sample diameter, and permeability were varied. Effects of those parameters on the fluid movement within the porous structure can be predicted with D'Arcy's law:

$$q = \frac{-\kappa}{\mu} \nabla p \quad (4.2)$$

Where q is the flux (in m^3/s), κ is the permeability or D'Arcy constant (in m^2), μ is the viscosity (in Pa s) and ∇p is the pressure gradient vector (Pa m). For a cylinder, which is compressed on the flat surfaces, this equation can be modified to¹⁵⁵ :

$$\frac{\partial e}{\partial t} = \frac{-\kappa}{\mu} \nabla^2 p \quad (4.3)$$

Where e is the displacement field:

$$e = \frac{1}{r} \frac{\partial}{\partial r} (r u_r) + \frac{1}{r} \frac{\partial u_\theta}{\partial \theta} \quad (4.4)$$

with u_r and u_θ as the radial and the circumferential displacements respectively,

and the Laplacian operator in polar coordinates is:

$$\nabla^2 = \frac{1}{r} \frac{\partial}{\partial r} \left(r \frac{\partial}{\partial r} \right) + \frac{1}{r^2} \frac{\partial^2}{\partial \theta^2} \quad (4.5)$$

These equations have been used to solve the stress and strain decay in a linear, isotropic elastic medium¹⁵⁵, however, the network phase here is the non-linear, anisotropic, and viscoelastic. It can be deduced from the change in the displacement field that the stress-relaxation will be slower: when the sample size is increased, when the permeability of the medium is lower, and when the viscosity of the solvent is higher.

The responses varied between collagen, and fibrin of a high and low concentration. The collagen networks showed pronounced differences in relaxation of both the storage moduli and axial stresses. The relaxation –normalized to the peak- is slower for larger samples and higher axial strains. The peak shear moduli -normalized to the unstressed value- and axial peak stresses also show an increase with sample diameter and axial strain. The addition of hyaluronic acid made the relaxation significantly slower and resulted in high peak shear moduli and high axial peak stresses. For these composite networks one has to take into consideration that the addition of hyaluronic acid is known to change the collagen network structure^{37,44}. It is not known if a portion of the HA is deposited on the collagen fibers or if it completely remains in the solvent phase. Nor has it been tested whether the HA is squeezed out of the network upon compression. These

two variables would have an influence on the charge balance when the networks are axially strained.

The trends in the 10 mg/ml fibrin networks were not as expected. There is a pronounced difference between a 1% and 10% axial strain for coarse clots of the same diameter. However, there is no obvious trend when the sample diameter is increased or the permeability is lowered. The axial peak stresses increase drastically between coarse and fine clots. The peak of the storage modulus in compression increases as well for the fine clot. However, when normalizing the relaxation of the storage moduli and axial stresses to the peak values, the coarse and fine 10 mg/ml clots relax remarkably similar, as do the samples for which the diameter was increased from 8 to 25 mm.

The 2 mg/ml fibrin samples were only tested at 5% compression. However, the difference between coarse and fine clots at this concentration is clear. The relaxation of both the storage modulus and axial stress is significantly slower for fine clots. The axial peak stress is higher for the fine clots as well. The coarse and fine clot storage modulus peaks are not different when normalized to the initial value. However, this could be due to the fact that the fine clots were followed at a lower sampling rate, which would make it likely the initial peak is underestimated.

The latter point touches on one of the many shortcomings of the presented experiments. The sampling rate of the shear rheometer is limited by the frequency used, which is 1 sample per 2 seconds at 10 rad/s. In order to increase the sampling speed one needs to increase the frequency, which is not always desirable. Another issue is the manual application of axial strains, which makes it difficult to apply axial strains as fast as possible and with high precision. It would be a possibility to fit the current data to get a more quantitative comparison on the peak moduli and stresses.

The results with the 10 mg/ml fibrin networks are inconsistent with what is expected from literature and what is seen with 2 mg/ml fibrin and collagen. It is expected that due to the poroelasticity of these networks, the increase in sample size or decrease in permeability would result in slower relaxations, which is not observed. The peaks of both the storage modulus and axial stress are higher for the fine clot indicating that there is a difference initially. However, the subsequent relaxation is not different. These results are likely to stem from network inhomogeneity. When a large pressure builds up in the network due to the axial strain application, the solvent will try to find the path of least resistance. Possibly there are 'weak' spots in the network structure where the network gets damaged as a result of the pressure and the solvent can flow 'freely' in and out. This principle was described for synthetic hydrogels in reference to epithelial sheet fracturing ¹⁵⁶.

Overall, the results here bolster the conclusion in Chapter 3 that the axial response of a sample during axial deformation is decoupled from its shear response during the same deformation. This is especially apparent in the small axial strains, where the storage modulus shows no apparent peak or relaxation, where the axial stress does. The absence of a peak in the shear modulus could be due to the small step size, between 0.25% and 1%, which is 2.5 - 10 μm . This step is on the same order of magnitude as the mesh size of the networks. The change in the storage modulus could be due to a collapse of only one or a few mesh sizes deep at the moving plate. This would still necessitate the movement of solvent and hence result in an axial stress peak, but which would not result in a rearrangement of the bulk of the network, and therefore not result in a large increase in the storage modulus. This localized compression or collapse at the moving plate (or piston) was seen in unconfined compression for fibrin ¹⁵⁷ and in confined compression

for collagen ¹³⁹. Fibrin networks were suggested to behave like a foam in axial compression, in this study where microscopy and shear rheometry were combined ¹⁵⁷.

Other explanations for the behavior of the storage modulus with small strains are feasible. The stability of these networks, that fall below the central-rigidity threshold (explained in Ch2), is hypothesized to come from internal stresses ^{62,158}. This is confirmed by the observation of modest negative axial stresses that the networks develop during polymerization. An internal stress decrease could account for the drop in the storage modulus in compression; for small compressions the dominating factor is the drop of tension on the network nodes as opposed to rearrangements of fibrils themselves or buckling.

When larger compressions are applied there are significant increases in the storage moduli of all systems, even in the compressed samples of which the modulus eventually relaxes to below the initial value. This peak is the result of the incompressibility of water, which results in a transient shape change, which in turn will result in transient radial extension of the network. The stress due to this extension is likely the cause for the shear modulus increase. The sample will revert back to its cylindrical shape as the solvent flows out of the free boundaries. In extension the same principle applies; a transient stress field will occur as the sample arches inward before fluid can flow in. However, in extension the viscoelasticity of the network phase is likely also a determinant after the fluid flow has subsided, which can be seen in the sustained relaxation of the storage modulus of collagen in 2.5% extension.

Another significant observation in this chapter is the large difference in the frequency dependence and stress-relaxation in shear, compression and extension. It shows a strong dependence in the axial direction, and a mild dependence in shear. The reported moduli

of especially collagen networks in literature vary dramatically. This variation is likely due to variability in testing parameters, which it was shown here can lead to differences of multiple orders of magnitude in the moduli. Hence, when comparing results of mechanical tests the experimental methods should be carefully evaluated.

Overall, the data presented here show differences between shear and axial responses to deformation. However, the interpretation of the results is clouded due to experimental difficulties. It would for example be interesting to compare relaxations of axial and shear stresses after application of axial strain, to better understand the stress field of the non-linear viscoelastic networks during these experiments. Additionally, it would be desirable to determine whether all of the relaxation is a direct result of fluid flow or not. It has been previously noted it is difficult to discern between poroelasticity and viscoelasticity in experiments ¹³⁹. Experimental data of high precision will have to be combined with one or more modelling approaches to accomplish this.

CHAPTER 5: THE EFFECT OF CELL CONTRACTILITY ON MULTIAXIAL RHEOLOGY OF EXTRACELLULAR MATRIX NETWORKS

(Partially adapted from: *Uncoupling shear and uniaxial elastic moduli of semiflexible biopolymer networks: compression-softening and stretch-stiffening*, Anne S. G. van Oosten, Mahsa Vahabi, Albert Licup, Abhinav Sharma, Fred C. MacKintosh, Paul A. Janmey, Scientific Reports, 2015)

5.1 Abstract

Cell traction is known to be an important modulator of tissue morphology. Contractile cells are also known to increase the modulus of biological hydrogels and diminish shear strain stiffening. Therefore, in this chapter cell traction is considered as an explanation for the differences observed between soft tissue and ECM rheology. This is investigated by comparing the rheology of plasma clots with and without platelets and whole blood clots in their native state and after inhibition of myosin IIa motors. The results show that the pre-stressed networks compression soften and extension stiffen, but the response is more symmetrical compared to collagen and fibrin networks. The absence of platelets or platelet contractility causes the clots to closely resemble reconstituted networks. There is little difference between the clots with and without red blood cells. Overall the results rule out cell traction induced pre-stress as the primary determinant of soft tissue mechanics. However, the results do contribute to the understanding of blood clot mechanics *in vivo*.

5.2 Introduction

Though the extracellular matrix (ECM) is commonly assumed to be the mechanical backbone of tissues; whole tissues show different mechanical behavior than reconstituted ECM networks. It was shown in Chapter 3 that semiflexible biopolymer networks, such as collagen and fibrin, show compression softening and extension stiffening. In addition the shear and axial moduli are uncoupled as a function of axial strain. Also, the collagen and fibrin networks tested show strain-stiffening. In contrast, brain, fat and liver tissue shear strain weaken ⁸²⁻⁸⁵. Additionally, these same tissues show an opposite response to multiaxial strain, showing hardening in compression and softening in extension ^{83,86,87,159}. However, a direct and comprehensive comparison of ECM and tissue mechanics has not been done.

The unexpected strength of semiflexible biopolymer networks has been hypothesized to originate from the bending rigidity of the fibers or pre-stress ^{62,64}. This pre-stress in tissues is likely to originate from cell traction on the network. The link between cell traction and tissue formation was described decades ago when Bell and colleagues monitored the contraction of collagen gels by fibroblasts. They observed how cells contracted collagen matrices, expelling water in the process, resulting in a 'tissue-like fabric'. Additionally they examined the effect of cytoskeletal disruption on the process ¹⁶⁰ Shortly after, Harris and Stopak investigated the traction potential of many cell types and found that fibroblasts exert forces much larger than needed for locomotion. They also made the observation that fibroblasts rearrange collagen networks in a manner that resembles tendon and organ capsules, concluding from this that the high cell traction was a means of controlling tissue morphology ¹⁶¹. Cell traction is now known to be an important factor of tissue morphogenesis ^{93,162,163}, but also to have a role in pathologies, most notably in metastasis ¹⁶⁴, fibrosis ^{89,165} and wound healing ^{166,167}.

Moreover, it was shown that cell traction can directly change network mechanics. The presence of platelets in plasma clots and fibrin gels, significantly increases the modulus of the gels and it results in a lower level of strain stiffening⁵⁶. Additionally, fibroblasts and mesenchymal stem cells were also shown to increase fibrin gel stiffness^{168,169}. The stiffness of a cell-seeded collagen gel is higher than that of an acellular gel¹⁷⁰.

In this chapter the effect of pre-stress in the network, imposed by cellular contractile forces, is investigated as a possible determinant of the discrepancy between tissue and ECM network mechanics. Hereto, plasma clots are prepared with and without platelets, and whole blood clots are prepared in their native state and compared to clots in which the contractile machinery of platelets is suppressed, by specifically inhibiting non-muscle myosin IIa. The results show that though changes in sample stiffness are observed, pre-stressed networks still compression weaken and extension stiffen. Differences are observed in the symmetry of the steady-state values and the dynamics of the systems.

5.3 Materials and methods

5.3.1 Preparation of platelet-rich and platelet-poor plasma

Blood donation were conducted in accordance with all appropriate guidelines and regulations and with approval of the Internal Review Board at the University of Pennsylvania (protocol nr. 805305). Human blood was drawn via venipuncture in K3EDTA, with informed consent from a healthy volunteer.

To prepare platelet-rich plasma the whole blood was prepared by spinning for 15 minutes at 120xG, from which the supernatant was removed and used. Platelet-poor plasma was prepared by spinning whole blood at 2200xG for 15 minutes. To prepare

plasma clots salmon thrombin and calcium was added to yield 2U thrombin /ml and 30mM Ca²⁺/ml. The samples were polymerized at 37°C.

5.3.2 Whole blood clots

Whole blood was pipetted directly between the rheometer plates prior to polymerization. For a number of samples blebbistatin was added to the blood at 5 µg/ml (17 µmol). The blood was polymerized between the rheometer plates for 1.5 hours at 37°C.

5.3.3 Rheometry

A strain-controlled rotational rheometer (RFS3, TA Instruments, New Castle, DE) was used with a parallel plate of 50 mm with a gap of 400 µm. The bottom plate incorporated a Peltier plate controlled the sample temperature at 37°C. The samples were pipetted between the plates prior to polymerization. After polymerization 1X phosphate-buffered saline with calcium and magnesium was pipetted around the free edge of the sample, to prevent drying and allow free fluid flow in and out of the sample. The shear moduli of the samples were measured by applying a low oscillatory shear strain of 1-2% at a frequency of 10 rad/sec. Axial strain was applied by changing the gap between the plates. Samples were subjected to small step-wise axial strains, between each consecutive step the samples were allowed to relax. Additionally, the samples were subjected to a 5% step-strain, either in compression, extension or shear. After which the storage modulus and stress (axial or shear) was monitored.

5.3.3 Imaging

Fibrin networks in whole blood clots were imaged by adding AlexaFluor-488 labelled fibrinogen (Life Technologies, Carlsbad, CA) in an estimated 1:40 molar ratio to blood samples. The samples were polymerized in between 2 glass slides with a Parafilm spacer.

The images were taken with a Leica DMIRE2 inverted fluorescent microscope. (Leica Microsystems, Buffalo Grove, IL).

5.4 Results

5.4.1 Platelet contractility increases storage moduli of whole blood and plasma clots

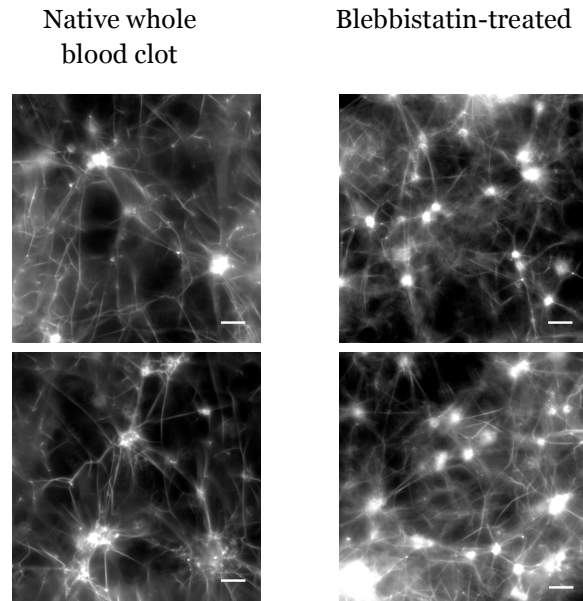
In Chapter 3 the strong effects of external stress on the shear moduli of collagen and fibrin networks were described. These results suggest that the generation of internal stresses within the network, such as are generated *in vivo* by cells, would alter the effects of axial strain on the shear rheology of the networks. To determine the effect of internal stress on fibrin networks, blood plasma was prepared with platelets (platelet-rich plasma, prp) and without platelets (platelet-poor plasma, ppp). Platelets bind the fibrin strands in a clot and put them under tension⁵⁶. Furthermore, whole blood clots were prepared in their native state and with the myosin IIa inhibitor, blebbistatin.

Blebbistatin was added to whole blood prior to polymerization, which prevents the actomyosin action in platelets and therefore the platelets ability to pull on the fibrin network. For whole blood clots the hematocrit of 40% is assumed to be the final red blood cell volume in the clots.

Because of the rigid adhesive boundaries the parallel plates provide, the fibrin networks in the clots with fully contractile platelets are put under significant stress. The development of axial stress, -46 Pa for prp (n=1) and -71.6 Pa \pm 2.9 for native whole blood clots, confirms this. The axial stress in the ppp and blebbistatin-treated samples is negative but small, in the order of single Pa. The axial stress was set to 0 Pa – by changing the off set in the software- at the start of every experiment.

The fibrin network of whole blood clots was imaged by incorporating Alexa Fluor-488 labeled fibrinogen. The imaging shows that the addition of blebbistatin to unpolymerized whole blood results in a well-developed fibrin network, with significant platelet aggregation. (Figure 5.1)

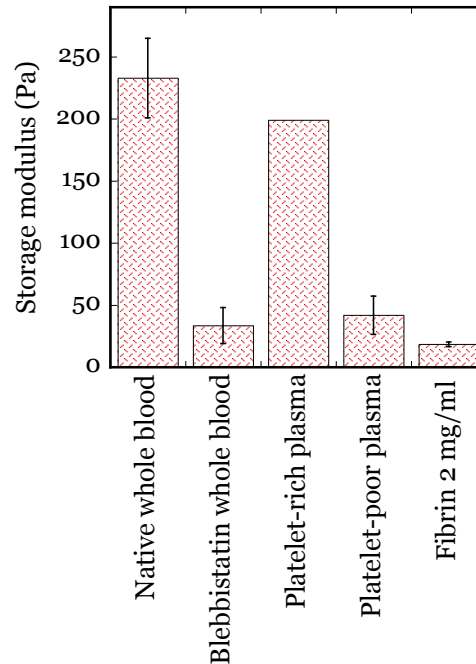
Figure 5.1: Imaging of fibrin network in whole blood clots. Native state (left) and with blebbistatin treatment (right). Fluorescent imaging of fibrin network by incorporation of Alexa Fluor 488-fibrinogen.



The presence of platelets or platelet contractility causes the moduli of the fibrin networks to increase drastically. The storage modulus of prp in absence of axial strain is 199 Pa (n=1), and that of ppp 41.9 Pa \pm 15.4 (n=2). The storage modulus of native whole clots is 232.0 Pa \pm 32, with blebbistatin 33.7 Pa \pm 14.5. Additionally fibrin at a concentration of 2 mg/ml (data from Chapter 3) is shown to compare the values to a fibrin network at physiological concentration, which has a modulus of 18.6 Pa \pm 1.9. (Figure 5.2)

All clots are highly elastic. The loss tangents of prp and ppp are 0.046, and 0.45 \pm 0.021 respectively. The loss tangents of whole clots are 0.038 \pm 0.006, and 0.070 \pm 0.02 for native and blebbistatin-treated clots, respectively.

Figure 5.2: Storage moduli of whole blood, plasma and fibrin clots. The storage modulus of whole blood clots at 1% shear strain; and of plasma clots and fibrin at 2% shear strain, all in absence of axial strain. For whole clots and fibrin the mean of 3 samples is shown \pm SD; for prp 1 sample is shown, for ppp the mean of 2 samples is shown \pm SD



5.4.2 Pre-stressed clots weaken when compressed and strengthen in extension, with symmetry between compression and extension.

After polymerization the clots were subjected to a series of incremental compressions, after which the gap was slowly returned to the original gap and a series of incremental extensions was applied. The moduli and axial stresses were monitored during this process. For both prp and native whole clots the storage modulus drops in compression and increases in extension. (Figure 5.3a) However, in contrast with the collagen and fibrin networks (Chapter 3), the slope of the storage modulus is linear over almost the whole range of axial strains. Note the axial strain range is larger than in Chapter 3. For native whole blood the axial stress is linear over the whole range of axial strains as well. For prp the slope in extension is higher than the slope in compression, but only about 3

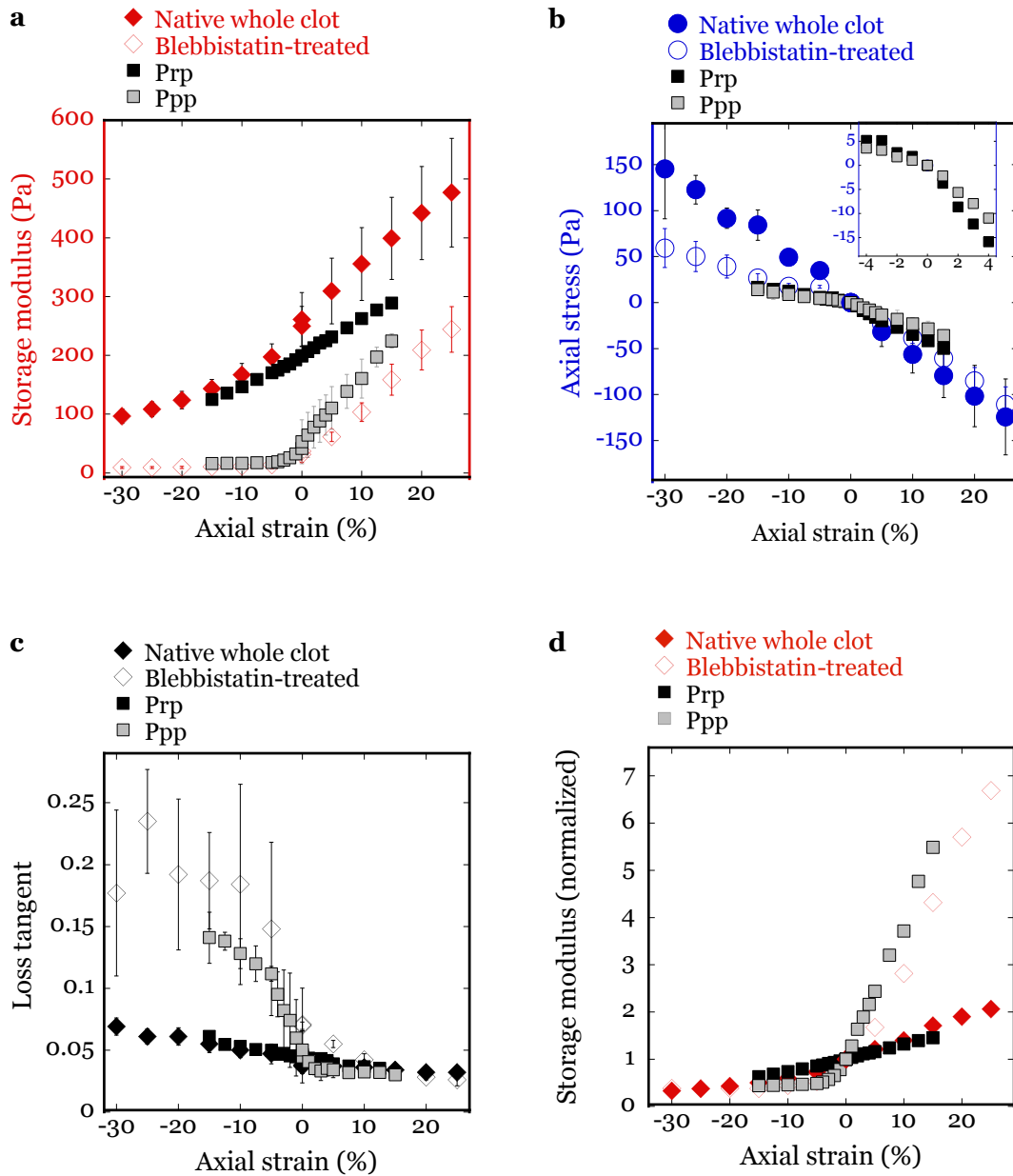


Figure 5.3: Native and blebbistatin-treated whole clots, platelet-rich and platelet-poor plasma clot show compression softening and extension stiffening. Rheology of native, blebbistatin-treated whole clots, ppp, and prp at low shear strains (1-2%) at increasing levels of axial strain, showing the storage moduli (a), axial stresses (b), loss tangents (c), and normalized storage moduli (d). The data from (a), (b) and (c) are obtained simultaneously with the shear rheometer. For prp 1 sample is shown. For ppp the mean of 2 samples \pm SD is shown, for whole clots 3 samples \pm SD.

times. (Figure 5.3**b**) The loss tangents of both prp and whole blood are small and change little with the application of axial strain. (Figure 5.3**c**)

5.4.3 Inhibiting platelet contractility in whole and plasma clots results in clots that resemble fibrin networks.

Ppp and blebbistatin-treated whole clots were tested and compared to prp and native whole clots, to elucidate the effect of platelets and specifically active contractility on clot mechanics. Ppp was tested similarly as prp and whole clots; blebbistatin-treated clots were axially strained either in compression or extension. The response of the storage modulus to axial strains shows asymmetry (Figure 5.3**a**) that compares well with a physiological concentration of fibrin (Figure 3.6). Figure 5.3**d** shows normalized storage moduli of all clots, which further illustrates the similarity between the clot types with contractile cells, and between the clot types without pre-stress.

The axial stress-strain curve of ppp shows a similar asymmetry compared to prp (see inset Figure 5.3**b**). Blebbistatin-treated clots show a higher asymmetry compared to native clots in the response to axial strain. However, the asymmetry in neither ppp nor blebbi-clots is as drastic as seen in 10 mg/ml fibrin and collagen networks. The loss tangents of ppp and blebbistatin-treated whole clots vary more with axial strain application compared to their counterparts with active cell contractility. Both types of clots quickly become more viscous in compression. (Figure 5.3**c**)

Figure 5.4 shows additional simulations of the networks comparing the curves in Figure 3.7, which were generated in absence of pre-stress, to networks with an imposed pre-stress equivalent to 10% extension and 10% compression. Both the storage moduli and axial stresses show a 10% shift in their response. The compressed networks stiffen later;

the extended networks stiffen earlier. As a result the extended curves show a symmetric response around 0% axial strain.

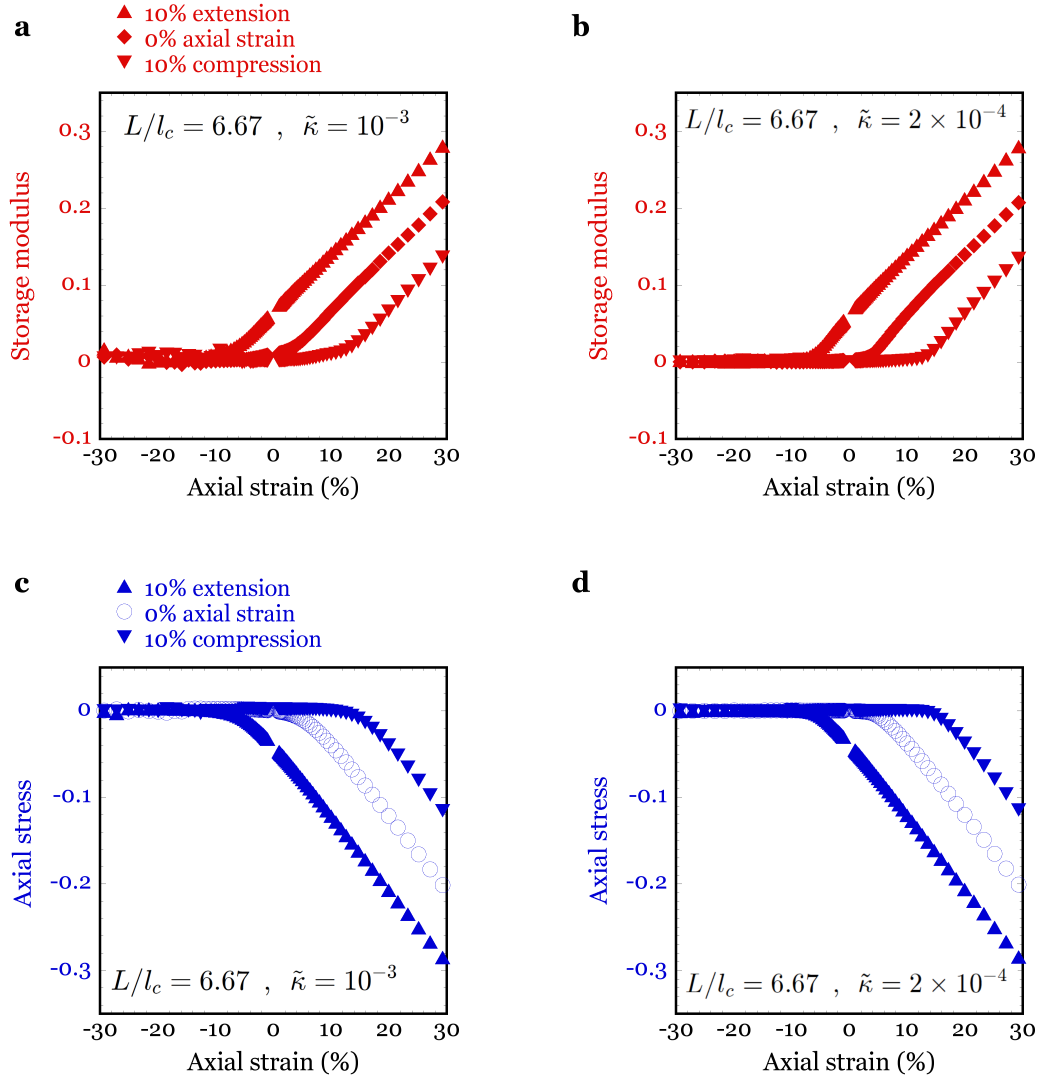


Figure 5.4: Simulations of storage moduli and axial stresses predict multiaxial behavior of semiflexible biopolymers. Simulation for a diluted phantomized triangular network (3D) with varying pre-stress and $L/L_c = 6.67$. **(a, c)** show the storage modulus, **(b, d)** show the axial stresses. The normalised bending modulus $\tilde{\kappa} = 10^{-3}$ corresponds with fibrin **(a, b)**, $\tilde{\kappa} = 2 \times 10^{-4}$ with collagen **(c, d)**.

Comparing prp to ppp and native to blebbistatin-treated whole clots reveals that the curves are not merely shifted. Prp and ppp would not overlap at any point within the tested range; even if the curve would be shifted on both the x and y axis. The whole blood clots do have the same slope at higher levels of extension. However, the storage moduli of the blebbistatin-treated clots level out quickly in compression, whereas the whole clots show a more gradual decrease after 10% compression.

5.4.4 Stress-relaxation is changed by platelet-contractility.

To further determine the mechanical behavior of pre-stressed networks, the dynamics of whole clots were followed as axial strains were applied. The networks were subjected to a 5% compression or extension; the storage moduli and axial stresses were followed over time. The storage moduli of whole clots do not show a peak or relaxation, both in compression and extension. During the application of axial strain, which starts at 5 sec, the storage modulus moves to the new value and stays fairly constant for the rest of the time. In compression, certain samples show a modest recovery after the compression is completed. Additionally, when extended samples are released to a lower level of extension, a more prominent recovery is seen. (data not shown) The axial stress of the same samples shows a strong increase and relaxation. (Figure 5.5a, b) Blebbistatin-treated clots have significant peak storage moduli both in extension and compression. After this the storage modulus drops; it falls below the initial modulus when compressed and levels out above the initial modulus when extended. The axial stresses of the blebbistatin-treated clots show peaks when axially strained.

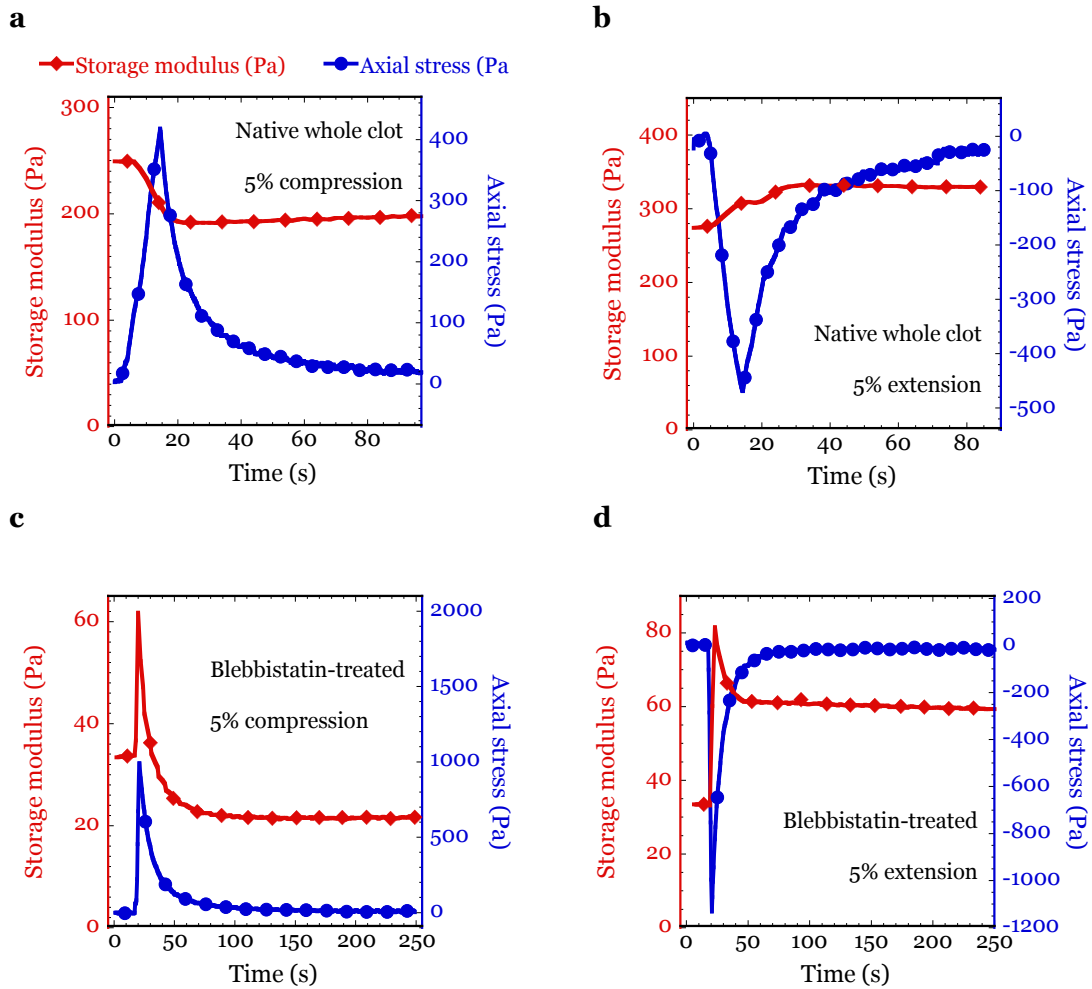


Figure 5.5: Dynamics of storage moduli and axial stresses of native and blebbistatin-treated whole blood clots. A 5% compression (a, c) or extension (b, d) was applied to native (a, b) or a blebbistatin-treated (c, d) clots. The storage modulus is measured with a 1% shear strain.

Next the relaxations of the storage moduli and axial stresses were looked at in more detail and compared to the relaxation of the shear stress after a 5% step shear strain. Even though the storage moduli of the blebbistatin-treated clots relax significantly compared to native clots (Figure 5.6a, b), the relaxation is less than what is observed for

2 mg/ml fibrin networks (Figure 4.8). Shear stresses of both native and blebbistatin-treated clots relax minimally compared to the axial stresses. The extensional stress of native clots levels off before the compressional stress. For blebbistatin-treated clots the compressional stress levels off before the extensional stress. (Figure 5.6c, d) This is different than 10mg/ml fibrin and collagen. (Figure 4.6, 4.7)

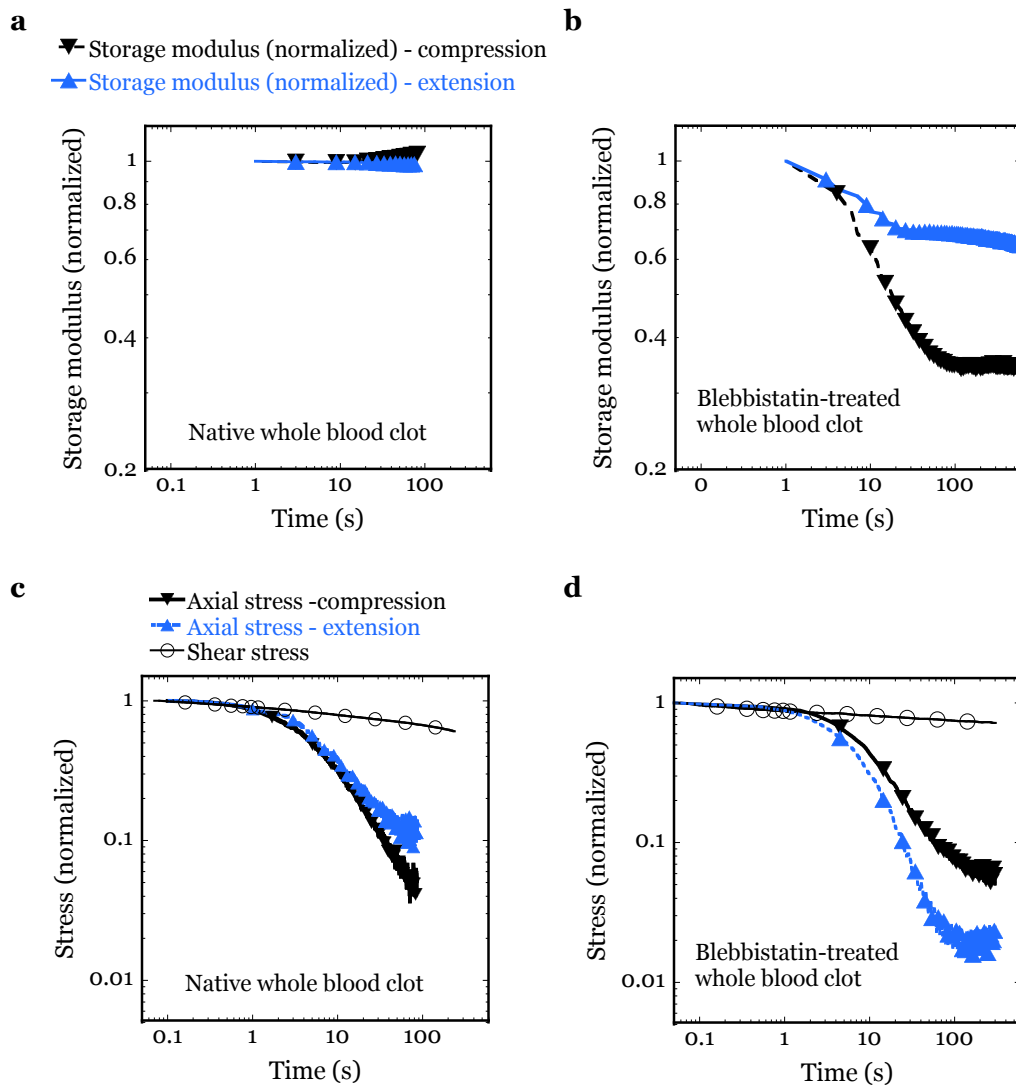


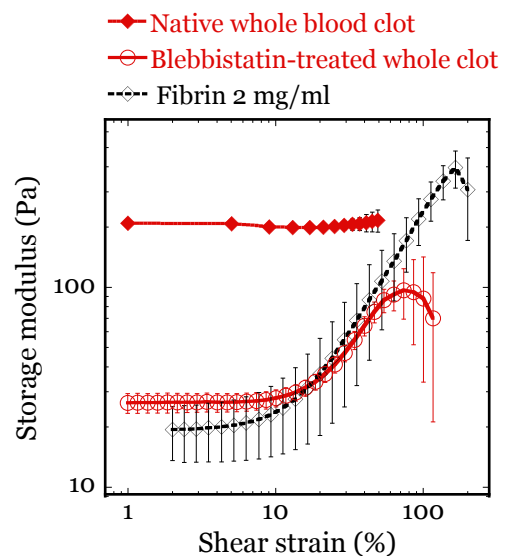
Figure 5.6: Stress-relaxation of native and blebbistatin-treated whole blood clots. The axial stress in compression and extension, and shear stress after a 5% strain is followed in time and normalized to the peak stress. The mean of 3 samples is shown.

5.4.5 Strain amplitude dependence decreases in pre-stressed networks

To further assess the effect of platelet contractility on clot mechanics the effect of an increasing strain-amplitude was investigated. Native whole clots show a very low level of strain-stiffening at the tested range of 1-50% shear strain. Inhibition of myosin IIa with blebbistatin restores the strain-stiffening in whole clots, though 2 mg/ml fibrin networks (from Figure 3.3c) strain-stiffen more dramatically. Both native and blebbistatin-treated whole clots show negative normal stresses with increasing shear strains. (data not shown)

In Figure 3.3 it was shown that the shear storage moduli of fibrin networks with and without pre-stress converge at high shear strains. When comparing the pre-stressed native whole clots and 2 mg/ml fibrin networks, it seems likely that the storage moduli would indeed converge- if native whole clots would have been tested up to higher shear strains.

Figure 5.7: Strain-amplitude dependence of the storage moduli of native and blebbistatin-treated clots compared to fibrin networks. The storage modulus is shown as a function of the applied shear strain at a constant frequency of 1 rad/s.



5.5 Discussion

In Chapter 3 it was shown that the Young's moduli of semiflexible biopolymer networks are not proportional to their shear moduli and both moduli are strongly affected by even modest degrees of axial strain, showing compression softening and extension stiffening. In an effort to elucidate the effect of cell traction mediated pre-stress on the network mechanics, plasma clots with and without platelets were compared as well as whole blood clots in their native state and after blebbistatin treatment to specifically inhibit myosin IIa. The results show that the pre-stressed networks also compression soften and extension stiffen. However, the asymmetry seen in fibrin and collagen networks in Chapter 3 is absent for the storage moduli. The axial stress of the native whole clots is symmetric over the whole range of axial strains as well. The prp sample shows some asymmetry in the axial stress response, though this is not different for ppp. When the pre-stress is absent the samples closely resemble collagen and fibrin networks described in Chapter 3.

The increase in storage moduli due to active pre-stress generation, as well as the diminished shear strain stiffening, has been described before with regular shear rheometry^{56,168,169}. The multiaxial rheology reveals several interesting features. Even though the networks still compression soften and extension stiffen, the symmetry of the response is greatly enhanced. The simulations reveal that a 10% extensional pre-stress results in a symmetric response between 7% compression and 29% extension. We can estimate the internal pre-stress in the experimental systems from the development of axial stress during polymerization, while the gap is kept at a constant height. For whole blood clots with an average storage modulus of 232 Pa the axial stress is on average -71.6 Pa, which is 30.9% of the storage modulus. For prp with a modulus of 199 Pa the axial stress is -46 Pa, which is 23.1%. Though this number cannot be compared directly to the

amount of pre-stress used in the simulations, it indicates that there is a higher pre-stress than 10%. It is therefore likely that the symmetry seen over the whole test range for prp and native whole clots, is due to the higher pre-stress imposed on the network.

The simulations show a simple shift in the response of the network to axial strain, with imposed pre-stress. This is not seen when comparing the non-stressed networks - collagen, fibrin, ppp, and blebbistatin-treated clots- to prp and native whole clots.

However, there are several parameters that could contribute to these differences. The platelets do not only put tension on the networks, they also form aggregates and form additional cross-links in the network¹³⁷. Ppp, fibrin and collagen are branched and entangled. Blood proteins other than fibrin that are present in the clots prepared from plasma and whole blood could also be important. Albumin, globulins and fibronectin are present in plasma and are known to influence fibrin structure and mechanics¹⁷¹⁻¹⁷³.

Between the plasma and whole blood clots, the obvious difference is the presence of 40% red blood cells, which alters network structure¹⁷⁴⁻¹⁷⁶. Also, to prepare plasma one or two spinning steps are necessary (for prp and ppp respectively). Whole blood is used directly to form clots for each experiment.

The stress relaxation of native whole blood clots shows an interesting feature. The storage modulus quickly reaches its new value when axially strained, without a pronounced peak, or relaxation otherwise. The same was observed with passive fibrin and collagen networks at very small axial strains in Chapter 4. However, in this system a 5% axial strain was applied to a sample with a large diameter (50mm). It is likely that the effect of the pre-stress is what dominates the response here. When a sample is compressed the tension on the network nodes is released and hence the shear modulus drops. This effect apparently dominates the stiffening effect that will arise due to

poroelastic effects. However, poroelastic effects are clearly present, concluding from the axial peak stress and subsequent relaxation. This is another indication that the axial and shear mechanics are decoupled in these systems. A subtle feature is that the storage moduli of whole blood clots sometimes modestly recover after a compression (and after deextension). This points towards active modulation of traction by platelets as a response to mechanical forces, which has been observed previously^{177,178}.

The axial stress-relaxation of blebbistatin-treated clots shows a deviation: extensional stresses of the biopolymer networks shown in Chapter 4 level out before the stresses in compression, for blebbistatin-treated clots this is reversed. This difference could originate in the presence of cross-linking in the clots, as well as the presence of red blood cells. The differences in the peak stresses of native and blebbistatin-treated clots are due to the speed at which the clots were axially strained, which was higher for the blebbistatin-treated clots.

An important conclusion from comparing plasma and whole blood is that the presence of red blood cells, at 40% hematocrit, has no apparent influence on the multiaxial rheology. When comparing the pre-stressed samples; prp clots, which have no red blood cells and whole blood with a 40% red cell density, there is very little difference. The differences seen – for example in the level of symmetry of the axial stress- could originate from the variability in preparation of the clots. Ppp, blebbistatin-treated clots and fibrin show little difference in their mechanical behavior, even though there are differences between these clots. Ppp and blebbistatin-treated clots contain a high amount of blood proteins, like albumin, globulin and fibronectin, which are absent in fibrin networks. Blebbistatin-treated whole clots also contain 40% red cells.

Concluding, though cell traction mediated pre-stress in semiflexible biopolymer

networks does change the mechanics of the networks, it does not explain the difference between biopolymer networks and whole tissues. The volume conserving effect of 40% red blood cells also does not switch the mechanical behavior of the clots to resemble whole tissues. Though these results exclude cell traction as the primary determinant of soft tissue mechanics, the results are relevant for understanding blood clots mechanics *in vivo*. Both whole blood and plasma clots form *in vivo* and are subject to compression and extensional deformation due to vessel dilation and contraction as well as shear stresses from blood flow.

Author Contributions

AvO and PAJ designed experiments. AvO performed experiments and data analysis. MV, AL, AS and FCM developed the computational model. MV and AL performed the simulations and MV analyzed the resulting data. AvO wrote manuscript.

CHAPTER 6: THE EFFECT OF CELL PACKING DENSITY ON MULTIAXIAL RHEOLOGY OF EXTRACELLULAR MATRIX AND MODEL TISSUES

6.1 Abstract

The discrepancy between the multiaxial rheology of soft tissues and extracellular matrix networks cannot be explained by pre-stress imposed on the networks by contractile cells. A red blood cell density around the natural hematocrit does not change the ECM mechanics to resemble tissues either. Therefore, fibrin networks with dense red blood cell or bead packing were tested. The results show that close red cell packing in blood clots reverses the behavior of the clots from compression softening to stiffening; and from extension and shear strain stiffening to softening, resembling soft tissues. The same effects can be mimicked by embedding chemically inert beads into a fibrin network at densities approaching the jamming threshold for granular and colloidal materials. It is suggested to approach soft tissues as jammed systems. More work needs to be done to understand the physics of these bead-network constructs. These results could have implications for understanding the mechanics of tissues *in vivo*.

6.2 Introduction

In this chapter the discrepancy between tissue and ECM mechanics is investigated further using blood clots as a simple tissue model. In Chapter 5 the effect of cell traction was investigated but it was found that the resulting pre-stress did not change the multiaxial rheology of porous biopolymer networks to resemble the mechanical behavior of whole tissues. Moreover, it became apparent that the presence of a 40% red blood cell volume in fibrin networks does not have a significant effect on multiaxial rheology either. Therefore, to assess cell density as a determinant of tissue mechanics, contracted clots

are tested here, in which the red cells are tightly packed. Additionally, the effect of cell packing on the multiaxial rheology of fibrin networks is explored further by embedding inert beads into the network in absence of contractile cells. The results show that contracted clots behave similarly to multiaxial strains as whole tissues. Furthermore, tissue-like behavior can be mimicked by embedding a high density of cross-linked dextran beads in the network, mimicking the presence of cells, even in the absence of platelets.

These findings will have implications on the understanding of the mechanical environment of cells *in vivo*; modeling of soft tissues as well as the use of tissue engineered constructs in clinical applications.

6.3 Materials and methods

6.3.1 Contracted clots from rat blood

Contracted clots were prepared from rat blood. The animals were sacrificed for the purpose of other experiments performed according to all appropriate national guidelines and with approval of Institutional Animal Care and Use Committee of the University of Pennsylvania. The blood was collected after dissecting the vena cava, without the use of anti-coagulant. The blood was immediately transferred to a tissue culture dish. The resulting disc-shaped contracted clots were detached from the well and transferred to the rheometer plate. To ensure proper attachment to the rheometer plates a high concentration fibrin solution (20-25 mg/ml) was used to glue the clots to the upper and lower plate.

6.3.2 Fibrin networks with beads

Fibrinogen (Fbg) isolated from human plasma (product # 342576, CalBioChem, EMD Millipore, Billerica, MA, USA) was dissolved at 42 mg/ml in 1X T7 buffer and dialyzed overnight.

Beads made from cross-linked dextran (Sephadex G-75, GE Health Sciences) were swollen with distilled water. The amount of water was adjusted to accomplish a 92% swelling. For rheometry, fibrinogen, 10X T7 buffer, CaCl₂ solution, thrombin and distilled water were added to a bead solution to yield a 5 mg/ml fibrin network in a 1X T7 buffer with 0.5U thrombin/mg fibrin and a 50%, 60% or 70% volume of beads, based on the presumed continued swelling of 92% swollen beads when placed in excess water. Samples were polymerized for 90 minutes at 37°C. Once fully swollen, the dextran beads have a diameter between 90 and 280 μm, have an exclusion limit of 80 kDa (hence fibrinogen is excluded), and behave like rigid spheres obeying D'Arcy's law.

6.3.3 Rheometry

A strain-controlled rotational rheometer (RFS3, TA Instruments, Newcastle, DE, USA) was used with a parallel plate of 25 mm diameter. The gap was dependent on sample thickness for contracted clots, ranging between 1.5 and 3 mm, and 1mm for all bead embedded-fibrin networks.

The bottom plate incorporated a Peltier plate allowing to control the samples temperature at 37°C. Appropriate buffer was pipetted around the free edge of the sample, to prevent drying and allow free fluid flow in and out of the sample if possible.

The shear moduli of the samples were measured by applying a low oscillatory shear strain of 2% at a frequency of 10 rad/sec. Axial stress was collected separately with a

ProLink instrument amplifier and Logger Lite software (Vernier, Beaverton, OR, USA). Axial strain was applied by changing the gap between the plates.

Samples were subjected to several tests varying the axial and shear strain. A number of samples was subjected to a series of incremental axial strains while measuring the axial stress and shear moduli. The step-size of the axial strain was relatively small and the samples were allowed to relax prior to applying another axial strain step. Other samples were subjected to a large step of strain (both shear and axial) after which the stress relaxation was recorded.

In addition to axial stresses collected with the shear rheometer, the axial stress of contracted clots was measured with a tensile tester (Instron 5564, Norwood, MA, USA).

6.4 Results

6.4.1 Contracted clots respond oppositely to axial strain as whole blood clots, plasma clots, and reconstituted networks.

The results in Chapter 5 revealed that cell traction and a 40% red blood cell volume do not cause the mechanics of blood clots to resemble tissues. Therefore, contracted blood clots are tested here to investigate the effect of dense cell packing on multiaxial rheology. Allowing whole blood to contract in a plate with some adhesion of the fibrin network to the side and bottom, results in disc-shaped contracted clots. These clots effectively have no free fluid in them, and the red blood cells will be packed together tightly. The contracted clots can easily be detached and transferred between the rheometer plates, without shape changes. To ensure proper adhesion, fibrin glue was used both on the bottom and upper plate.

When performing extension and compression series, contracted clots show behavior opposite from whole blood clots, and similar to liver, fat and brain. The storage moduli increase linearly with compression and show a decrease in extension, which levels off at higher extensions. The axial stress shows asymmetry but opposite from ECM networks, the slope in compression is larger than in extension. In extension the axial stress levels off. The loss tangent of contracted clots is higher than the reconstituted networks and other clots tested previously. Also, the loss tangent shows a decreasing trend in compression, which is opposite from what was observed in reconstituted networks, blood, and plasma clots. (Figure 6.1)

6.4.2 Shear rheology of contracted clots can be mimicked by embedding beads in a fibrin network, in absence of contractile cells

The large difference between whole clots, with 40% red blood cells, and contracted clots, with >90% red blood cells, motivated looking closer at the possibility that the rheology of contracted clots and tissues is dominated by dense cell packing alone.

A fibrin network of 5 mg/ml fibrin was prepared with several volume densities of beads. The initial bead volumes were 50%, 60% and 70%. The fluid that remains in these constructs can flow in and out of the network, therefore the bead volume ratio will change with applied axial strain. The constructs were imaged with Alexa Fluor-488

Contracted rat blood clots

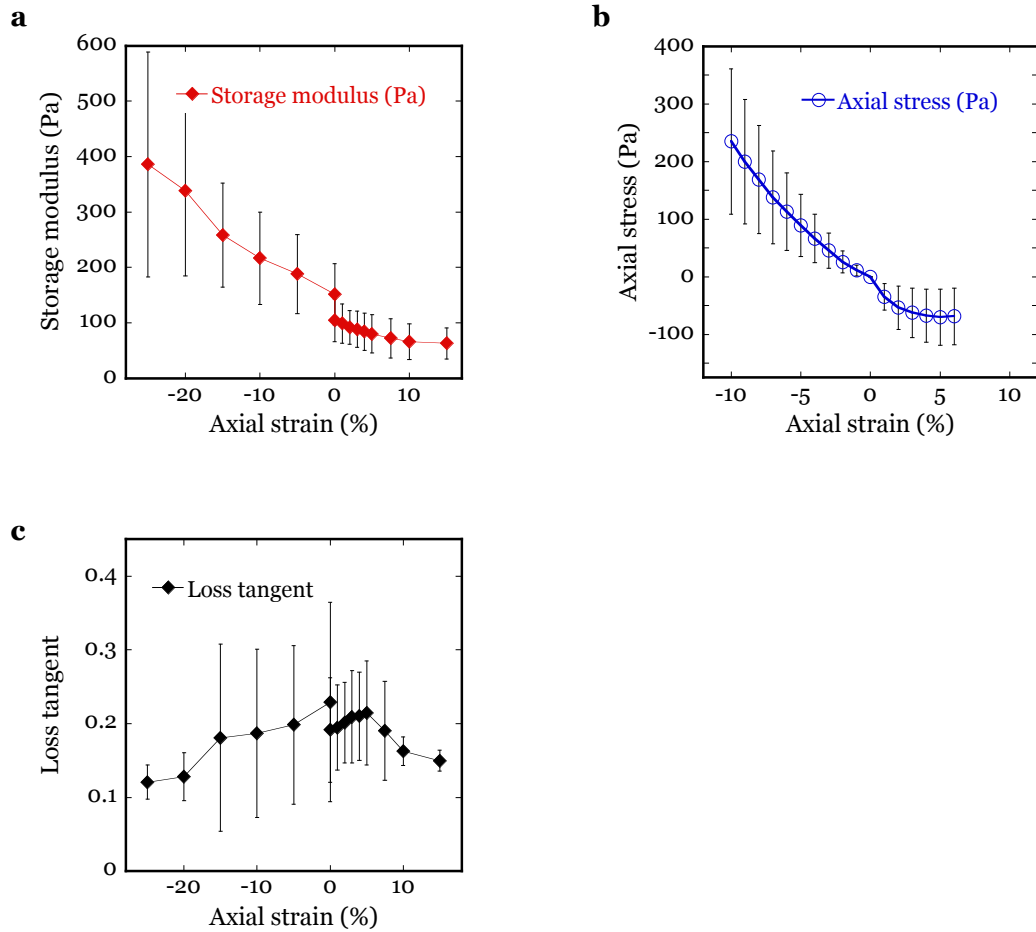


Figure 6.1: Contracted clots compression stiffen and extension weaken. Rheology of contracted rat blood clots at low shear strains (2%) at increasing levels of axial strain, showing the storage modulus (a), axial stress (b) and loss tangent (c). The data from (a), and (c) are obtained simultaneously with the shear rheometer. The axial stress data in (b) are obtained with the tensile tester. The mean of 5 samples is shown \pm SD.

fibrinogen added to the fibrinogen solution at a 1:40 molar ratio. This revealed that the beads are orders of magnitude larger than the mesh size of the network. In between the packed beads sits a well-developed network. At the positions where beads get in close proximity of each other there is still fibrin present. However, the images indicate that -as expected from the exclusion limit of the beads- the fibrin network is fully excluded from the beads. (Figure 6.2)

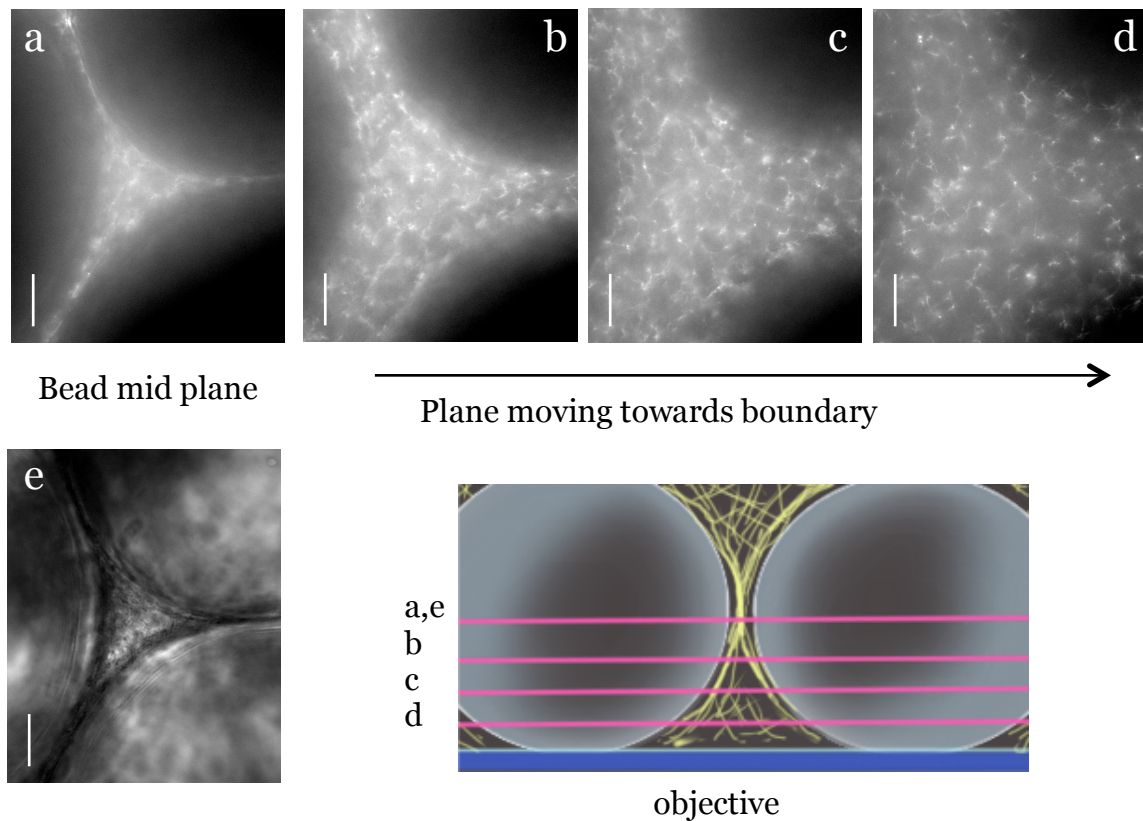


Figure 6.2: Imaging of 3 jammed beads within fibrin network at different depths. A 50% bead- fibrin construct is shown. Images show fibrin network imaged with ALEXA-488 Fbg incorporation (**a**, **b**, **c**, **d**). Phase contrast image of beads (**e**) corresponding with fluorescent image (**a**).

Figure 6.3 shows the response of the storage modulus, axial stress and loss tangent to axial strain for all three constructs. The storage modulus of networks with an initial bead volume of 50% shows an initial decrease in compression; similar to fibrin, ppp and whole clots. However, after a couple of percent compression the trend reverses and the constructs start to stiffen with increasing compression. The storage modulus increases with extension. For constructs with a 60% and 70% initial bead volume there is no

significant weakening in compression; the constructs stiffen fairly constantly over the whole range of compression. In extension the 60% bead constructs stiffen similarly as the 50% constructs. However, the 70% bead constructs stiffen less in extension.

The axial stress of the 50% constructs shows similar asymmetry as fibrin and ppp between -7.5% and 20% axial strain. It has a small slope in the initial phase of compression, however, the slope increases at higher compressions. The axial stresses of the 60% and 70% bead constructs behave almost identically. The slope of the axial stress is similar in extension and the initial phase of compression, at higher levels of compression the axial stress curves up. The axial stresses of the 60% and 70% bead constructs have larger slopes over the whole range of compression compared to the 50% constructs.

The loss tangents of all constructs drop in extension. In compression the loss tangents initially increase, however, for all constructs this trend reverses. This reversal is most pronounced and has the earliest onset in the 70% bead constructs.

When a 70% bead solution is put between the rheometer plates, there is no significant storage modulus. When compressed up to 35% the storage modulus is $92 \text{ Pa} \pm 85 \text{ Pa}$, with a loss tangent of $0.35 \text{ Pa} \pm 0.21$ ($n=4$) (data not shown). Additionally, the storage modulus of the fibrin used for the constructs was tested in absence of beads at 5 mg/ml, which was $87.5 \text{ Pa} \pm 30.3 \text{ Pa}$ ($n=4$) (data not shown).

In addition to using dextran beads, this experiment was also performed with 10 mg/ml fibrin networks with densely packed red blood cells which were lightly fixed with 0.5% glutaraldehyde. The results in these constructs show extensive compression stiffening and mild extension stiffening, similar to the 70% bead – fibrin constructs (data not

shown), indicating that the results are independent of the size and shape of the embedded particles.

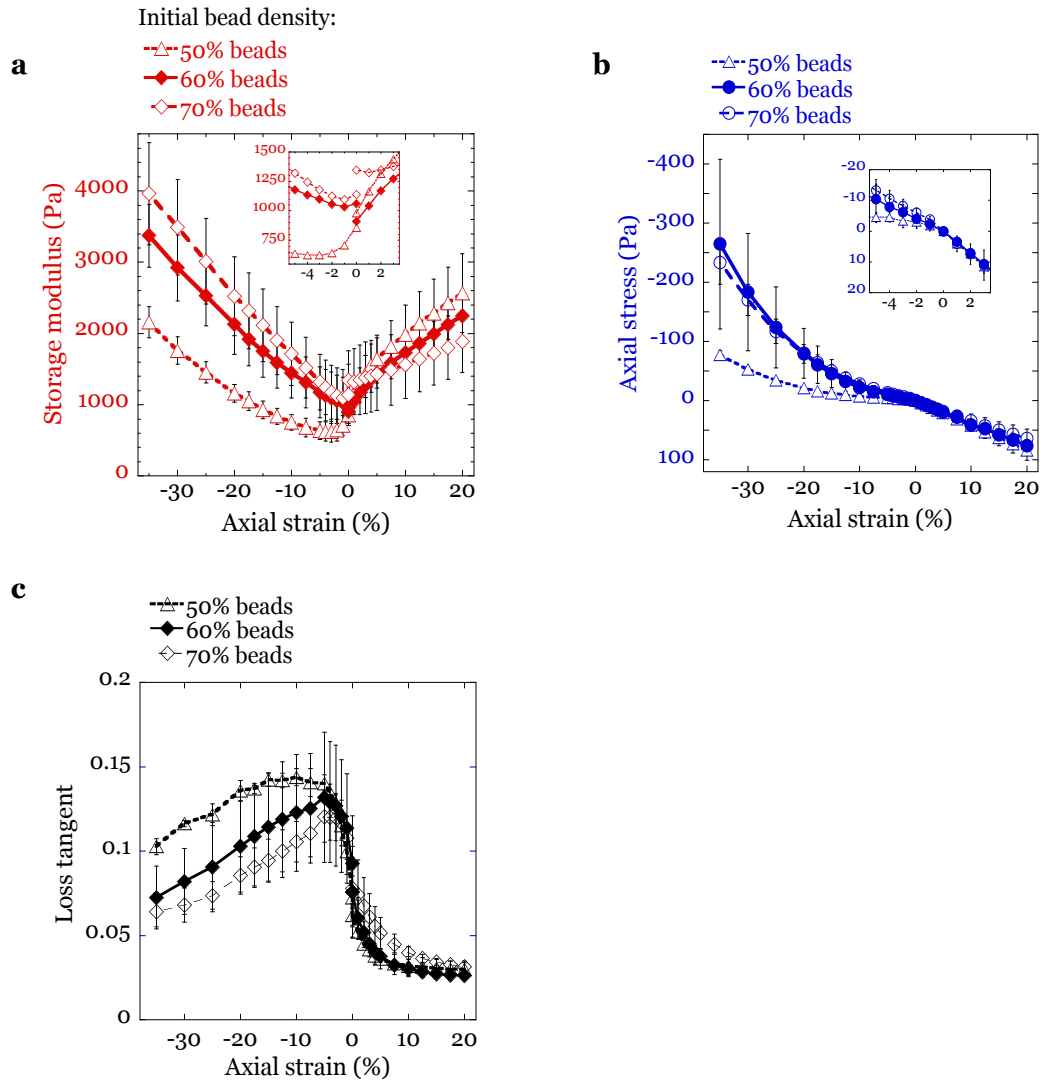


Figure 6.3: Beads embedded in a fibrin network change multiaxial rheology to resemble tissues when bead density reaches a critical value. Rheology of fibrin-bead constructs at low shear strains (2%) at increasing levels of axial strain, showing the storage modulus (a), axial stress (b) and loss tangent (c). The data from (a), (b) and (c) are obtained simultaneously with the shear rheometer.

6.4.3 Dynamics and stress-relaxation of contracted clots and constructs

As a follow up on the equilibrium results the dynamics of the storage moduli and axial stresses of contracted clots and fibrin-bead constructs were investigated. The dynamics of the storage moduli and axial stresses of the contracted clots and fibrin-bead constructs were followed for a 5% step compression or extension (Figure 6.4), which is applied quickly at $t = 10$ seconds. The storage moduli of contracted clots do not show a peak. In compression the storage modulus keeps increasing slightly after the compression has been applied. The axial stress in compression shows a continued relaxation. The storage modulus of the 50% beads still resembles a fibrin network, with a pronounced peak and a drop below the initial modulus. The peak decreases with increasing bead density, and the modulus stays above the initial value. The storage modulus shows no visible peak in extension for the 50% and 60% constructs, the 70% construct does show a peak, however, the storage modulus drops back to a value close to the original value. The relaxation of the storage modulus, normalized to the peak value, confirms the trends in the dynamics. (Figure 6.5) Here the values are plotted for longer time periods. In compression, it shows that at a longer time scale the storage modulus curves up mildly.

Figure 6.6 shows the axial stress relaxation after the 5% step axial strain and additionally the shear stress after a 5% step shear strain. The shear stress and axial stress relaxations are small for contracted clots, and both slower and less dramatic compared to the whole clots. (Figure 5.7) The bead- fibrin constructs with an initial bead density of 50% show quick relaxation in the axial direction, the stress in extension levels out quicker than compression. This behavior is very similar to the stress-relaxation of fibrin and collagen described in Chapter 4 (Figure 4.6). However, with 60% and 70% beads the axial stress in compression levels out before the stress in extension. The level of extensional relaxation stays roughly constant in all bead-fibrin constructs.

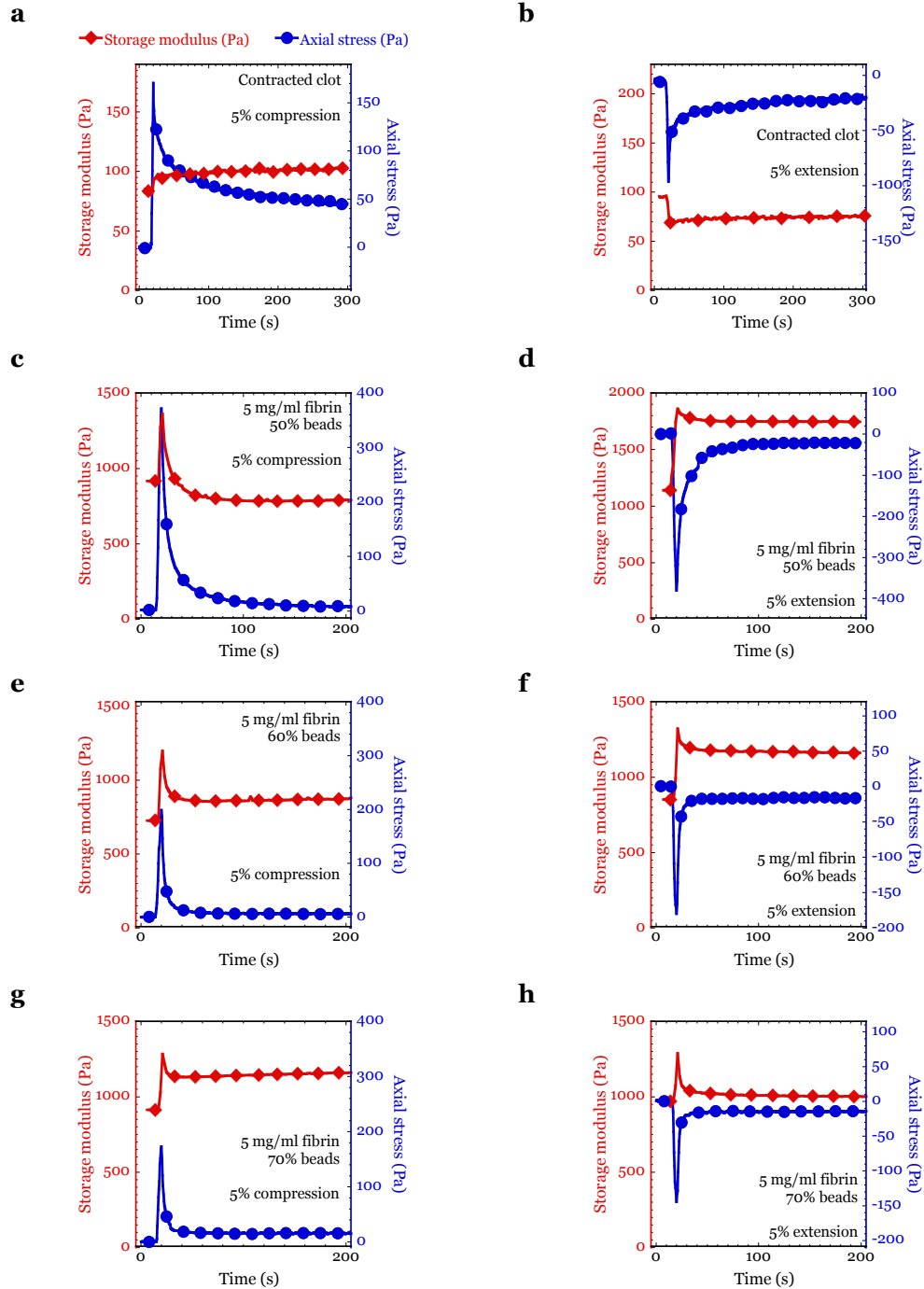


Figure 6.4: Dynamics of storage moduli and axial stresses of contracted clots and fibrin-bead constructs. A 5% compression (**a, c, e, g**) or extension (**b, d, f, h**) was applied, to contracted clots (**a, b**), and 5 mg/ml fibrin networks with 50% beads (**c, d**), 60% beads (**e, f**), and 70% beads (**g, h**). The mean of 3 samples is shown, except for compressed contracted clots and 70% ($n=4$). 3-5% of data points is depicted with a symbol.

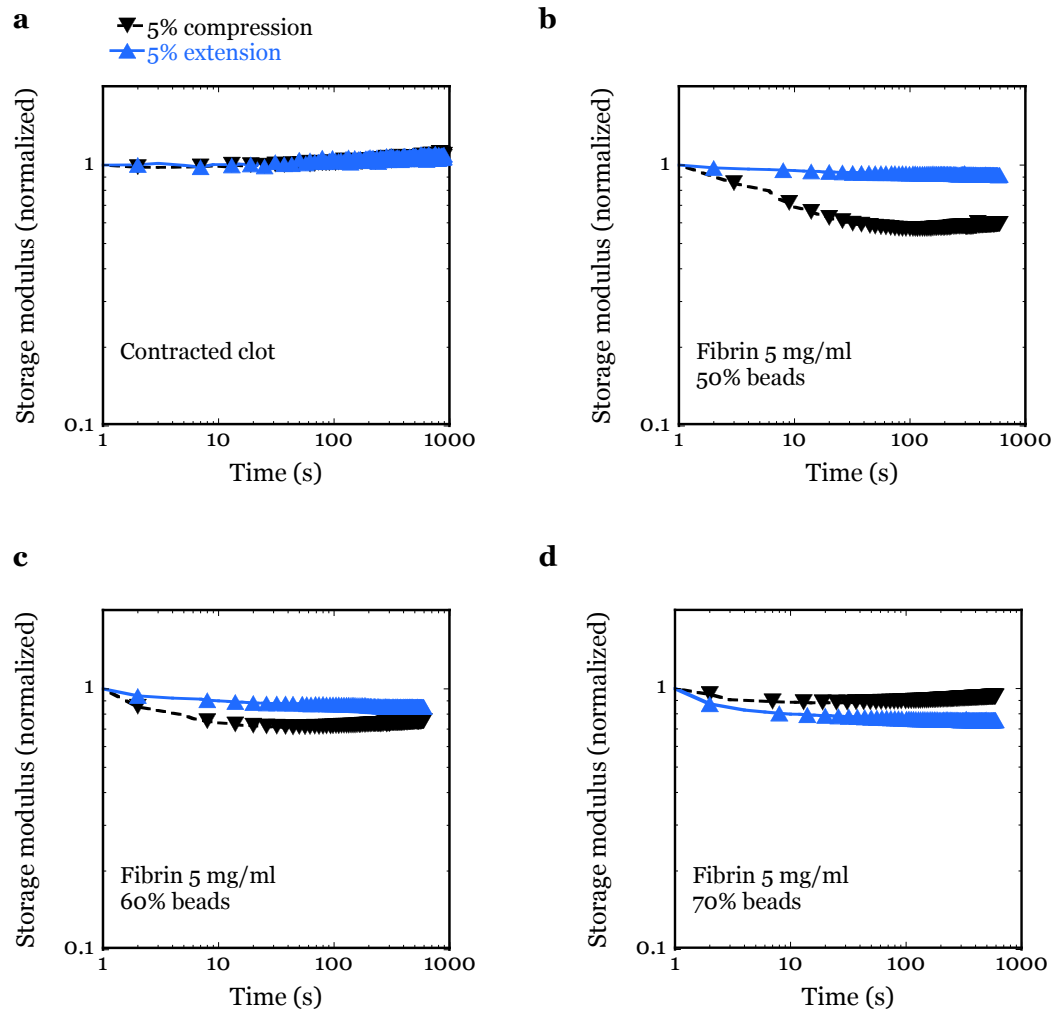


Figure 6.5: Relaxation of storage modulus after axial strain application of contracted clots and fibrin-bead constructs Stress-relaxation in compression, extension and shear is shown, normalized to the peak stress of (a) contracted clots (b) fibrin-bead construct with 50% beads, (c) constructs with 60% beads and (d) constructs with 70% beads.

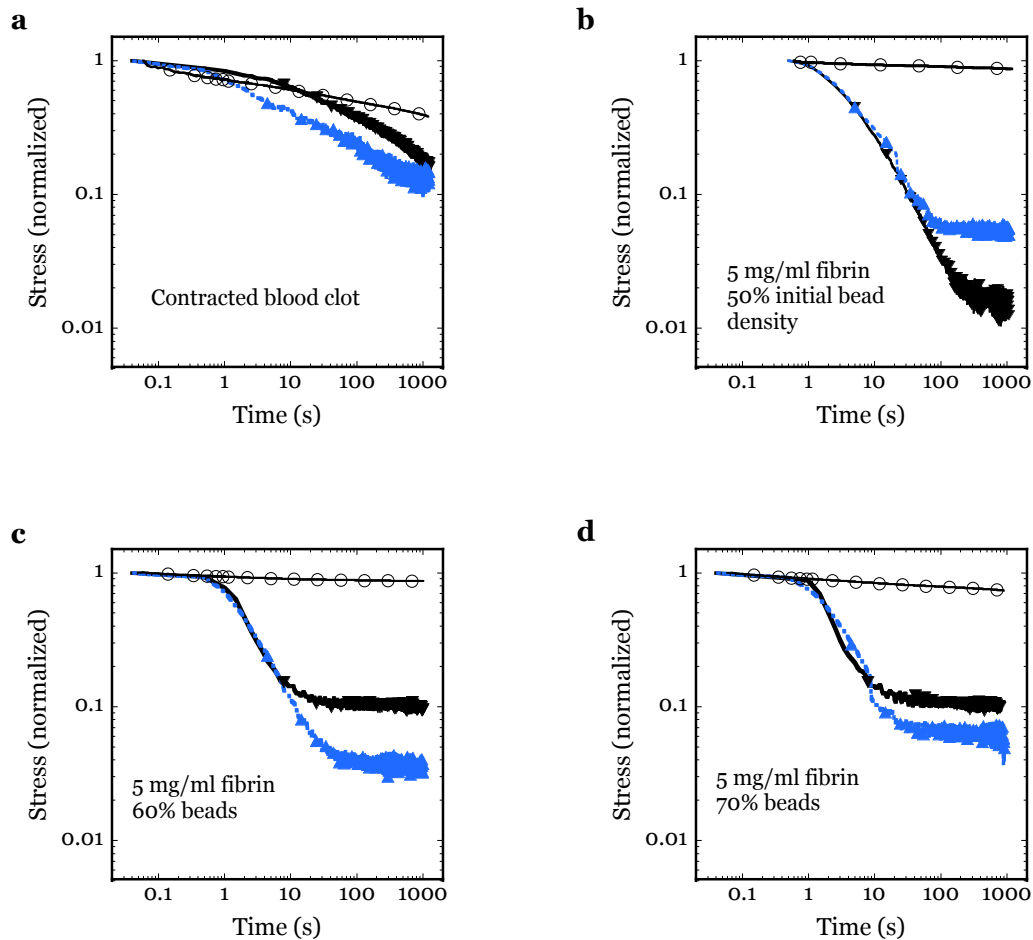


Figure 6.6: Stress-relaxation of contracted clots and fibrin-bead constructs after a step axial or shear strain. Stress-relaxation in compression, extension and shear is shown, normalized to the peak stress of **(a)** contracted clots **(b)** fibrin-bead construct with 50% beads, **(c)** constructs with 60% beads and **(d)** constructs with 70% beads.

6.4.4 Non-linear behavior at high shear strains changes at high cell and bead packing densities

Strain-stiffening is a feature often seen in biopolymer networks, but not in soft tissues. To further elucidate the nature of this divergence, the behavior of contracted clots and bead-fibrin constructs when subjected to increasing shear strains is compared. Contracted clots show shear strain weakening (Figure 6.7).

Figure 6.7: Strain amplitude dependence of contracted clots. The storage modulus of contracted rat blood clots is shown with increasing shear strains.

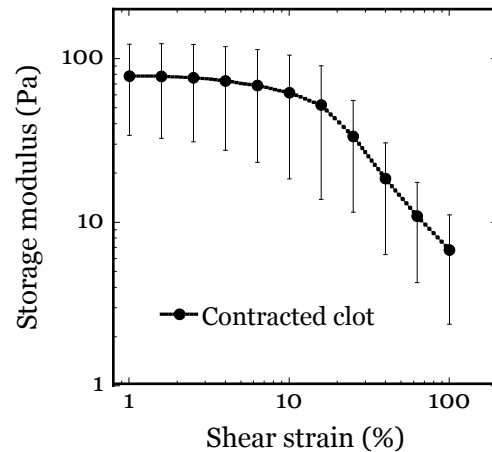


Figure 6.8 shows strain amplitude dependence of bead-fibrin constructs. All constructs were tested in absence of axial strain, at 35% compression, and 20% extension. In absence of axial strain the networks with 50% beads show strain-stiffening behavior similar to fibrin by itself. However, the 60% bead constructs show strain-weakening up to 15% shear strain after which strain-stiffening occurs, which is less pronounced than that of the 50% bead networks. The 70% bead constructs show an even more distinct initial strain-weakening, up to 50% shear strain, after which the samples stiffen again but do not reach a modulus higher than was measured at 2% shear strain.

When compressed, the 50% constructs show an initial weakening followed by strain-stiffening that does not fully return the moduli to the initial value (comparable to 70% constructs in absence of axial strain). Constructs with 60% beads show strain-weakening over almost the whole range when compressed, only showing a slight restoration between 100-200% shear strain. When the 70% bead constructs were compressed the samples show strain-weakening over the whole range of shear strains. The extended 50% and 60% constructs show very weak strain-stiffening and both have a lower critical strain than the compressed samples. The 70% constructs show little strain-stiffening when extended and do not show signs of a shift in critical strain. Overall the constructs seem to converge at higher levels of shear strain.

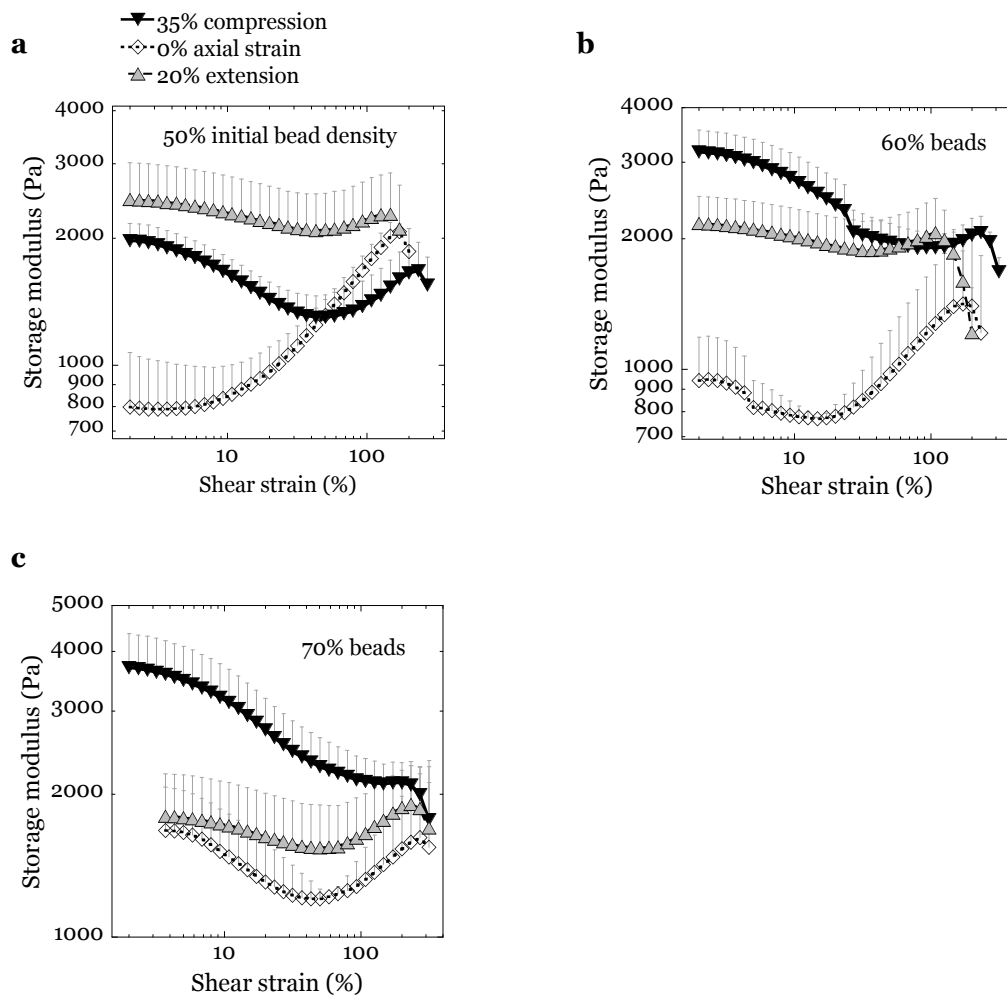
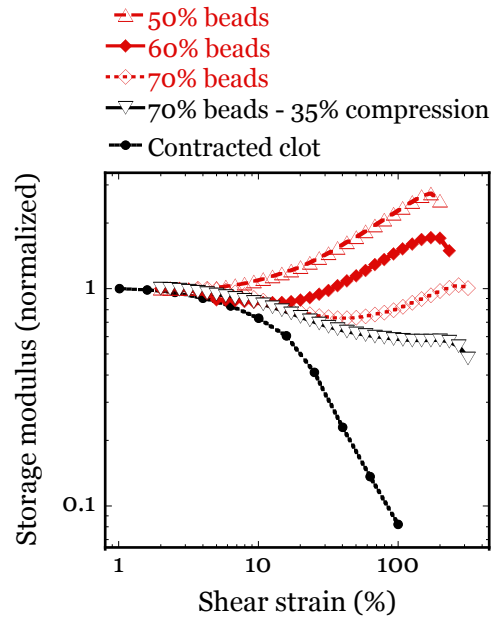


Figure 6.8: Strain amplitude dependence of fibrin-bead constructs at varying axial strain. The storage modulus of fibrin-bead constructs with a bead density of (a) 50% (b) 60% and, (c) 70% is shown with increasing shear strains at 20% extension, 35% compression and 0% axial strain.

To better compare the effect of bead density on strain-stiffening, the normalized storage moduli of contracted clots, all bead-fibrin constructs in absence of axial strain and the 70% construct at 35% compression were plotted. (Figure 6.9) From this graph it becomes

clear that the higher the density of the beads in the network is, the more pronounced strain-weakening becomes.

Figure 6.9: Overview of strain-stiffening and weakening behavior, comparing normalized storage moduli of contracted clots and fibrin-beads constructs. The storage modulus was normalized to the value at the lowest shear stress (1% for contracted clots, 2% for constructs).



6.5 Discussion

In this chapter the possibility that the multiaxial macrorheology of soft tissues is dominated by cell packing was investigated. Contracted blood clots were tested; in which the platelets contract the fibrin network, hence squeezing out plasma and trapping red blood cells. With these experiments it was shown that contracted clots show multiaxial mechanics closely resembling whole tissues. Experiments using fibrin networks in which dextran beads were embedded indicated that this behavior is not dependent on cell traction. Differences are observed between the contracted clots and embedded bead-fibrin networks, for example the modest extension and shear-strain stiffening seen in the bead-fibrin constructs. These differences could be explained by the fact that it is impossible to embed the beads into a fibrin network as densely packed as in a contracted clot. Also, the platelets in the contracted clots put the network under significant stress;

and platelets cause the network to be cross-linked, whereas the fibrin network in the constructs has entanglements only. Other blood proteins could further add to the deviation between contracted clot and bead-fibrin construct mechanics.

An important difference between tissues and the tested samples here is that in tissues the volume conserving cells are attached to the ECM network. Red blood cells do have receptors on their cell membrane, for example integrin $\alpha_4\beta_1$ that can attach to -for example- fibronectin. However, they are generally considered not adhesive and they will not exert forces on the network if they attach to it ¹⁷⁹.

6.5.1 Jamming to explain tissue rheology

From the experiments it seems likely that jamming plays a role in the macroscopic response of tissues and contracted clots to multiaxial deformations. Jamming has been related to cells in tissues, however, not directly related to the mechanical properties of the tissues. Often the experiments focussed on cell movement in monolayers ¹⁸⁰⁻¹⁸³, for example during bronchospasms ^{181,183}. Interestingly, compressive stress was shown to cause unjamming in a confluent monolayer of human bronchial epithelial cells ^{181,184}, where compression results in jamming in our system. Three dimensional movement was followed in jammed embryonic tissues ¹⁸⁵ and cells during malignant invasion in a collagen network ¹⁸⁶.

Here we consider jamming of cells and beads mechanically as described for granular materials ¹⁸⁷, colloids ¹⁸⁸, glasses ¹⁸⁹ and foams ¹⁹⁰. In granular systems the jamming transition was determined to be dependent on temperature, volume density and applied load ¹⁹¹. In colloidal systems or bead suspensions the jamming transition lays around 64% at ambient temperatures ¹⁹²⁻¹⁹⁴.

Both the 60% and 70% constructs compression stiffen. The 70% constructs extension stiffen, but less than the 50% and 60% bead constructs, and especially less than fibrin networks.

Interpreting these results is challenging as jammed systems and viscoelastic networks are not fully understood by themselves. Jamming of particles embedded in a network has not been studied. Closer approximations of the beads or cells in networks would be given by attractive colloids, for which the jamming phase-diagram differs from hard spheres^{188,195}. Colloidal suspensions can be strain-stiffening¹⁹⁶. More recently jammed colloid systems were developed from droplets between which bonds can be formed through biotin and streptavidin embedded on the surface. However, these have so far only been used to study the mechanics of cell adhesion, not the rheology of jammed suspensions¹⁹⁷.

In the systems described here it seems likely that the network will have an effect on the jammed particles, by limiting the ability of the particles to move freely as a response to shear. This is possibly seen in the current experiments, as the reversal of the compression-softening in the 50% constructs is seen around 5% compression. The 60% constructs do not significantly weaken in compression even though it should still fall below the jamming threshold. An exact quantification of the transition point of compression-softening to compression-stiffening needs to be done, in order to determine at what bead density the reversal happens.

Vice versa, jammed beads will likely have an effect on network properties, by limiting the ability of the network fibers to move. Evidence for this is also seen in the experiments:

the storage modulus of a 5 mg/ml fibrin network is much lower than that of the constructs, even with 50% beads. Since the fibrin cannot penetrate the beads, the effective concentration of fibrin is higher in the free fluid of the construct. In the 50% bead constructs this will lead to an effective fibrin concentration of 10 mg/ml. Though fibrin has not been tested at this concentration (note, the fibrin used here is different than that used in Ch3-5); the modulus can be approximated by multiplying it by $2^{2.5}$ (from Eq 2.14), which would result in a storage modulus around 500 Pa. Embedded objects –below the jamming threshold- are known to have an effect on fibrin structure and mechanics ¹⁷⁴⁻¹⁷⁶. Therefore, even though it is possible that the high storage modulus in the constructs is caused by spatial limitations of the fibrin network, this comparison is not proof that jamming induces network stiffening. Other factors like compaction of fibrin fibers should be considered, which was recently shown to increase clot stiffness ¹⁹⁸. Compaction possibly also lies at the basis of the mild increase of the storage moduli during experiments when contracted clots and fibrin-bead constructs are compressed. Though in the case of the clots, active remodeling as a result of the applied compression should not be ruled out.

Fiber constriction possibly also lies at the basis of the strain-amplitude dependence of the constructs, which show combinations of shear-weakening and stiffening at bead density of 60% and higher. In the current set-up the beads are so large compared to the mesh size that a normal fibrin network can exist in between the beads, which makes it hard to interpret the data, specifically for the strain amplitude behavior.

Hence, the fibrin-bead experiments need to be repeated with beads that are closer to the mesh size of the network. Most importantly, the experiments need to be repeated with a

linear network with beads embedded so that contributions of the network can be considered to remain stable.

Overall it seems likely that jamming plays an important role in tissue mechanics, which could have serious implications for modeling of tissues and understanding the mechanical environment *in vivo*. More work needs to be done to fully understand these systems.

CHAPTER 7: CONCLUSIONS AND FUTURE DIRECTIONS

7. 1 Summary of results

The goal for this thesis was to elucidate the factors determining the discrepancy between extracellular matrix and soft tissue mechanics. This was done with a novel multiaxial rheology approach, allowing to monitor shear rheology and axial stresses while applying compression or extension. By using this approach, the effects of physiologically relevant but rarely considered combinations of shear and compression or extension are addressed. Several other features were studied such as strain-amplitude dependence, frequency dependence, and stress-relaxation.

The results in Chapter 3 show that semiflexible ECM networks, fibrin and collagen, soften in compression and stiffen in extension. Over the tested range of axial strains, the elastic shear moduli increase linearly in extension. In compression the shear moduli initially drop, however, the values level off and stay constant after a few percent of compression. The apparent Young's moduli in extension are orders of magnitude larger compared to those in compression. Overall, the relation between the shear modulus and Young's modulus is decoupled. In Chapter 4 the dynamics of these systems showed this decoupling as well. However, higher quality data and modeling approaches are necessary to quantitatively compare shear and axial relaxation of networks during axial deformations. Shear stress relaxation after a step shear is significantly less pronounced than axial stress relaxation after an axial deformation. Compressive and extensional stress relaxation is similar at early time points. As a result, large differences in the frequency dependence are observed in shear and axially.

In Chapter 5 the effect of cell traction induced pre-stress on the networks was investigated. It became apparent that cell traction imposed on fibrin networks does not

flip the behavior of the networks to resemble whole tissues. The pre-stressed networks compression weaken and extension stiffen though the asymmetry is strongly decreased. Additionally, comparing clots made with whole blood and plasma, showed a 40% red blood cell volume had no apparent effect on multiaxial rheology. Therefore, the effect of a higher red cell density was investigated in Chapter 6, by letting clots contract fully. These contracted clots showed shear strain and extension softening, and compression stiffening, like soft tissues. Additionally, embedding a sufficient amount of beads into a reconstituted fibrin network can mimic this effect in absence of platelets, showing that the tissue-like behavior is independent of cell traction. The swift transition between compression softening and compression hardening is reminiscent of a jammed system. These results are significant from both a fundamental as well as a translational point of view. The results in Chapter 3 give new insights in the physics of semiflexible biopolymer networks. Moreover, collagen and fibrin hydrogels are used in numerous biomedical applications in which they are subject to multiaxial deformations. The results in Chapter 5 contribute to the understanding of the mechanical responses of blood clots in their *in vivo* environment. Chapter 5 and 6 show that not cell traction but cell jamming is likely to be the determining factor of soft tissue mechanics. This has implications for the understanding of tissue mechanics in physiological and pathological situations as well as the modeling of tissues. Moreover, the fundamental understanding of jammed particles inside a network is a new niche in physics.

7.2 Future directions

The results presented in this thesis bring up many new questions. The reconstituted biopolymer networks, constructs, and blood clots tested form a good model system but

several features are highly simplified. This forms the basis of designing future experiments continuing on this research highlighted below.

7.2.1 Deepening the understanding of semiflexible network physics

In the presented experiments stress responses in shear were collected and processed with the rheometer software. Hereto, the average stress is computed from the first harmonic of the sinusoidal torque signal measured. Though this approach is satisfactory in the linear regime, there is much insight to be gained from the waveforms of the raw data output in the non-linear regime. Raw waveforms can be analyzed by means of Bowditch - Lissajous curves ^{199,200} or Fourier transforms ²⁰¹, which have been used previously to analyze fibrin ²⁰²⁻²⁰⁵, collagen ⁴⁵ and soft tissues ^{85,206} in shear. Measuring the differential moduli of networks, obtained by superimposing a small oscillatory strain on a large step strain, is another method to more sensitively probe the non-linear regime of networks ^{32,207}.

7.2.2 Stress-relaxation

The stress-relaxation experiments presented here were limited and often collected in the effort of obtaining steady state values. For better evaluation of stress-relaxation it would be desirable to obtain higher quality data. Most importantly the axial stress application should be as quick and precise as possible, and stresses should be collected at higher sampling rates. This would allow for better quantification of the stress relaxation, enhance the ability to model the systems and determine which constitutive equations can be used to describe and predict the behavior.

A continuation on the stress-relaxation experiments would be to examine shear stress-relaxation and frequency dependence at different levels of axial strain, similar to the

strain-amplitude experiments done at different levels of axial strain as shown in Figure 3.3 and Figure 6.5.

7.2.3 Generalization of multiaxial rheology principles to rigid, and flexible biopolymers, and polyelectrolytes.

Tissues *in vivo* contain a wide spectrum of biopolymers, which are found both inside and outside cells. This thesis was primarily focused on two semiflexible, uncharged, extracellular components, collagen and fibrin. To fully understand tissue mechanics it would be desirable to extend experiments on multiaxial mechanics to include both extracellular and intracellular components with varying physical properties.

As shown in Chapter 3, gels prepared from lightly cross-linked, flexible and charged hyaluronic chains show very different behavior than collagen and fibrin. As a continuation on this, it would be interesting to extend the multiaxial rheology method to other ECM components, including other types of collagen and proteoglycans, and composites of 2 or more constituents.

Biopolymers that are found inside cells include actin, intermediate filaments, and microtubules, which form the cytoskeleton. Microtubules are very rigid compared to other biopolymers; and though not having been studied much, networks of microtubules can be formed^{31,208,209}. Actin and intermediate filaments are both considered semiflexible, though actin is more rigid; and both carry a significant charge, intermediate filaments more so than actin. Testing actin and intermediate filaments could provide insights in the effect of charges on the multiaxial rheology of semiflexible biopolymers; preliminary results with vimentin point towards it behaving more like cross-linked HA gels. Additionally, as cytoskeletal components form interactions with each other *in vivo*, composite networks of cytoskeletal constituents would be a logical next step^{210,211}. For

both extracellular and intracellular biopolymers testing of composite networks is especially interesting in the multiaxial set-up. It was shown that the mechanical properties of the solvent phase can significantly change buckling properties, which was observed with microtubules in a cross-linked actin gel and illustrated with a plastic rod in gelatin ²¹².

7.2.4 Influence of platelet contraction on fibrin network mechanics

The focus in this thesis is on soft tissue mechanics. However, as blood clots are used as a soft tissue model, these results can be applied to understand the mechanical behavior of blood clots *in vivo*. From literature ^{177,178} and presented experiments there are indications that platelets actively adjust tension to accommodate to mechanical changes in the network as a result of axial strain. To directly investigate the reactivity of platelets to changes in network stress it would be interesting to probe myosin activity right after applied axial strains, for example by using Western blots for total myosin and phosphorylated myosin.

7.2.5 Jamming of beads inside networks

The theory that (red blood) cells in tissues and contracted clots are a jammed system has been investigated with constructs consisting of a fibrin network and embedded dextran beads. More work needs to be done to understand this system better. Several construct variables can be simplified to allow for better interpretation of jamming in a network, and subsequently the properties of the constructs used in this thesis can be reintroduced to make this applicable to biological systems.

The variables causing complexity are the mechanics of the network and the bead size.

The fibrin network exhibits non-linear rheology at relatively modest shear strains.

Experiments as presented here should be repeated with a linear network with beads

embedded so that contributions of the network can be considered to remain stable.

Polyacrylamide would be an ideal candidate as it was shown already that the mechanics of these networks do not change with shear or axial strains. However, as the mesh-size of PAA is very small, other options would include cross-linked hyaluronic acid gels used in Chapter 3, which are known to be linear at high shear strains ^{213,214}.

The beads used in the presented experiments are polydisperse, and much larger than the network mesh size. The polydispersity is quite dramatic, with beads varying between 90 and 280 μm , which is known to influence jamming behavior ^{205,215}. Hereto, it would be ideal to keep the bead diameter within a 5% fluctuation, which would allow to use theory for monodisperse beads ²¹⁶. Specifically for jamming experiments with fibrin networks, there is a need to repeat measurements with beads that are closer to the mesh size of the fibrin network. In the current set-up the beads are so large compared to the mesh-size that a normal fibrin network can exist in between the beads. This makes it hard to interpret the data, specifically the strain amplitude behavior.

The exact bead density at the transition point of compression-softening to compression-stiffening needs to be determined, in order to determine how the presence of a network shifts the jamming transition. An option to make this determination easier is to use N-isopropyl acrylamide beads. The diameter of these beads varies with temperature, even at the small temperature range of 25°C to 37°C at which fibrin networks are tested commonly ^{205,217-219}. Using this system would allow to increase the bead density at small increments after full polymerization of the network without compression.

7.2.6 Effect of cell attachments on multiaxial rheology

In this thesis only cell traction mediated pre-stress on the ECM network and the dense cell packing were investigated directly, but a third determinant of tissue mechanics could

be the interaction between cells and the network. Cell-ECM interactions introduce an abundance of cross-links and hereby restrain the network, which is not the case in the current experiments. Here, the red blood cells are generally considered non-adhesive, and the used dextran beads are chemically inert. To investigate this effect the fibrin-bead constructs could be made with beads with adhesive properties like polystyrene or dextran beads with specific surface modifications to make the beads adherent to the network.

7.2.7 Extension of multiaxial rheology to tissues with varying cell to ECM ratio; cellular traction and anisotropy

Ultimately the goal of the research presented here is to better understand the mechanics of tissue *in vivo* and to be able to use that knowledge in applied fields like tissue engineering and regenerative medicine. In order to get a full understanding of multiaxial tissue mechanics this approach should be tried on multiple types of tissues, with varying levels of cell densities and cell traction forces.

The bottom-up approach –testing intra- and extracellular components separately and in composites- can be combined with data from the top down approach –testing tissues of varying compositions - to construct a phase diagram for tissue mechanics in which different regimes of tissue mechanics (jamming/cell traction/ECM dominated, for example) are linked to mechanical determinants.

BIBLIOGRAPHY

- 1 Physiological gels research group website,
www.math.utah.edu/research/mathbio/groups/gels/gel_firbin_page.html
- 2 Macosko. *Rheology: Principles, Measurements, and Applications*. (Wiley-VCH, 1994).
- 3 Karp. *Cell and Molecular Biology Concepts and Experiments* (Wiley).
- 4 Rockwood, G. *Fractures in Adults*. 6th edn, (2006).
- 5 Martini, B. *Essentials of Anatomy & Physiology*. 5th edn, (Pearson Education).
- 6 Wikipedia. en.wikipedia.org/wiki/Hooke's_law
- 7 Kruger, T. E., Miller, A. H. & Wang, J. Collagen scaffolds in bone sialoprotein-mediated
bone regeneration. *The Scientific World Journal* **2013** (2013).
- 8 Storm, C., Pastore, J. J., MacKintosh, F. C., Lubensky, T. C. & Janmey, P. A. Nonlinear
elasticity in biological gels. *Nature* **435**, 191-194 (2005).
- 9 van der Giessen, E. Materials physics: Bending Maxwell's rule. *Nature Physics* **7**, 923-924
(2011).
- 10 Janmey, P. A. *et al.* Negative normal stress in semiflexible biopolymer gels. *Nature*
materials **6**, 48-51 (2006).
- 11 Weisel, J. W. Fibrinogen and fibrin. *Advances in protein chemistry* **70**, 247-299 (2005).
- 12 Cines, D. B. *et al.* Clot contraction: compression of erythrocytes into tightly packed
polyhedra and redistribution of platelets and fibrin. *Blood* **123**, 1596-1603 (2014).
- 13 DAVIS, H. G. Conservative Surgery, as Exhibited in Remediating Some of the Mechanical
Causes That Operate Injuriouly Both in Health and Disease. *New York, D. Appleton and*
Company (1867).
- 14 Volkmann, R. Beiträge zur Anatomie und Chirurgie der Geschwülste [Contributions to
the anatomy and surgery of growth]. *Langenbecks Arch Chir* **15**, 556-561 (1873).
- 15 Hueter, C. Anatomische studien an den extremitätengelenken neugeborener und
erwachsener. *Virchows Archiv* **26**, 484-519 (1863).
- 16 Wolff, J. Das gesetz der transformation der knochen. *DMW-Deutsche Medizinische*
Wochenschrift **19**, 1222-1224 (1892).
- 17 D'arcy, W. T. On growth and form. *Cambridge Univ. Pr* (1917).
- 18 Petri, R. J. Eine kleine Modification des Kochschen Plattenverfahrens. *Centralbl*
Bacteriol Parasitenkunde **1**, 279-280 (1887).
- 19 Harris, A. K., Wild, P. & Stopak, D. Silicone rubber substrata: a new wrinkle in the study
of cell locomotion. *Science* **208**, 177-179 (1980).
- 20 Pelham, R. J. & Wang, Y.-l. Cell locomotion and focal adhesions are regulated by
substrate flexibility. *Proceedings of the National Academy of Sciences* **94**, 13661-13665
(1997).
- 21 Solon, J., Levental, I., Sengupta, K., Georges, P. C. & Janmey, P. A. Fibroblast adaptation
and stiffness matching to soft elastic substrates. *Biophysical Journal* **93**, 4453-4461
(2007).
- 22 Yeung, T. *et al.* Effects of substrate stiffness on cell morphology, cytoskeletal structure,
and adhesion. *Cell motility and the cytoskeleton* **60**, 24-34 (2005).
- 23 Discher, D. E., Janmey, P. & Wang, Y. Tissue cells feel and respond to the stiffness of
their substrate. *Science* **310**, 1139 (2005).
- 24 Alberts, J., Lewis, Raff, Roberts, Walter. *The molecular biology of the cell*. 5th edn,
(Garland Science).
- 25 Kreis, T. *Guidebook to the extracellular matrix, anchor, and adhesion proteins*. (A
Sambrook and Tooze Publication at Oxford University Press, 1999).
- 26 Brinckmann, J., Notbohm, H. & MÅ¼aller, P. K. *Collagen: primer in structure,*
processing and assembly. (Springer, 2005).

- 27 Fratzl, P. *Collagen: structure and mechanics*. (Springer Science & Business Media, 2008).
- 28 Gerth, C., Roberts, W. W. & Ferry, J. D. Rheology of fibrin clots II: Linear viscoelastic behavior in shear creep. *Biophysical chemistry* **2**, 208-217 (1974).
- 29 Roberts, W. W., Kramer, O., Rosser, R. W., Nestler, F. H. M. & Ferry, J. D. Rheology of fibrin clots. I.: Dynamic viscoelastic properties and fluid permeation. *Biophysical chemistry* **1**, 152-160 (1974).
- 30 Janmey, P., Shah, J., Janssen, K. & Schliwa, M. Viscoelasticity of intermediate filament networks. *Sub-cellular biochemistry* **31**, 381 (1998).
- 31 Janmey, P. A., Euteneuer, U., Traub, P. & Schliwa, M. Viscoelastic properties of vimentin compared with other filamentous biopolymer networks. *The Journal of cell biology* **113**, 155-160 (1991).
- 32 Gardel, M. *et al.* Elastic behavior of cross-linked and bundled actin networks. *Science* **304**, 1301-1305 (2004).
- 33 Fung, Y. *Biomechanics: mechanical properties of living tissues*. 1993. *New York, NY*.
- 34 Cowin, S. C. & Doty, S. B. *Tissue mechanics*. (Springer Science & Business Media, 2007).
- 35 Piechocka, I. K., van Oosten, A. S., Breuls, R. G. & Koenderink, G. H. Rheology of heterotypic collagen networks. *Biomacromolecules* **12**, 2797-2805, doi:10.1021/bm200553x (2011).
- 36 Stuart, K. & Panitch, A. Characterization of gels composed of blends of collagen I, collagen III, and chondroitin sulfate. *Biomacromolecules* **10**, 25-31 (2008).
- 37 Yang, Y.-l. *et al.* Influence of chondroitin sulfate and hyaluronic acid on structure, mechanical properties, and glioma invasion of collagen I gels. *Biomaterials* **32**, 7932-7940 (2011).
- 38 Guarneri, D. *et al.* Effects of fibronectin and laminin on structural, mechanical and transport properties of 3D collagenous network. *Journal of Materials Science: Materials in Medicine* **18**, 245-253 (2007).
- 39 Motte, S. & Kaufman, L. J. Strain stiffening in collagen I networks. *Biopolymers* **99**, 35-46 (2013).
- 40 Wilson, S. L. *et al.* A microscopic and macroscopic study of aging collagen on its molecular structure, mechanical properties, and cellular response. *The FASEB Journal* **28**, 14-25 (2014).
- 41 Wu, C.-C., Ding, S.-J., Wang, Y.-H., Tang, M.-J. & Chang, H.-C. Mechanical properties of collagen gels derived from rats of different ages. *Journal of Biomaterials Science, Polymer Edition* **16**, 1261-1275 (2005).
- 42 Vader, D., Kabla, A., Weitz, D. & Mahadevan, L. Strain-induced alignment in collagen gels. *PloS one* **4**, e5902 (2009).
- 43 Velegol, D. & Lanni, F. Cell traction forces on soft biomaterials. I. Microrheology of type I collagen gels. *Biophysical journal* **81**, 1786-1792 (2001).
- 44 Yang, Y. & Kaufman, L. J. Rheology and confocal reflectance microscopy as probes of mechanical properties and structure during collagen and collagen/hyaluronan self-assembly. *Biophysical journal* **96**, 1566-1585 (2009).
- 45 Kurniawan, N. A., Wong, L. H. & Rajagopalan, R. Early stiffening and softening of collagen: interplay of deformation mechanisms in biopolymer networks. *Biomacromolecules* **13**, 691-698 (2012).
- 46 Lopez-Garcia, M., Beebe, D. & Crone, W. Young's modulus of collagen at slow displacement rates. *Bio-medical materials and engineering* **20**, 361-369 (2010).
- 47 Roeder, B. A., Kokini, K., Sturgis, J. E., Robinson, J. P. & Voytik-Harbin, S. L. Tensile mechanical properties of three-dimensional type I collagen extracellular matrices with varied microstructure. *Journal of biomechanical engineering* **124**, 214-222 (2002).
- 48 Ozerdem, B. & Tözeren, A. Physical response of collagen gels to tensile strain. *Journal of biomechanical engineering* **117**, 397-401 (1995).

- 49 Pryse, K. M., Nekouzadeh, A., Genin, G. M., Elson, E. L. & Zahalak, G. I. Incremental mechanics of collagen gels: new experiments and a new viscoelastic model. *Annals of biomedical engineering* **31**, 1287-1296 (2003).
- 50 Sheu, M.-T., Huang, J.-C., Yeh, G.-C. & Ho, H.-O. Characterization of collagen gel solutions and collagen matrices for cell culture. *Biomaterials* **22**, 1713-1719 (2001).
- 51 Knapp, D. M. *et al.* Rheology of reconstituted type I collagen gel in confined compression. *Journal of Rheology (1978-present)* **41**, 971-993 (1997).
- 52 Münster, S. *et al.* Strain history dependence of the nonlinear stress response of fibrin and collagen networks. *Proceedings of the National Academy of Sciences* **110**, 12197-12202 (2013).
- 53 Ahmed, T. A. E., Dare, E. V. & Hincke, M. Fibrin: A versatile scaffold for tissue engineering applications. *Tissue Engineering Part B-Reviews* **14**, 199-215, doi:10.1089/ten.teb.2007.0435 (2008).
- 54 Laudano, A. P. & Doolittle, R. F. SYNTHETIC PEPTIDE DERIVATIVES THAT BIND TO FIBRINOGEN AND PREVENT POLYMERIZATION OF FIBRIN MONOMERS. *Proceedings of the National Academy of Sciences of the United States of America* **75**, 3085-3089, doi:10.1073/pnas.75.7.3085 (1978).
- 55 Brown, A. E., Litvinov, R. I., Discher, D. E., Purohit, P. K. & Weisel, J. W. Multiscale mechanics of fibrin polymer: gel stretching with protein unfolding and loss of water. *Science* **325**, 741-744, doi:10.1126/science.1172484 (2009).
- 56 Shah, J. V. & Janmey, P. A. Strain hardening of fibrin gels and plasma clots. *Rheologica Acta* **36**, 262-268 (1997).
- 57 Weisel, J. W. The mechanical properties of fibrin for basic scientists and clinicians. *Biophysical Chemistry* **112**, 267-276, doi:10.1016/j.bpc.2004.07.029 (2004).
- 58 Ryan, E. A., Mockros, L. F., Weisel, J. W. & Lorand, L. Structural origins of fibrin clot rheology. *Biophys J* **77**, 2813-2826 (1999).
- 59 MacKintosh, F., Käs, J. & Janmey, P. Elasticity of semiflexible biopolymer networks. *Physical review letters* **75**, 4425 (1995).
- 60 Janmey, P. A. *et al.* The mechanical properties of actin gels. Elastic modulus and filament motions. *Journal of Biological Chemistry* **269**, 32503-32513 (1994).
- 61 Maxwell, J. C. L. on the calculation of the equilibrium and stiffness of frames. *The London, Edinburgh, and Dublin Philosophical Magazine and Journal of Science* **27**, 294-299 (1864).
- 62 Broedersz, C. P., Mao, X., Lubensky, T. C. & MacKintosh, F. C. Criticality and isostaticity in fibre networks. *Nature Physics* **7**, 983-988 (2011).
- 63 Sheinman, M., Broedersz, C. & MacKintosh, F. Actively stressed marginal networks. *Physical review letters* **109**, 238101 (2012).
- 64 Huisman, E. & Lubensky, T. C. Internal stresses, normal modes, and nonaffinity in three-dimensional biopolymer networks. *Physical review letters* **106**, 088301 (2011).
- 65 Chien, S. Shear dependence of effective cell volume as a determinant of blood viscosity. *Science* **168**, 977-979 (1970).
- 66 Dippy, J. & Davis, S. Rheological assessment of mucolytic agents on sputum of chronic bronchitics. *Thorax* **24**, 707-713 (1969).
- 67 Ogston, A. & Stanier, J. The physiological function of hyaluronic acid in synovial fluid; viscous, elastic and lubricant properties. *The Journal of physiology* **119**, 244-252 (1953).
- 68 Suki, B. & Bates, J. H. Lung tissue mechanics as an emergent phenomenon. *Journal of Applied Physiology* **110**, 1111-1118 (2011).
- 69 Shadwick, R. E. Mechanical design in arteries. *Journal of Experimental Biology* **202**, 3305-3313 (1999).
- 70 Hjortdal, J. Ø. Extensibility of the normo-hydrated human cornea. *Acta Ophthalmologica Scandinavica* **73**, 12-17 (1995).
- 71 Tong, P. & Fung, Y.-C. The stress-strain relationship for the skin. *Journal of Biomechanics* **9**, 649-657 (1976).

- 72 Silver, F. H., Freeman, J. W. & DeVore, D. Viscoelastic properties of human skin and
processed dermis. *Skin Research and Technology* **7**, 18-23 (2001).
- 73 Min, Y. B., Titze, I. R. & Alipour-Haghighi, F. Stress-strain response of the human vocal
ligament. *Annals of Otology, Rhinology & Laryngology* **104**, 563-569 (1995).
- 74 Noyes, F. R. Functional properties of knee ligaments and alterations induced by
immobilization: a correlative biomechanical and histological study in primates. *Clinical
orthopaedics and related research* **123**, 210-242 (1977).
- 75 Fratzl, P. *et al.* Fibrillar structure and mechanical properties of collagen. *Journal of
structural biology* **122**, 119-122 (1998).
- 76 Carlstedt, C. A. & Nordin, M. Biomechanics of tendons and ligaments. *Basic
biomechanics of the musculoskeletal system* **3**, 59-74 (1989).
- 77 Woo, S.-Y. in *Frontiers in biomechanics* 180-195 (Springer, 1986).
- 78 Kenedi, R., Gibson, T., Evans, J. & Barbenel, J. Tissue mechanics. *Physics in medicine
and biology* **20**, 699 (1975).
- 79 Mow, V. C., Ateshian, G. A. & Spilker, R. L. Biomechanics of diarthrodial joints: a review
of twenty years of progress. *Journal of biomechanical engineering* **115**, 460-467 (1993).
- 80 Dobrin, P. B. Vascular mechanics. *Comprehensive Physiology* (1983).
- 81 Ommaya, A. K. Mechanical properties of tissues of the nervous system. *Journal of
Biomechanics* **1**, 127-138 (1968).
- 82 Brands, D., Bovendeerd, P., Peters, G. & Wismans, J. The large shear strain dynamic
behaviour of in-vitro porcine brain tissue and a silicone gel model material. *Stapp car
crash journal*, 249-260 (2000).
- 83 Pogoda, K. *et al.* Compression stiffening of brain and its effect on mechanosensing by
glioma cells. *New Journal of Physics* **16**, 075002 (2014).
- 84 Perepelyuk, M. *et al.* Hepatic stellate cells and portal fibroblasts are the major cellular
sources of collagens and lysyl oxidases in normal liver and early after injury. *American
Journal of Physiology-Gastrointestinal and Liver Physiology* **304**, G605-G614 (2013).
- 85 Tan, K., Cheng, S., Jugé, L. & Bilston, L. E. Characterising soft tissues under large
amplitude oscillatory shear and combined loading. *Journal of biomechanics* **46**, 1060-
1066 (2013).
- 86 Mihai, L. A., LiKang Chin, & Paul A. Janmey, A. G. A comparison of hyperelastic
constitutive models applicable to brain and fat tissues. (2015).
- 87 Chin, L., Bobby Monks, Morris J. Birnbaum, Paul A. Janmey, Makoto Funaki. Collagen VI
knockout abrogates obesity-related adipose tissue stiffening. *ADA 74th Scientific sessions*
(2014).
- 88 Bailey, A. & Light, N. in *Ciba Foundation Symposium 114-Fibrosis*. 80-96 (Wiley Online
Library).
- 89 Hinz, B. *et al.* The myofibroblast: one function, multiple origins. *The American journal of
pathology* **170**, 1807-1816 (2007).
- 90 Afdhal, N. H. & Nunes, D. Evaluation of liver fibrosis: a concise review. *The American
journal of gastroenterology* **99**, 1160-1174 (2004).
- 91 Grenard, P. *et al.* Transglutaminase-mediated cross-linking is involved in the
stabilization of extracellular matrix in human liver fibrosis. *Journal of hepatology* **35**,
367-375 (2001).
- 92 Selman, M., King, T. E. & Pardo, A. Idiopathic pulmonary fibrosis: prevailing and
evolving hypotheses about its pathogenesis and implications for therapy. *Annals of
internal medicine* **134**, 136-151 (2001).
- 93 Huang, S. & Ingber, D. E. Cell tension, matrix mechanics, and cancer development.
Cancer cell **8**, 175-176 (2005).
- 94 Lopez, J. I., Kang, I., You, W.-K., McDonald, D. M. & Weaver, V. M. In situ force mapping
of mammary gland transformation. *Integrative Biology* **3**, 910-921 (2011).
- 95 Fenner, J. *et al.* Macroscopic Stiffness of Breast Tumors Predicts Metastasis. *Scientific
reports* **4** (2014).

- 96 Baker, A., Bird, D., Lang, G., Cox, T. R. & Erler, J. Lysyl oxidase enzymatic function increases stiffness to drive colorectal cancer progression through FAK. *Oncogene* **32**, 1863-1868 (2013).
- 97 Venkatesh, S. K. *et al.* Magnetic resonance elastography of liver tumors-preliminary results. *AJR. American journal of roentgenology* **190**, 1534 (2008).
- 98 Levental, K. R. *et al.* Matrix crosslinking forces tumor progression by enhancing integrin signaling. *Cell* **139**, 891-906 (2009).
- 99 Paszek, M. J. *et al.* Tensional homeostasis and the malignant phenotype. *Cancer Cell* **8**, 241-254 (2005).
- 100 Wang, H., Haeger, S. M., Kloxin, A. M., Leinwand, L. A. & Anseth, K. S. Redirecting valvular myofibroblasts into dormant fibroblasts through light-mediated reduction in substrate modulus. *PLoS One* **7**, e39969 (2012).
- 101 Balestrini, J. L., Chaudhry, S., Sarrazy, V., Koehler, A. & Hinz, B. The mechanical memory of lung myofibroblasts. *Integrative Biology* **4**, 410-421 (2012).
- 102 Rocco, P. R. *et al.* Lung tissue mechanics and extracellular matrix remodeling in acute lung injury. *American journal of respiratory and critical care medicine* **164**, 1067-1071 (2001).
- 103 Eisenberg, J. L. *et al.* Substrate stiffness regulates extracellular matrix deposition by alveolar epithelial cells. *Research and reports in biology* **2011**, 1 (2011).
- 104 Liu, F. *et al.* Feedback amplification of fibrosis through matrix stiffening and COX-2 suppression. *The Journal of cell biology* **190**, 693-706 (2010).
- 105 Georges, P. C. *et al.* Increased stiffness of the rat liver precedes matrix deposition: implications for fibrosis. *American Journal of Physiology-Gastrointestinal and Liver Physiology* **293**, G1147-G1154 (2007).
- 106 Olsen, A. L. *et al.* Hepatic stellate cells require a stiff environment for myofibroblastic differentiation. *American Journal of Physiology-Gastrointestinal and Liver Physiology* **301**, G110-G118 (2011).
- 107 Guvendiren, M., Perepelyuk, M., Wells, R. G. & Burdick, J. A. Hydrogels with differential and patterned mechanics to study stiffness-mediated myofibroblastic differentiation of hepatic stellate cells. *Journal of the mechanical behavior of biomedical materials* **38**, 198-208 (2014).
- 108 Hansen, L. K., Wilhelm, J. & Fassett, J. T. Regulation of hepatocyte cell cycle progression and differentiation by type I collagen structure. *Current topics in developmental biology* **72**, 205-236 (2005).
- 109 Semler, E. J., Ranucci, C. S. & Moghe, P. V. Mechanochemical manipulation of hepatocyte aggregation can selectively induce or repress liver-specific function. *Biotechnology and bioengineering* **69**, 359-369 (2000).
- 110 McEniery, C. M., Hall, I. R., Qasem, A., Wilkinson, I. B. & Cockcroft, J. R. Normal vascular aging: differential effects on wave reflection and aortic pulse wave velocity: the Anglo-Cardiff Collaborative Trial (ACCT). *Journal of the American College of Cardiology* **46**, 1753-1760 (2005).
- 111 van Popele, N. M. *et al.* Association between arterial stiffness and atherosclerosis The Rotterdam Study. *Stroke* **32**, 454-460 (2001).
- 112 Boutouyrie, P. *et al.* Aortic stiffness is an independent predictor of primary coronary events in hypertensive patients a longitudinal study. *Hypertension* **39**, 10-15 (2002).
- 113 Huynh, J. *et al.* Age-related intimal stiffening enhances endothelial permeability and leukocyte transmigration. *Science translational medicine* **3**, 112ra122-112ra122 (2011).
- 114 Stroka, K. M. & Aranda-Espinoza, H. Endothelial cell substrate stiffness influences neutrophil transmigration via myosin light chain kinase-dependent cell contraction. *Blood* **118**, 1632-1640 (2011).
- 115 Galie, P., van Oosten, A., Chen, C. & Janmey, P. Application of multiple levels of fluid shear stress to endothelial cells plated on polyacrylamide gels. *Lab on a Chip* (2015).
- 116 Lin, Y.-C. *et al.* Origins of elasticity in intermediate filament networks. *Physical review letters* **104**, 058101 (2010).

- 117 Tharmann, R., Claessens, M. & Bausch, A. Viscoelasticity of isotropically cross-linked
actin networks. *Physical review letters* **98**, 088103 (2007).
- 118 Piechocka, I. K., van Oosten, A. S. G., Breuls, R. G. M. & Koenderink, G. H. Rheology of
heterotypic collagen networks. *Biomacromolecules* **2011**, 2797-2805.
- 119 Yang, Y.-l., Leone, L. M. & Kaufman, L. J. Elastic moduli of collagen gels can be predicted
from two-dimensional confocal microscopy. *Biophysical journal* **97**, 2051-2060 (2009).
- 120 Piechocka, I. K., Bacabac, R. G., Potters, M., MacKintosh, F. C. & Koenderink, G. H.
Structural hierarchy governs fibrin gel mechanics. *Biophysical journal* **98**, 2281-2289
(2010).
- 121 Alexander, S. Amorphous solids: their structure, lattice dynamics and elasticity. *Physics
reports* **296**, 65-236 (1998).
- 122 Onck, P., Koeman, T., Van Dillen, T. & Van der Giessen, E. Alternative explanation of
stiffening in cross-linked semiflexible networks. *Physical review letters* **95**, 178102
(2005).
- 123 Michaud, S. E. *et al.* Purification of salmon thrombin and its potential as an alternative to
mammalian thrombins in fibrin sealants. *Thrombosis research* **107**, 245-254 (2002).
- 124 Smith, J. R. *et al.* Salmon and Human Thrombin Differentially Regulate Radicular Pain,
Glial-Induced Inflammation and Spinal Neuronal Excitability through Protease-Activated
Receptor-1. *PLoS one* **8**, e80006 (2013).
- 125 Boudou, T., Ohayon, J., Picart, C. & Tracqui, P. An extended relationship for the
characterization of Young's modulus and Poisson's ratio of tunable polyacrylamide gels.
Biorheology **43**, 721-728 (2006).
- 126 Lindström, S. B., Vader, D. A., Kulachenko, A. & Weitz, D. A. Biopolymer network
geometries: characterization, regeneration, and elastic properties. *Physical Review E* **82**,
051905 (2010).
- 127 Conti, E. & MacKintosh, F. C. Cross-linked networks of stiff filaments exhibit negative
normal stress. *Physical review letters* **102**, 088102 (2009).
- 128 Broedersz, C., Sheinman, M. & MacKintosh, F. Filament-length-controlled elasticity in
3D fiber networks. *Physical review letters* **108**, 078102 (2012).
- 129 Toole, B. P. Hyaluronan: from extracellular glue to pericellular cue. *Nature Reviews
Cancer* **4**, 528-539 (2004).
- 130 Heussinger, C., Schaefer, B. & Frey, E. Nonaffine rubber elasticity for stiff polymer
networks. *Physical Review E* **76**, 031906 (2007).
- 131 Heussinger, C. & Frey, E. Floppy modes and nonaffine deformations in random fiber
networks. *Physical review letters* **97**, 105501 (2006).
- 132 Vaughan Jr, B. L., Galie, P. A., Stegemann, J. P. & Grotberg, J. B. A Poroelastic Model
Describing Nutrient Transport and Cell Stresses Within a Cyclically Strained Collagen
Hydrogel. *Biophysical Journal* **105**, 2188-2198 (2013).
- 133 Kim, O. V., Litvinov, R. I., Weisel, J. W. & Alber, M. S. Structural basis for the nonlinear
mechanics of fibrin networks under compression. *Biomaterials* (2014).
- 134 Lakes, R. S. & Wineman, A. On Poisson's ratio in linearly viscoelastic solids. *Journal of
Elasticity* **85**, 45-63 (2006).
- 135 Choi, J. & Lakes, R. Non-linear properties of polymer cellular materials with a negative
Poisson's ratio. *Journal of Materials Science* **27**, 4678-4684 (1992).
- 136 Hayes, W. & Bodine, A. Flow-independent viscoelastic properties of articular cartilage
matrix. *Journal of Biomechanics* **11**, 407-419 (1978).
- 137 Weisel, J. W. The mechanical properties of fibrin for basic scientists and clinicians.
Biophysical chemistry **112**, 267-276 (2004).
- 138 Barocas, V. H. & Tranquillo, R. T. An anisotropic biphasic theory of tissue-equivalent
mechanics: the interplay among cell traction, fibrillar network deformation, fibril
alignment, and cell contact guidance. *Journal of biomechanical engineering* **119**, 137-145
(1997).

- 139 Chandran, P. L. & Barocas, V. H. Microstructural mechanics of collagen gels in confined
compression: poroelasticity, viscoelasticity, and collapse. *Journal of biomechanical
engineering* **126**, 152-166 (2004).
- 140 Hu, Y. & Suo, Z. Viscoelasticity and poroelasticity in elastomeric gels. *Acta Mechanica
Solida Sinica* **25**, 441-458 (2012).
- 141 Galli, M., Comley, K. S., Shean, T. A. & Oyen, M. L. Viscoelastic and poroelastic
mechanical characterization of hydrated gels. *Journal of Materials Research* **24**, 973-979
(2009).
- 142 Mow, V., Kuei, S., Lai, W. & Armstrong, C. Biphasic creep and stress relaxation of
articular cartilage in compression: theory and experiments. *Journal of biomechanical
engineering* **102**, 73-84 (1980).
- 143 Biot, M. General three-dimensional theory of poroelasticity. *J. Appl. Phys* **12**, 155-164
(1941).
- 144 Setton, L. A., Zhu, W. & Mow, V. C. The biphasic poroviscoelastic behavior of articular
cartilage: role of the surface zone in governing the compressive behavior. *Journal of
biomechanics* **26**, 581-592 (1993).
- 145 Mak, A. Unconfined compression of hydrated viscoelastic tissues: a biphasic
poroviscoelastic analysis. *Biorheology* **23**, 371-383 (1985).
- 146 Gasser, T. C., Ogden, R. W. & Holzapfel, G. A. Hyperelastic modelling of arterial layers
with distributed collagen fibre orientations. *Journal of the royal society interface* **3**, 15-
35 (2006).
- 147 Triantafyllidis, N. & Aifantis, E. C. A gradient approach to localization of deformation. I.
Hyperelastic materials. *Journal of Elasticity* **16**, 225-237 (1986).
- 148 Ogden, R. & Isherwood, D. Solution of some finite plane-strain problems for
compressible elastic solids. *The Quarterly Journal of Mechanics and Applied
Mathematics* **31**, 219-249 (1978).
- 149 Wang, H., Abhilash, A., Chen, C. S., Wells, R. G. & Shenoy, V. B. Long-Range Force
Transmission in Fibrous Matrices Enabled by Tension-Driven Alignment of Fibers.
Biophysical journal **107**, 2592-2603 (2014).
- 150 Abhilash, A., Baker, B. M., Trappmann, B., Chen, C. S. & Shenoy, V. B. Remodeling of
Fibrous Extracellular Matrices by Contractile Cells: Predictions from Discrete Fiber
Network Simulations. *Biophysical journal* **107**, 1829-1840 (2014).
- 151 Lai, W., Hou, J. & Mow, V. A triphasic theory for the swelling and deformation behaviors
of articular cartilage. *Journal of biomechanical engineering* **113**, 245-258 (1991).
- 152 MÅller, M. F., Ris, H. & Ferry, J. D. Electron microscopy of fine fibrin clots and fine
and coarse fibrin films: Observations of fibers in cross-section and in deformed states.
Journal of Molecular Biology **174**, 369-384 (1984).
- 153 Janmey, P. A., Amis, E. J. & Ferry, J. D. Rheology of fibrin clots. VI. Stress relaxation,
creep, and differential dynamic modulus of fine clots in large shearing deformations.
Journal of Rheology (1978-present) **27**, 135-153 (1983).
- 154 Nelb, G. W., Gerth, C., Ferry, J. D. & Lorand, L. Rheology of fibrin clots: III. Shear creep
and creep recovery of fine ligated and coarse unligated clots. *Biophysical chemistry* **5**,
377-387 (1976).
- 155 Osman, A. S. & Randolph, M. F. Response of a solid infinite cylinder embedded in a
poroelastic medium and subjected to a lateral load. *International Journal of Solids and
Structures* **47**, 2414-2424 (2010).
- 156 Casares, L. *et al.* Hydraulic fracture during epithelial stretching. *Nature materials* **14**,
343-351 (2015).
- 157 Kim, O. V. *et al.* Foam-like compression behavior of fibrin networks. *Biomechanics and
modeling in mechanobiology*, 1-16 (2015).
- 158 Licup, A. J. *et al.* Stress controls the mechanics of collagen networks. *arXiv preprint
arXiv:1503.00924* (2015).

- 159 Perepelyuk, M., LiKang Chin, Xuan Cao, Anne van Oosten, Vivek B. Shenoy, Paul A. Janmey, Rebecca G. Wells. Normal and fibrotic rat livers demonstrate strain softening and compression stiffening: a model for soft tissue mechanics. (2015).
- 160 Bell, E., Ivarsson, B. & Merrill, C. Production of a tissue-like structure by contraction of collagen lattices by human fibroblasts of different proliferative potential in vitro. *Proceedings of the National Academy of Sciences* **76**, 1274-1278 (1979).
- 161 Harris, A. K., Stopak, D. & Wild, P. Fibroblast traction as a mechanism for collagen morphogenesis. (1981).
- 162 Czirók, A., Rongish, B. J. & Little, C. D. Extracellular matrix dynamics during vertebrate axis formation. *Developmental biology* **268**, 111-122 (2004).
- 163 Korff, T. & Augustin, H. G. Tensional forces in fibrillar extracellular matrices control directional capillary sprouting. *Journal of Cell Science* **112**, 3249-3258 (1999).
- 164 Paszek, M. J. & Weaver, V. M. The tension mounts: mechanics meets morphogenesis and malignancy. *Journal of mammary gland biology and neoplasia* **9**, 325-342 (2004).
- 165 Tomasek, J. J., Gabbiani, G., Hinz, B., Chaponnier, C. & Brown, R. A. Myofibroblasts and mechano-regulation of connective tissue remodelling. *Nature Reviews Molecular Cell Biology* **3**, 349-363 (2002).
- 166 Hinz, B., Mastrangelo, D., Iselin, C. E., Chaponnier, C. & Gabbiani, G. Mechanical tension controls granulation tissue contractile activity and myofibroblast differentiation. *The American journal of pathology* **159**, 1009-1020 (2001).
- 167 Gabbiani, G., Ryan, G. & Majno, G. Presence of modified fibroblasts in granulation tissue and their possible role in wound contraction. *Experientia* **27**, 549-550 (1971).
- 168 Jansen, K. A., Bacabac, R. G., Piechocka, I. K. & Koenderink, G. H. Cells actively stiffen fibrin networks by generating contractile stress. *Biophysical journal* **105**, 2240-2251 (2013).
- 169 Winer, J. P., Oake, S. & Janmey, P. A. Non-linear elasticity of extracellular matrices enables contractile cells to communicate local position and orientation. *PloS one* **4**, e6382 (2009).
- 170 Raub, C., Putnam, A., Tromberg, B. & George, S. Predicting bulk mechanical properties of cellularized collagen gels using multiphoton microscopy. *Acta biomaterialia* **6**, 4657-4665 (2010).
- 171 Nair, C. & Dhall, D. Studies on fibrin network structure: the effect of some plasma proteins. *Thrombosis research* **61**, 315-325 (1991).
- 172 Okada, M., Blombäck, B., Chang, M.-D. & Horowitz, B. Fibronectin and fibrin gel structure. *Journal of Biological Chemistry* **260**, 1811-1820 (1985).
- 173 Carr, M. E. Fibrin formed in plasma is composed of fibers more massive than those formed from purified fibrinogen. *Thrombosis and haemostasis* **59**, 535-539 (1988).
- 174 Tutwiler, V. *et al. Effects of Platelets and Erythrocytes on the Dynamic Size and Mechanical Properties of Blood Clots during Contraction*. Vol. 124 (2014).
- 175 Gersh, K. C., Nagaswami, C. & Weisel, J. W. Fibrin network structure and clot mechanical properties are altered by incorporation of erythrocytes. *Thrombosis and haemostasis* **102**, 1169 (2009).
- 176 Carr, M. & Hardin, C. L. Fibrin has larger pores when formed in the presence of erythrocytes. *American Journal of Physiology-Heart and Circulatory Physiology* **253**, H1069-H1073 (1987).
- 177 Lam, W. A. *et al.* Mechanics and contraction dynamics of single platelets and implications for clot stiffening. *Nature materials* **10**, 61-66 (2010).
- 178 Muthard, R. W. & Diamond, S. L. Blood Clots Are Rapidly Assembled Hemodynamic Sensors Flow Arrest Triggers Intraluminal Thrombus Contraction. *Arteriosclerosis, thrombosis, and vascular biology* **32**, 2938-2945 (2012).
- 179 Telen, M. J. in *Seminars in hematology*. 130-142 (Elsevier).
- 180 Nnetu, K. D., Knorr, M., Käs, J. & Zink, M. The impact of jamming on boundaries of collectively moving weak-interacting cells. *New Journal of Physics* **14**, 115012 (2012).

- 181 Park, J.-A. *et al.* Maturation of the human bronchial epithelial cell (HBEC) layer causes a
jamming transition, but compression of the layer, as in bronchospasm, causes
unjamming. *The FASEB Journal* **29**, 671.671 (2015).
- 182 Bi, D., Lopez, J., Schwarz, J. & Manning, M. L. A density-independent glass transition in
biological tissues. *arXiv preprint arXiv:1409.0593* (2014).
- 183 Park, J.-A. *et al.* Unjamming and cell shape in the asthmatic airway epithelium. *Nature
materials* (2015).
- 184 Mitchel, J. *et al.* Maturation Of The Human Bronchial Epithelial Cell (hbec) Layer Causes
A Jamming Transition, But Compression Of The Layer, As In Bronchospasm, Causes
Unjamming. *Am J Respir Crit Care Med* **191**, A5580 (2015).
- 185 Schötz, E.-M., Lanio, M., Talbot, J. A. & Manning, M. L. Glassy dynamics in three-
dimensional embryonic tissues. *Journal of The Royal Society Interface* **10**, 20130726
(2013).
- 186 Haeger, A., Krause, M., Wolf, K. & Friedl, P. Cell jamming: collective invasion of
mesenchymal tumor cells imposed by tissue confinement. *Biochimica et Biophysica Acta
(BBA)-General Subjects* **1840**, 2386-2395 (2014).
- 187 Keys, A. S., Abate, A. R., Glotzer, S. C. & Durian, D. J. Measurement of growing dynamical
length scales and prediction of the jamming transition in a granular material. *Nature
physics* **3**, 260-264 (2007).
- 188 Jorjadze, I., Pontani, L.-L., Newhall, K. A. & Brujić, J. Attractive emulsion droplets probe
the phase diagram of jammed granular matter. *Proceedings of the National Academy of
Sciences* **108**, 4286-4291 (2011).
- 189 Lee, H.-N., Paeng, K., Swallen, S. F. & Ediger, M. Direct measurement of molecular
mobility in actively deformed polymer glasses. *Science* **323**, 231-234 (2009).
- 190 Katgert, G. & van Hecke, M. Jamming and geometry of two-dimensional foams. *EPL
(Europhysics Letters)* **92**, 34002 (2010).
- 191 Wyart, M. & Cates, M. Discontinuous shear thickening without inertia in dense non-
Brownian suspensions. *Physical review letters* **112**, 098302 (2014).
- 192 Berryman, J. G. Random close packing of hard spheres and disks. *Physical Review A* **27**,
1053 (1983).
- 193 Scott, G. & Kilgour, D. The density of random close packing of spheres. *Journal of
Physics D: Applied Physics* **2**, 863 (1969).
- 194 Bernal, J. & Mason, J. Packing of spheres: Coordination of randomly packed spheres.
Nature, 910-911 (1960).
- 195 Trappe, V., Prasad, V., Cipelletti, L., Segre, P. & Weitz, D. Jamming phase diagram for
attractive particles. *Nature* **411**, 772-775 (2001).
- 196 Gisler, T., Ball, R. C. & Weitz, D. A. Strain hardening of fractal colloidal gels. *Physical
review letters* **82**, 1064 (1999).
- 197 Pontani, L.-L., Jorjadze, I., Viasnoff, V. & Brujic, J. Biomimetic emulsions reveal the
effect of mechanical forces on cell-cell adhesion. *Proceedings of the National Academy
of Sciences* **109**, 9839-9844 (2012).
- 198 Kurniawan, N., Grimbergen, J., Koopman, J. & Koenderink, G. Factor XIII stiffens fibrin
clots by causing fiber compaction. *Journal of Thrombosis and Haemostasis* **12**, 1687-
1696 (2014).
- 199 Cho, K. S., Hyun, K., Ahn, K. H. & Lee, S. J. A geometrical interpretation of large
amplitude oscillatory shear response. *Journal of Rheology (1978-present)* **49**, 747-758
(2005).
- 200 Yao, N. Y., Larsen, R. J. & Weitz, D. A. Probing nonlinear rheology with inertio-elastic
oscillations. *Journal of Rheology (1978-present)* **52**, 1013-1025 (2008).
- 201 Wilhelm, M. Fourier-Transform Rheology. *Macromolecular materials and engineering*
287, 83-105 (2002).
- 202 van Kempen, T. H., Peters, G. W. & van de Vosse, F. N. A constitutive model for the time-
dependent, nonlinear stress response of fibrin networks. *Biomechanics and modeling in
mechanobiology*, 1-12 (2015).

- 203 Fahimi, Z. *et al.* A new approach for calculating the true stress response from large
amplitude oscillatory shear (LAOS) measurements using parallel plates. *Rheologica Acta*
53, 75-83 (2014).
- 204 Kang, H. *et al.* Nonlinear elasticity of stiff filament networks: Strain stiffening, negative
normal stress, and filament alignment in fibrin gels[†]. *The Journal of Physical Chemistry*
B **113**, 3799-3805 (2009).
- 205 Basu, A. Shear deformation in polymer gels and dense colloidal suspensions. (2012).
- 206 Naseri, E., Du, M. & Chan, R. W. Nonlinear viscoelastic properties of human vocal fold
tissues under large-amplitude oscillatory shear. *The Journal of the Acoustical Society of*
America **130**, 2551-2551 (2011).
- 207 Gardel, M. *et al.* Stress-dependent elasticity of composite actin networks as a model for
cell behavior. *Physical review letters* **96**, 088102 (2006).
- 208 Lin, Y.-C., Koenderink, G. H., MacKintosh, F. C. & Weitz, D. A. Viscoelastic properties of
microtubule networks. *Macromolecules* **40**, 7714-7720 (2007).
- 209 Bausch, A. & Kroy, K. A bottom-up approach to cell mechanics. *Nature physics* **2**, 231-
238 (2006).
- 210 Brangwynne, C. P., Koenderink, G. H., MacKintosh, F. C. & Weitz, D. A. Nonequilibrium
microtubule fluctuations in a model cytoskeleton. *Physical review letters* **100**, 118104
(2008).
- 211 Pelletier, V., Gal, N., Fournier, P. & Kilfoil, M. L. Microrheology of microtubule solutions
and actin-microtubule composite networks. *Physical review letters* **102**, 188303 (2009).
- 212 Brangwynne, C. P. *et al.* Microtubules can bear enhanced compressive loads in living cells
because of lateral reinforcement. *The Journal of cell biology* **173**, 733-741 (2006).
- 213 Vanderhoff, J. L., Alcoutlabi, M., Magda, J. J. & Prestwich, G. D. Rheological Properties
of Cross-Linked Hyaluronan–Gelatin Hydrogels for Tissue Engineering. *Macromolecular*
bioscience **9**, 20-28 (2009).
- 214 Ghosh, K. *et al.* Rheological characterization of in situ cross-linkable hyaluronan
hydrogels. *Biomacromolecules* **6**, 2857-2865 (2005).
- 215 Corwin, E. I., Clusel, M., Siemens, A. O. & Brujić, J. Model for random packing of
polydisperse frictionless spheres. *Soft Matter* **6**, 2949-2959 (2010).
- 216 Hermes, M. & Dijkstra, M. Jamming of polydisperse hard spheres: The effect of kinetic
arrest. *EPL (Europhysics Letters)* **89**, 38005 (2010).
- 217 Senff, H. & Richtering, W. Influence of cross-link density on rheological properties of
temperature-sensitive microgel suspensions. *Colloid and Polymer Science* **278**, 830-840
(2000).
- 218 Nordstrom, K. N. *et al.* Centrifugal compression of soft particle packings: Theory and
experiment. *Physical Review E* **82**, 041403 (2010).
- 219 Pelton, R. Temperature-sensitive aqueous microgels. *Advances in colloid and interface*
science **85**, 1-33 (2000).